Design, Implementation and BCI-based Control of a Series Elastic Mobile Robot for Home-based Physical Rehabilitation

by

Mine Saraç

Submitted to the Graduate School of Sabancı University
in partial fulfillment of the requirements for the degree of
Master of Science

Sabancı University

October, 2013

Design, Implementation and BCI-based Control of a Series Elastic Mobile Robot for Home-based Physical Rehabilitation

APPROVED BY:

Assoc. Prof. Volkan Patoğlu
(Thesis Advisor) .....

Assoc. Prof. Müjdat Çetin
(Thesis Co-Advisor) .....

Assoc. Prof. Kemalettin Erbatur .....

Assoc. Prof. Ali Koşar .....

Assist. Prof. Naime Özben Önhon .....

DATE OF APPROVAL: 25.10.2013

Design, Implementation and BCI-based Control of a Series Elastic Mobile Robot for Home-based Rehabilitation

Mine Saraç
ME, Master of Science, 2013
Thesis Supervisor: Assoc. Prof. Volkan Patoğlu
Thesis Co-supervisor: Assoc. Prof. Müjdat Çetin

Keywords: Robotic Rehabilitation, Series Elastic Actuation, Passive Velocity Field Control, Brain-Computer Interaction.

Abstract

We present the design, control and human-machine interface of AssistOn-Mobile, a series elastic holonomic mobile platform aimed to administer therapeutic table-top exercises to patients who have suffered injuries that affect the function of their upper extremities.

AssistOn-Mobile is designed as a multi-DoF series elastic actuator based on a holonomic mobile platform consisting of four actuated Mecanum wheels. Thanks to its mobile base, it is a compact and portable device that can cover whole human workspace for planar reaching exercises. Even though the mobile platform is not passively backdriveable due to the Mecanum wheels, a low-cost, compliant mechanism based, multi-DoF series elastic element is introduced to transform the holonomic mobile platform into a series elastic actuator and to ensure actively backdriveability of the overall system. Implementation of series elastic actuation results in many advantages, such as eliminating the need for costly force sensors, improving the performance of force control, and increasing the impact resistance and robustness of the overall system.

For the control of AssistOn-Mobile, in addition to admittance controllers used for active backdriveability, passive velocity field control (PVFC) is implemented for contour following tasks. PVFC minimizes the contour error by decoupling the task (path tracking) and the timing of the task, while also ensuring the coupled stability of the human-in-the-loop system by rendering the system passive with respect to externally applied forces. Furthermore, since AssistOn-Mobile is an end-effector type device, patients' shoulder movements are continually tracked utilizing a Kinect (RGBD) sensor such that compensatory movements of the patients (e.g, leaning) are limited by providing online feedback to the patients (for instance, by modulating the speed of the contour tracking task). With these controllers in place, AssistOn-Mobile becomes a highly backdriveable, force-controlled robotic interface that can provide required amount of assistance/resistance to patients, while performing omni-directional movements on a plane.

To enable patients with severe disabilities (e.g., spinal cord injury patients with no residual movements on their affected limb) to interact with AssistOn-Mobile and to provide assist-as-needed rehabilitation protocols to such patients, we introduce a systematic approach for online modification of robot assisted rehabilitation exercises by continuously monitoring intention levels of patients utilizing an electroencephalogram (EEG) based Brain-Computer Interface (BCI). In one implementation, we utilize posterior probabilities extracted from an LDA classifier as the continuous-valued outputs to PFVC. This way, PVFC modulates the speed of contour following tasks with respect to intention levels of motor imagery.

The efficacy of our proposed robotic BCI framework with online modification of task speed is investigated by a set of human subject experiments with healthy volunteers. In particular, our approach is compared with the existing BCI-based virtual reality and robot-assisted rehabilitation techniques. Within this experiment, we have collected statistically significant evidence of the beneficial effect of the haptic feedback during the mental imagery of subjects. Results also indicate that using BCI continuously rather than to initialize the movement only may be preferable to ensure active participation of patients throughout the therapy. Finally, using the proposed BCI-based rehabilitation protocol shows no statistically significant difference in terms of mental imagery activity, compared to the rehabilitation protocol where the subjects are actively performing the real movement.

Evde Kullanılabilen Seri Elastik Mobil Rehabilitasyon Robotunun Tasarımı, Uygulaması ve Beyin-Bilgisayar Arayüzü Tabanlı Kontrolü

Mine Saraç
Yüksek Lisans Tezi, 2013
Tez Danışmanı: Doç. Dr. Volkan Patoğlu
Tez Eş-danışmanı: Doç. Dr. Müjdat Çetin

Anahtar Kelimeler: Robot Destekli Rehabilitasyon, Seri-Elastik Eyleyici, Holonomik Platform, Pasif Hız Alanı Kontrolü, Beyin-Bilgisayar Etkileşimi.

Özet

Bu tezde üst uzuvların robot destekli masa üstü rehabilitasyonunda kullanılmak üzere, seri elastik holonomik gezgin platform AssistOn-Mobile' ın tasarımını, kontrolünü ve insan etkileşimi için kullanılan arayüzünü sunmaktayız.

AssistOn-Mobile, dört aktif Mecanum tekerlekli holonomik gezgin platform tabanlı, çok serbestlik dereceli seri elastik eyleyici olarak tasarlanmıştır. Gezgin tabanı sayesinde kompakt ve taşınabilir olan bu cihaz, insan kolunun ulaşabileceği çalışma alanında dönme ve ilerleme hareketlerini bağımsız yapabildiği gibi tüm yatay uzanma hareketlerini de gerçekleştirebilir. Mekanum tekerlekler yüzünden pasif olarak geri sürülebilir olmayan bu cihazı, düşük maliyetli, esnek mekanizma tabanlı, çok serbestlik dereceli seri elastik eleman kullanarak seri elastik eyleyiciye dönüştürdük ve sisteme aktif geri sürülebilirlik kazandırdık. Seri elastik eyleyiciye sahip holonomik platform, yüksek maliyetli kuvvet sensörlerine olan ihtiyacı ortadan kaldırmakta ve yüksek kazanımlara sahip kapalı döngü kuvvet kontrolü uygulamasına olanak tanımaktadır. Aynı zamanda sistemin pasif empedansını düşürüp darbelere karşı sistem gürbüzlüğünün artmasını da mümkün kılmaktadır.

AssistOn-Mobile'ın kontrolü için, aktif geri sürülebilirliği sağlayan admitans kontrolörüne ek olarak, rota takip etme uygulamaları için pasif hız alanı kontrolörü (PVFC) de sentezledik. PVFC, takip edilmesi istenilen rotayı ve rotayı tamamlamak için gereken zamanı birbirinden ayırmakta ve rota hatalarını küçültmektedir. Aynı zamanda, döngü içerisinde insan da olan sistemin dışarıdan uygulanan kuvvetlere karşı pasif olmasını sağlayarak, toplam sistemin kararlılığını garanti etmektedir. AssistOn-Mobile hasta ile robotun sadece sonlandırıcıda fiziksel etkileşim içinde olması üzere tasarlandığından, egzersizler sırasında hastaların telafi edici hareketlerini (örneğin, eğilme hareketi) engelleyememektedir. Terapi sırasında istenmeyen bu hareketleri limitlemek için, Kinect (RGBD) sensörü ile hastaların omuz hareketlerini anlık olarak takip edilmiş ve AssistOn-Mobile'ın hızı bu ölçümlere göre değiştirilerek hastalara anlık geri besleme verilmiştir. Bu kontrolörlerin kullanımı

sayesinde AssistOn-Mobile, hastalara yatay düzlemde çok yönlü hareketleri gerekli miktarda destek veya direnç göstererek gerçekleştirebilen, kuvvet kontrolörlü ve geri sürülebilir bir robot ara yüzü haline getirilmiştir.

Ağır sakatlıkları bulunan hastaların (örneğin sakatlıktan etkilenmiş kolu ile hiç bir hareketi gerçekleştiremeyen hastalar veya omurilik rahatsızlıkları bulunan hastalar) AssistOn-Mobile ile etkileşimlerini mümkün kılabilmek ve bu hastalara da ihtiyaç duydukları kadar destek verebilen rehabilitasyon protokollerini uygulayabilmek amacı ile Elektroensefalografi (EEG) tabanlı Beyin-Bilgisayar Arayüzleri (BBA) sisteme entegre edilmiştir. Bu tezde; hastaların hareketi ne kadar gerçekleştirmek istedikleri BBA tarafından görüntülenerek robot destekli rehabilitasyon egzersizlerinin hızının sürekli olarak değiştirildiği sistematik bir yaklaşım sunulmuştur. Bir uygulamada, LDA sınıflandırıcısından gelen bilgilerin ardıl olasılıklarını sürekli değerli sonuç verecek şekilde hesaplayarak PVFC'nin hız katsayısını değiştirecek şekilde kullanılmıştır. Böylece, AssistOn-Mobile'ın PVFC sayesinde belirlenen rotayı takip edeceği hız, hastaların hareketi gerçekleştirme isteği doğrultusunda değiştirilmiştir.

Sunmuş olduğumuz hareket hızının çevrimiçi değiştirildiği BBA tabanlı rehabilitasyon yönteminin etkinliğini, sağlıklı gönüllülerin katıldığı insanlı deneyler ile gözlemledik. Bu deneylerde, sunmuş olduğumuz yöntemi mevcut BBA tabanlı sanal gerçeklik ve robot destekli rehabilitasyon teknikleri ile karşılaştırdık. Bu insan deneylerinin sonuçları gösterdi ki, sunmuş olduğumuz robot destekli BBA sistemi, hastaların rehabilitasyon egzersizlerine daha fazla katılım göstermesini sağlamakla beraber rehabilitasyon protokolünde hastaların aktif olmasını garanti etmektedir. Bu deneyin sonucunda, hastalara terapi sırasında verilen robotik geri beslemenin istatistiksel önemini gözlemledik. Ayrıca, BBA sistemini hareketi başlatmak yerine düzenli olarak kullanmanın daha tercih edilebilir olduğu sonucuna vardık. Son olarak, sonuçlarımız, önerdiğimiz BBA yöntemi ile kullanıcıların hareketi fiziksel ve aktif gerçekleştirlemeleri arasında beyin aktivitesi açısından istatistiksel bir fark olmadığınını göstermektedir.

Acknowledgement

It is a great pleasure to extend my gratitude to my thesis advisor Assoc. Prof. Dr. Volkan Patoğlu and my co-advisor Assoc. Prof. Dr. Müjdat Çetin for their guidance and support. I am indepted to them for their supervision, advices and support during my Master study. I would gratefully thank Assoc. Prof. Dr. Kemalettin Erbatur, Assoc. Prof. Dr. Ali Koşar, and Assist. Prof. Dr. Naime Özben Önhon for their feedbacks and spending their time to serve as mu jurors.

I would like to acknowledge the financial support provided by The Scientific & Technological Research Council of Turkey (TÜBİTAK) under the project grant of 111M186 and Sabanci University for waiving the tuition through my Master education.

It was a pleasure to work with Ahmetcan Erdoğan and Ela Koyaş and I am thankful to them for their collaboration during the project. Many thanks to my group friends, Giray Havur, Mustafa Yalçın, Beşir Çelebi, Ozan Tokatlı, Elif Hocaoğlu for their support and invaluable help. Moreover, my good friends, Soner Ulun, Eray Baran, Beste Bahçeci, İlker Sevgen and many others for making the laboratory enjoyable and memorable. Also, special thanks to İlker Sevgen for his support throughout my research and for sharing his experience and technical knowledge and saving my day many times. I want to express my gratitude to Mustafa Yalçın, Ozan Tokatlı, Emre Özeren, Alper Yıldırım, Ezgi Karakaş, Taygun Kekeç, Çağdaş Erk, Eray Baran, Beste Bahçeci and others for their voluntarily participation to the joint experiments.

I owe my deepest gratitude to my family for all their love and support throughout my life. I am thankful for my great friends Bengi Deniz Kırındı, Sena Ayhun, Ceren Aşkın, Ahmet Gülsat, Anıl Özdemirli, Bahadır Dindar, Erkin Yücel and many others for behaving like my sisters and brothers. Without their love, support and help, this research would not have been possible.

Contents

List of Figures

List of Tables

Chapter I

1 Introduction

This section discusses physical rehabilitation for stroke, its burden on both therapists and patients, and main notions of upper limb rehabilitation. Also, the importance of assist-as-needed based rehabilitation therapies is emphasized for patients with residual movement ability. Then, Brain-Computer Interaction (BCI) based rehabilitation is introduced to implement assist-as-needed therapies for patients with severe disabilities and no ability to function their limbs. The introduction chapter ends with the contributions and outline of the thesis.

1.1 Physical Rehabilitation

The nervous system consists of the brain, spinal cord and an intricate network of nerves throughout the body and is an incredibly complex communication system that controls and regulates the functions of body. Unfortunately, this extraordinary system is vulnerable to disease and injury [1]. Neurological injuries are the leading cause of serious, long-term disabilities that restrict the daily functions of millions of patients. Stroke is one of the most serious neurological injuries and approximately 9 million people had a stroke in 2008 and 30 million people have previously had a stroke and are still alive [2].

After neurological injuries, 75% of stroke survivors suffer from the disabilities that affect their daily living routines physically, mentally, and emotionally [3]. Physical rehabilitation is an indispensable solution to treat those patients who are dealing with disabilities of neurological injuries and to help those patients regain their functional abilities for the activities of daily living (ADLs) skills. Rehabilitation therapies are shown to be more effective when they are repetitive [4], intense [5], long term [6] and task specific [7].

For upper limb rehabilitation, one of the major aims of the physical therapy is to increase the effective range of motion of the patient arm. An effective way of increasing the range of motion is to administer reaching movements to the patient. Although human arm is capable of performing more complex movements, many practical tasks in our daily lives only require planar reaching movements. Therefore, table top exercises where the weight of the patient's arm is supported are widely administered as upper limb rehabilitation exercises.

During conventional physical rehabilitation, therapists guide patients to move their upper and/or lower limbs by physical interaction. Manual administration of such therapies are costly due to physical burden involved.

Robotic Rehabilitation

Utilization of robotic devices to provide repetitive and physically involved rehabilitation exercises eliminate the physical burden of the therapy for the therapists, while motivating the patients to endure long, intense therapy sessions. Besides, the the lack of physical interaction between the therapists and the patients allows the therapists to deal with multiple patients at a time and decreases the cost of the treatment. Robot assistance during reha-

bilitation also increases the reliability and accuracy of desired tasks, ensuring that the same task is repeated by patients, while also providing quantitative measurements to track the patients' progress.

Clinical trials investigate the efficacy of robotic rehabilitation and provide evidence that robotic therapy is effective for motor recovery and possesses high potential for improving functional independence of patients [8–11]. Moreover, robotic devices may provide "assist-as-needed" (AAN) control to patients by allowing them to complete the tasks with their own efforts and assist them as much as they need. In particular, AAN control helps patients to follow a desired path, while assisting them to prevent large errors along the path.

Rehabilitation robots can loosely by categorized as exoskeleton and end-effector types. Exoskeleton type robots correspond with the human joints individually. In particular, exoskeletons are capable of delivering specific joint therapies decoupled from movements of other joints, as well as task specific therapies coupling different joint movements. Thanks to individual joint control, compensatory movements are prevented by the exoskeleton devices. Many exoskeleton type upper limb rehabilitation robots have been developed successfully in the literature, such as [12–24]. Despite of their advantages, the exoskeleton type robots are complex in terms of their physical design and have higher cost. Besides, most of these devices require cumbersome adjustments as misalignments between the robot and the arm of patient may be harmful for patients during the treatment process.

AssistOn-Mobile

In this thesis, we propose utilizing an end-effector type holonomic mobile platform to administer active therapeutic table-top exercises to patients who have suffered injuries that affect the function of upper extremities. In particular, we introduce the design of AssistOn-Mobile, a series-elastic actuation based mecanum-wheeled holonomic mobile platform for upper arm rehabilitation. Unlike the other therapeutic mobile devices that only sustain passive and resistive modes, the proposed holonomic mobile platform is an active rehabilitation device for home-based therapies. AssistOn-Mobile can assist patients to complete table-top reaching tasks, help improve the accuracy of movement therapy and the efficacy of rehabilitation protocols. With the integration of a compliant element which estimates the applied forces by measuring the deflections, the holonomic mobile platform is turned into a series elastic actuator, AssistOn-Mobile to achieve active back-driveability. The mobile platform and the compliant element can be used as measurement tools to characterize the range of motion, isometric strength of the injured arm and functional ability to apply forces. The force estimation enables AssistOn-Mobile to measure interaction forces between the device and the patients and to provide adaptive assistance to patients based on their contribution as in AAN methods. Since AssistOn-Mobile is an end-effector type device, we also continually track shoulder movements of patients utilizing a Kinect (RGBD) sensor such that compensatory movements of the patients (e.g, leaning) are limited by providing online feedback to the patients (for instance, by modulating the speed of the contour tracking task).

1.2 Brain Computer Interface (BCI) based Rehabilitation

Current rehabilitation devices that provide AAN therapies are based on the interaction forces between the device and the patient; hence, cannot be used with severely injured patients that have low residual movement on their upper limbs (e.g., spline cord injury patients). Since activity-dependent plasticity requires that patients actively recruit their own neural pathways to the best of their ability, the mental effort of patients is as important as their physically involvement during the treatment process. Moreover, studies [25] show that patient passive physical therapy routines do not provide lasting positive effect on chronic stroke patients, especially for patients without any residual functionality. Motor imagery training in combination with physical therapy creates favorable conditions to induce neuroplasticity with the aid of visual and haptic feedback. Brain-Computer Interface (BCI) systems provide a systematic approach for the mental imagery tasks, quantitative measurements and possibility for visual and haptic integrations.

A BCI system generates commands by measuring the brain activity. In particular, a non-invasive electroencephalogram (EEG) method is commonly used to measure the electrical activity of the brain from the outside of the scalp for rehabilitation integration. Collecting these electric potentials is more practical, less expensive and safer for the patients compared to other alternative methods. Using different features to understand EEG signals gives the opportunity to control prostheses [26], wheelchairs [27, 28], a cursor [29, 30], and robots [31–33]. Recently, there has been much interest in developing BCI technology to help restore function for patients with severe motor disabilities, including patients with severe trauma due to stroke, cere-

bral palsy, or injury to spinal cord or brain.

EEG-based BCI technology promises an alternative pathway to guide rehabilitation protocols to effectively induce activity-dependent brain plasticity and to restore neuromuscular function by monitoring the electrical activity with brain signals. Experimental evidence shows that the brain has a cortical plasticity which can be stimulated by a learning process. A BCI system can exploit the plasticity of the Central Nervous System (CNS) to restore some functionality [34]. Experimental studies in [35, 36] showed that stroke patients could learn to operate a BCI system. Furthermore, in [37], it is stated that the success rate of stroke patients on using a BCI system is close to the rate of healthy subjects. [38] investigated the effect of BCI systems with a set of experiments for 32 chronic stroke patients with severe hand weaknesses. The subjects are separated as experimental and control group, where the hand/arm orthosis is controlled via BCI system or randomly. The results indicate that the BCI training may improve the functional treatment when it is combined with the traditional physical practice.

In the literature, EEG-based BCI systems are integrated with either virtual reality (VR) environment or robotic devices for the rehabilitation. During VR integration, the intention for the movement is represented visually with no physical feedback. The robotic device integration provides haptic feedback to patients related to their intentions. During BCI integration with robotic devices, the patients are in contact with the rehabilitation device; therefore, the patients also complete physical tasks as well as mental imagery tasks. The robotic devices are mostly triggered with the intention levels; however, as stated in [39], online adaptation between the physical movement and the mental state of patients are crucial in terms of generating

a true pathway during therapies.

Proposed BCI Integration

We propose a novel systematic approach that enables online modification/adaptation of robot assisted rehabilitation exercises by continuously monitoring intention levels of patients utilizing an EEG-based BCI system. In particular, we use Linear Discriminant Analysis (LDA) to classify event-related synchronization/desynchronization (ERD/ERS) patterns associated with motor imagery; however instead of using binary outputs, at first, we utilize posterior probabilities extracted from LDA classifier as the continuous-valued outputs to control AssistOn-Mobile. Passive Velocity Field Control (PVFC) has been used as the underlying controller to map instantaneous levels of motor imagery during the movement to the speed of contour following tasks applied to AssistOn-Mobile. In other words; PVFC changes the speed of contour tracking tasks with respect to intention levels of motor imagery. PVFC also decouples the task and the speed of the task from each other while ensuring coupled stability of the overall robot patient system. Giving patients online control over the speed of the task, the proposed approach ensures active involvement of patients throughout exercise routines. To prove the efficacy of the proposed BCI-based rehabilitation protocol with online modification, a set of experiments with 13 healthy subjects have been performed. In this experiment; the subjects are asked to perform all existing BCI-based rehabilitation methods as well as conventional robot assisted rehabilitation tasks in a randomized order to show the effect of robotic assistance and online modification between the mental state and the movement in the rehabilitation protocols.

1.3 Contributions

- We propose an active holonomic mobile platform based multi degrees of freedom (DoF) series elastic actuator, AssistOn-Mobile to administer therapeutic table-top exercises to patients who have suffered injuries that affect the functionality of their upper extremities. In particular, AssistOn-Mobile consists of a holonomic mobile platform and a compliant element that transforms the mobile platform into series elastic actuator. Thanks to the compliant element; the externally applied forces can be estimated to control the interaction forces with the device. Unlike the mobile rehabilitation devices in the literature, multi DoF series elastic actuator, AssistOn-Mobile is able to measure the interaction forces between the patients and the subjects to provide "assist-as-needed" control therapies while avoiding the necessity to use high cost, high stiffness force sensors.

  - A 3-Dof active holonomic mobile platform with unlimited workspace is designed with 4 Mecanum wheels. Due to the four actuated wheels, the system is redundant. Redundancy allows the use for smaller actuators and provides better dead-reckoning accuracy. Each wheel is belt-driven with a tensioning mechanism. A suspension system ensures that the system is in contact with the ground at all times. Although the motors are passively backdriveable, due to mecanum wheels; the mobile platform is not passively backdriveable.

  - For localization of AssistOn-Mobile, odometry is integrated with the data from the optical flow sensors to help compensate for

the lateral slip of the wheels. For combination of different sensor measurements; 3 sensor fusion techniques based on Kalman filter have been implemented and compared for AssistOn-Mobile.

  - A multi-DoF compliant element is introduced between the mobile base and the users to transform the active holonomic platform into a multi-DoF series elastic actuator. In particular, forces applied at the end-effector are estimated by measuring the deflections of the grounded prismatic joints of the compliant mechanism using linear encoders. As a result, in addition to inheriting the advantages of series elastic actuation for the system, applied forces are estimated with a low-cost design.

  - To limit the amount of compensatory movements that are inevitable for end-effector type devices, a Kinect (RGBD) sensor is integrated to the system such that the movements of AssistOn-Mobile is regulated to provide online feedback to the patient when the undesired level of compensatory shoulder movements take place.

- We have implemented passive velocity field control (PVFC) for AssistOn-Mobile to provide required amount of assistance to the patients, such that the mobile platform follows a desired velocity field while maintaining passivity with respect to external applied forces.

  - PVFC is particularly suitable for rehabilitation robotics, since this contour tracking controller ensures coordination and synchronization between various degrees of freedom, while allowing patients to complete the task.

  - PVFC decouples the desired contour following task and timing along the path; therefore patients are free to determine the speed of the task while PVFC assists them to stay on the path.
  - PVFC not only minimizes the contour error, but also renders the closed loop system passive with respect to external forces, ensuring coupled stability; hence safety, of the overall human-robot system.

- As a collaborative work with Sabanci University Computer Vision and Pattern Analysis Laboratory (VPA), we propose a novel BCI-based robot-assisted rehabilitation framework, where the task speed is adjusted with respect to the subjects' intention levels obtained by the EEG-based BCI system. Within this joint work, we have controlled the AssistOn-Mobile by adjusting the task speed using continuously estimated intention levels of subjects which has been covered in **??**.
  - To enable online adaptation of robot assisted rehabilitation exercises with respect to the intention levels of the patients, posterior probabilities extracted from the LDA classifier of a BCI system are used as continuous valued outputs to PVFC. Such outputs correspond to instantaneous levels of motor imagery during the movement and are used to modulate the speed coefficient in PVFC algorithm. Therefore, with increased level of "intention", a higher speed to complete the task is supplied to the patient. Such an online feedback is aimed to encourage the active participation of the patient.
  - A human subject experiment is designed and conducted to compare the efficacy of the proposed robotic BCI framework with on-

line modification of task speed with the existing BCI protocols used for stroke rehabilitation.

– This human subject experiment has provided statistically significant evidence of the beneficial effect of robotic assistance during the mental imagery tasks of subjects. Moreover, the results indicate that using the BCI system continuously rather than to trigger the movement only may be preferable to impose active participation of patients throughout the therapy. Finally, the use of proposed BCI-based rehabilitation protocol under robot assistance with online modification of task speed have no statistically significant difference in the brain activity, compared to the rehabilitation protocol where the subjects are actively performing the real movement.

1.4 Outline

The rest of the thesis is organized as follows. The design of rehabilitation robot for the upper extremities are discussed and design decisions are detailed in Chapter 2. In particular, Section 2.1 describes the kinematics and dynamics of the holonomic mobile platform. Section 2.2 details the integration of optical flow sensors to improve the localization performance of the mobile platform and discusses the sensor fusion techniques employed. Section 2.3 focuses on the design and implementation of the compliant element that transforms the mobile holonomic platform into a multi-DoF series elastic actuator. Section 2.4 details the integration of Kinect sensor to prevent compensatory movements. Chapter 3 reviews the control algorithms implemented on AssistOn-Mobile. In particular, Section 3.1 details the

admittance control, while Section 3.2 presents the Passive Velocity Field Control. Chapter 4 focuses on the implementation of an EEG-based Brain-Computer Interface for modifying the task speed with respect to intention levels of subjects. Chapter 5 explains the experimental procedure to compare the proposed BCI-assisted rehabilitation robotic system with existing rehabilitation techniques and discusses the results. Finally, Chapter 6 concludes the thesis and gives brief description of the future work.

Chapter II

2 AssistOn-Mobile

This chapter discusses the robot-assisted rehabilitation devices in the literature and presents the implementation of AssistOn-Mobile [40], a series elastic holonomic mobile platform depicted in Figure 2.1. This mobile platform has a rectangular shape of 340 mm x 160 mm x 85 mm and possesses 3-DoF to sustain all possible planar movements: 2 DoF translations and 1 DoF rotation in plane. The size of this device is optimized to be light and portable while providing enough space to enable patients to place their arms on it to support the weight of their arms.

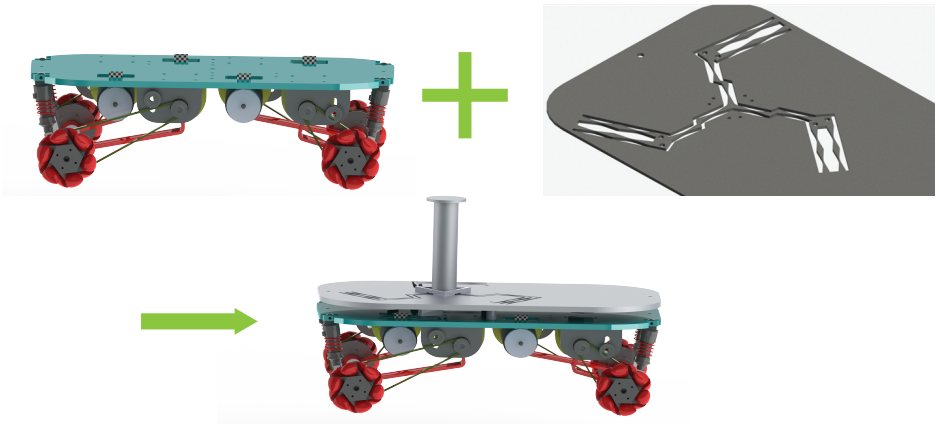

Figure 2.1: AssistOn-Mobile: A holonomic mobile platform with a multi-DoF compliant element

2.0.1 Robot Assisted Rehabilitation

End-effector type rehabilitation devices interface with the human arm only at only the end-effector and aim to control the human arm as a whole. This type of connection may allow patients to move their bodies while their arm is connected to the device. Such compensatory movements are undesirable during rehabilitation therapies. In particular, such devices can only administer controlled therapeutic movements in the task space. Yet, the end-effector type devices are advantageous because of their relatively simpler kinematic structure and lower cost. End-effector devices can further be categorized as fixed-base and mobile devices with respect to their portability.

Fixed-base end-effector devices are mounted to the ground and their stationary structure allow them to include heavy and powerful actuators and transmission units. Moreover, such devices do not suffer from localization problems, since the global configuration of the end-effector can be directly measured. MIT-Manus [41] is a well-known fixed-base end-effector type rehabilitation device. In particular, it is an impedance-type robot that possesses two grounded direct-drive motors to provide assistance or resistance to patients. Gentle/S [42] is an admittance-type robot, which uses HapticMaster device [43] along with a gimbal mechanism for the connection with the human wrist. As a second prototype, Gentle/A [44] has been developed. This device can either perform position controlled movements or active-assisted movements where the patients are asked to initialize the movement. Reha-Slide is designed to administer resistive movement therapies [45]. The diamond robot (DR) parallel rehabilitation device in [46] provides horizontal movements for the therapy. It has quasi-3-DoF space movements and its magnetic clutch provides safety. Even though fixed-base end-effector type

devices have been shown to be effective in delivering therapies in a clinical setting, their adaptation for the home-based therapies has not been very feasible. Therefore, such devices are limited in the number of sessions they can deliver therapy to a patient.

Unlike fixed-base devices, mobile end-effector type rehabilitation devices are designed as light, portable and compact; which make them suitable for the home-based robotic therapies. Although the mobility introduces a challenge in the localization accuracy, these devices can be implemented with much lower manufacturing cost. Several low-cost, home-based rehabilitation robots have been designed in the literature. A well-known low-cost, passive mobile device is the arm skate [47], which is a passive device equipped with reed-relays and magnets to link the objects defined in a virtual environment with the physical environment and to determine the robot position. Due to its high-cost, a later version with 4 omni-directional wheels has been implemented to provide resistance to patients [48]. Another example of low-cost table-top devices is Rutgers Arm II [49] which uses teflon balls to slide over a table. The table is manually tilted to provide limited assistance or resistance to patients passively and the movements are tracked with cameras and displayed in a virtual environment. Even though these passive mobile devices are low-cost and potentially effective in motivating patients and providing quantitative measurements of patients' progress, they do not include any actuators to guide patients to complete the desired tasks.

There are several active mobile-based rehabilitation devices in the literature. The first prototype of ArmAssist [50] has been designed to provide passive planar movements using three omni-directional wheels. A force sensor has been integrated to this device to measure the out-of-plane forces.

For the second prototype [51]; three DC motors have also been added to the device to drive the mobile module and deliver position tracking tasks. But, this device does not measure the interaction forces to provide assist-as-needed type therapies. MOTORE [52] is an active mobile device which uses 3 actuated omni-directional wheels and two load cells at the handle to measure in-plane forces. MOTORE implements admittance controllers during trajectory tracking tasks. Reha-Maus [53, 54] is another active mobile device with 3 omni-directional wheels driven by geared motors and a force/torque sensor. These active devices rely on high fidelity commercial force sensors to achieve active backdriveability under control. However, the use of high fidelity force sensors significantly increases the system cost and limits the performance of these device due to low force controller gains. Besides, explicit force control is vulnerable to instability due to sensor actuator non-collocation imposed by the higher order dynamics of the system [55, 56]. Therefore, there is still need for low-cost, high performance mobile end-effector devices for upper arm rehabilitation in the literature.

2.1 Holonomic Mobile Platform

The holonomic mobile platform in Figure 2.2 is designed so that the forearm and the wrist of a patient can be comfortably placed on the robot, relieving patients from the burden of supporting the weight of their own arm. In particular; the holonomic mobile platform can independently control all possible planar DoFs thanks to the use of 4 Mecanum wheels. Mecanum wheels are omni-directional wheels with 45° angled rollers. Evidence in the literature suggests that Mecanum wheels can provide enhanced traction, smoother motion and less slip during movements compared to omni-directional wheels [57].

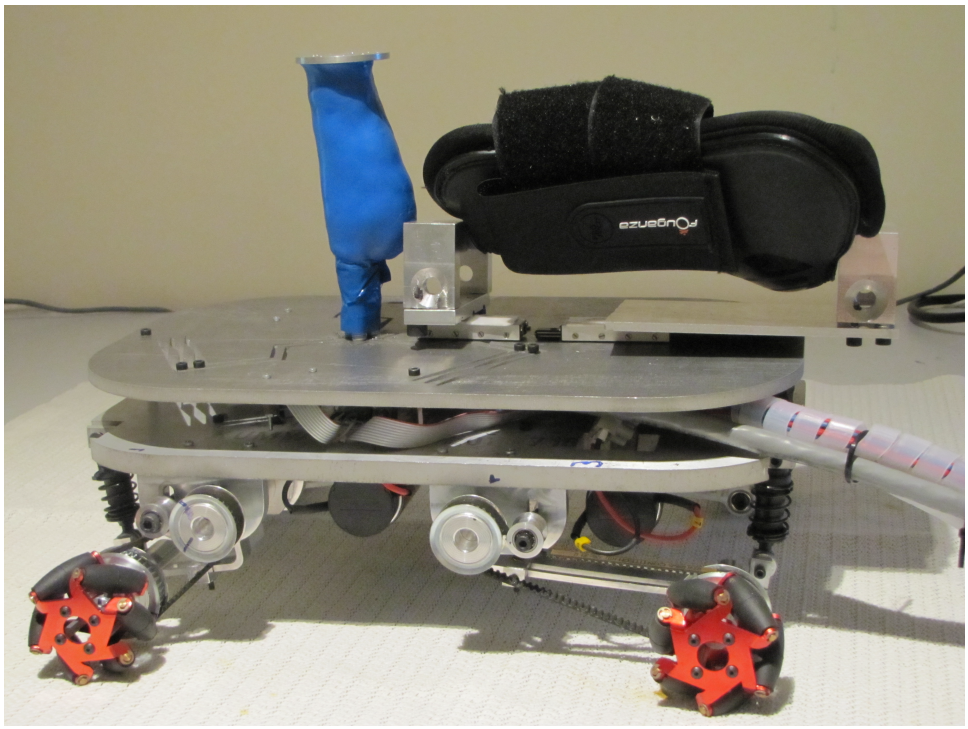

Figure 2.2: A prototype of AssistOn-Mobile

Mecanum wheels are placed on the mobile platform such that the rollers of first and fourth wheels and rollers of second and third wheels possess a 90° orientation difference about the vertical axis. The use of 4 actuated Mecanum wheels renders the mobile platform redundant. Redundant actuation has advantages such as allowing the use of lower power actuators and smaller transmission units, allowing achievement of high forces/torques at the task space and providing better dead-reckoning accuracy with the use of 4 encoders. The proposed mobile platform has a suspension system for each wheel to ensure that all wheels are in contact with the ground at all times. Specifically, the suspension springs are chosen among the commercially available suspension components for RC cars and have 10 mm stroke. The connec-

tion parts and upper body of the robot are manufactured from aluminum and stainless steel. The actuators of the mobile robot are chosen as brushed DC motors with 180 mNm continuous torques and with 4.8 : 1 integrated gearboxes. The power generated by the motors is transmitted to the wheels via a belt driven transmission with a torque amplification ratio of 42 : 30. A handle and an arm support are also designed for the comfort of patients during the therapies; supporting the weight of their arms while providing a stable connection between the patients and the device. The components of the AssistOn-Mobile has been shown in Figure 2.3.

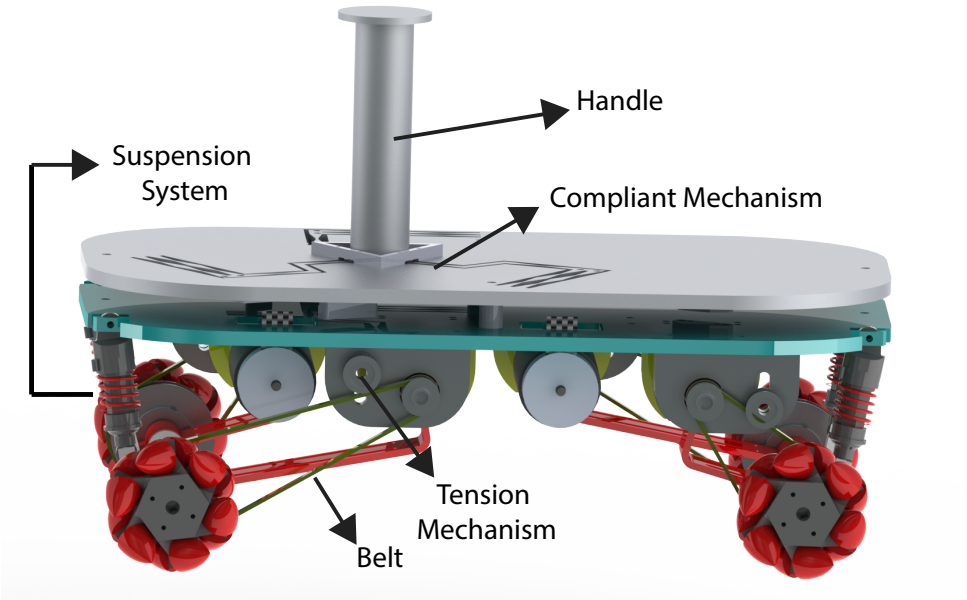

Figure 2.3: The components of AssistOn-Mobile

2.1.1 Kinematics

Figure 2.4 shows the CAD model of the holonomic mobile platform where the significant points, frames and bodies are marked. N, H, W_i and S_i with

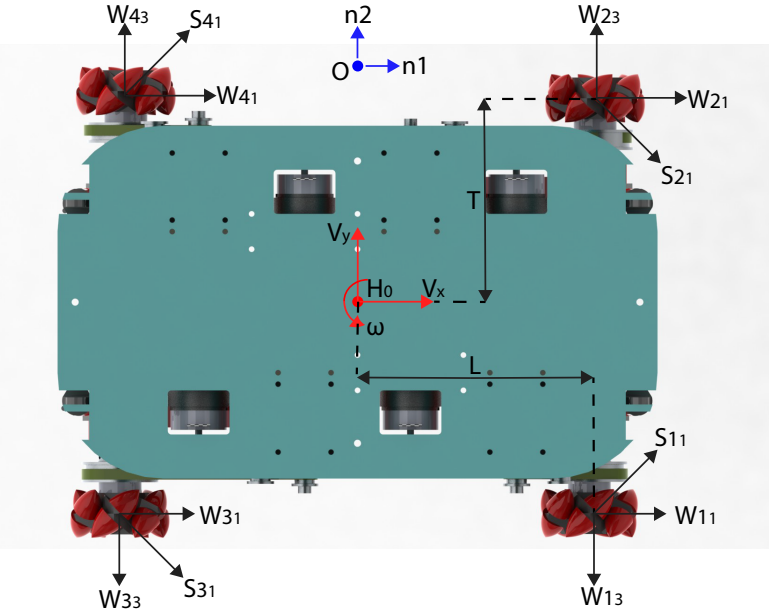

Figure 2.4: CAD model of AssistOn-Mobile

$(i = 1, 2, 3, 4)$ frames represent Newtonian reference frame, mobile platform frame, wheels' frames and angled roller frames on the Mecanum wheels. The center points are O for Newtonian frame and H_0 for mobile platform. L and T represent the distances from H_0 to the wheels' center.

The velocity of the mobile platform can be defined with respect to the frame N as in Equation (1).

$$^{N}\vec{V}^{M} = V_x\vec{n}_1 + V_y\vec{n}_2 = {}^{W}R_A^T \tag{1}$$

where V_x and V_y are the velocities along $\vec{n}_1$ and $\vec{n}_2$ directions. Equation (2) shows the angular velocity of the system with respect to N.

$$^{N}\vec{\omega}^{M} = \omega\vec{n}_3 \tag{2}$$

The angular velocity of each wheel with respect to the frame H is given in Equation (3).

$$^{H}\vec{\omega}^{W_i} = \dot{\theta}_i \vec{\omega}_{i_2} \qquad \text{for i=1,..,4} \tag{3}$$

where $\dot{\theta}_i$ are the magnitudes of angular velocities of each wheel respectively. The velocity of the center of 45^o shifted rollers S_{i_o} that are in contact with the ground can be driven as in Equation (4).

$$^{N}\vec{V}^{S_{i_o}} = {}^{N}\vec{V}^{H_o} + {}^{N}\vec{\omega}^{H} \times \vec{r}^{H_o W_{i_o}} + {}^{H}\vec{\omega}^{W_i} \times \vec{r}^{W_{i_o} S_{i_o}} \tag{4}$$

where $\vec{r}^{H_o W_{i_o}}$ is the position vector from the center of the platform to the center of each wheel and $\vec{r}^{W_{i_o} S_{i_o}}$ is the position vector from the wheel centers to the contacting roller centers for each wheel. Assuming that the rollers touching the ground cannot slip sideways; the $\vec{s}_{i_2}$ components of the velocities $^{N}\vec{V}^{S_{i_o}}$ are set to zero as non-holonomic constraints to restrict the motion of the robot as Equation (5).

$$^{N}\vec{V}_{S_{i_o}} . \vec{s_{i_2}} = 0 \qquad \text{for i=1,..,4} \tag{5}$$

Given these definitions, Equation (6) presents the motion level inverse kinematics of the mobile platform with respect to the H frame.

$$\begin{bmatrix} \dot{\theta}_1 \\ \dot{\theta}_2 \\ \dot{\theta}_3 \\ \dot{\theta}_4 \end{bmatrix} = J^{-1} \begin{bmatrix} Vx \\ Vy \\ \omega \end{bmatrix} \tag{6}$$

The inverse Jacobian matrix J^{-1} is calculated as Equation (7).

$$J^{-1} = \frac{1}{R}\begin{bmatrix} 1 & -1 & -(L+T) \\ 1 & 1 & (L+T) \\ 1 & 1 & -(L+T) \\ 1 & -1 & (L+T) \end{bmatrix} \tag{7}$$

where R is the radius of the Mecanum wheels, L and T are vertical and horizontal distances from the center of mobile platform to the center of wheels. Due to the redundancy of mobile platform, J^{-1} is not a square matrix and motion level inverse kinematics is computed using pseudo-inverse method as in Equation (8).

$$J^{\dagger} = (J^T \times J)^{-1} \times J^T \tag{8}$$

As a result; the kinematic Jacobian J characterizing the the motion level kinematics can be explicitly stated as in Equation (9).

$$J = \frac{R}{4}\begin{bmatrix} 1 & 1 & 1 & 1 \\ -1 & 1 & 1 & -1 \\ \frac{-1}{L+T} & \frac{1}{L+T} & \frac{-1}{L+T} & \frac{1}{L+T} \end{bmatrix} \tag{9}$$

2.1.2 Dynamics

The dynamic equations governing the motion of the mobile platform is derived using Kane's method [58]. The external forces along x and y directions, torque about z direction at the end effector and the motor torques at each wheel are identified as F_x, F_y, τ_z, and τ_i, respectively. To implement Kane's method, acceleration level kinematics of the device is derived and partial

velocities of the mass centers and forces acting points are formed. Inertia of each component of the robot is estimated from its CAD model. Finally, the equations of motion of the robot are derived symbolically and task space inertia and Coriolis matrices are extracted for use in controls.

2.2 Localization

The easiest way to calculate the configuration of a mobile robot is to rely on odometry/dead-reckoning techniques. The odometry keeps track of the angular movement of each wheel, by possibly utilizing encoders attached to the motor. Using the kinematic model of the robot, the end-effector position of the mobile device can then be estimated. Although these techniques are quite common for localization, they are vulnerable to the errors caused by the slip of the wheels causing the position estimate errors to increase cumulatively over time.

In this work, optical flow sensors are introduced to help compensate the position errors due to the (especially lateral) slip of the wheels. These sensors measure the displacement along x and y directions, provide good local positioning accuracy with a range of millimeter, are low-cost, light-weight, with very low-power consumption. For our current prototype, we have integrated high-performance, low-cost optical mouse sensor $ADNS2620$ with an Arduino board as optical flow sensors.

To correspond with all possible DoFs the mobile platform can cover; 2 optical flow sensors have been integrated to the mobile device. The smoothness of the surface is crucial for proper operation of an optical flow sensor as it may fail on an uneven surface. As unevenness of the surface will introduce measurement errors, the optical sensors are used with the existing odome-

try methods. To be able to systematically integrate these methods together for the best configuration estimation over time, Kalman filter based sensor fusion methods are employed.

The use of Extended Kalman filter [59] is a well-known, efficient method for the dead-reckoning of mobile robots, estimating the configuration of the robotic system.

2.2.1 Extended Kalman Filter

The Extended Kalman Filter is a recursive linear estimator which calculates an estimate for a discrete state on the basis of periodic observations. Equation (10) shows the generalized non-linear system dynamics in discrete-time.

$$\begin{aligned} x(k) &= x(k-1) + f[x(k-1, u(k-1), v(k-1), k] \\ z(k) &= h[x(k), u(k), w(k), k] \end{aligned} \tag{10}$$

where $x(k)$ is the state of interest, $u(k)$ is control input, S is the sampling time, $f[.,.,.]$ is the function of state velocity, $v(k)$ is the state noise, $z(k)$ is the observation, $h[.,.,.]$ is the function of observations and $w(k)$ is the measurement noise. The state and measurement noises $v(k)$ and $w(k)$ are assumed to be Gaussian with zero mean and their covariance matrices are proposed as Q_k and R_k respectively. The non-linear system in Equation (10) is linearized as in Equation (11).

$$A_k = \nabla f_x, \qquad B_k = \nabla f_u, \qquad H_k = \nabla h_x \tag{11}$$

Discrete Kinematics Model

Using the state-space equation of the holonomic mobile platform in continuous time space as in Equation (12)

$$\dot{x}(t) = A_k x(t) + B_k u(t) \tag{12}$$

where $u(t) = \dot{q}$, A_k is identity matrix, and the kinematic Jacobian matrix B_k has been evaluated in Equation (9) with respect to mobile platform itself. Equation (12) with respect to Newtonian can be expressed as:

$$B_k = \frac{R}{4} \begin{bmatrix} s\theta + c\theta & c\theta - s\theta & c\theta - s\theta & s\theta + c\theta \\ s\theta - c\theta & s\theta + c\theta & s\theta + c\theta & s\theta - c\theta \\ \frac{-1}{L+T} & \frac{1}{L+T} & \frac{-1}{L+T} & \frac{1}{L+T} \end{bmatrix} \tag{13}$$

Finally, the discrete-time model of the mobile platform can be obtained as in Equation (14).

$$\begin{bmatrix} x_k \\ y_k \\ \theta_k \end{bmatrix} = \begin{bmatrix} x_{k-1} \\ y_{k-1} \\ \theta_{k-1} \end{bmatrix} + B_k \begin{bmatrix} \delta\theta_{1k} \\ \delta\theta_{2k} \\ \delta\theta_{3k} \\ \delta\theta_{4k} \end{bmatrix} \tag{14}$$

A fixed coordinate frame and a mobile one M attached to the mobile platform have been defined in Figure (2.5). The origin of the mobile system has coordinates (xm, ym) in the fixed system. θ represents the rotation of the mobile platform with respect to the fixed coordinate. Two optical flow sensors have been inserted to the mobile platform located at the coordinates $(xo1, yo1)$ and $(xo2, yo2)$.

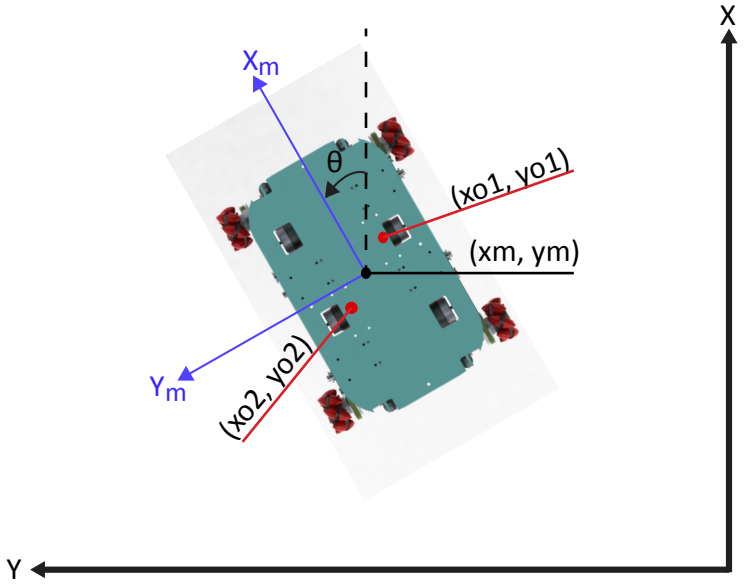

Figure 2.5: Mobile M and fixed coordinate frames

The relationship between the mobile and fixed coordinate frames is given in Equation (15)

$$\begin{aligned} x^F &= x_m cos(\theta) - y_m sin(\theta) \\ y^F &= x_m sin(\theta) + y_m cos(\theta) \end{aligned} \tag{15}$$

Similar equation can be written for both optical sensors as in Equation (16)

$$\begin{aligned} x^F i &= x_{oi} cos(\theta) - y_{oi} sin(\theta) \\ y^F i &= x_{oi} sin(\theta) + y_{oi} cos(\theta) \end{aligned} \tag{16}$$

where $i = 1, 2$

The measurement matrices are defined as $z1(k)$ and $z2(k)$, respectively. The observation models for those sensors are given in Equation (17).

$$
\begin{aligned}
H1 &= \begin{bmatrix} cos\theta & -sin\theta & -x_{o1}sin\theta - y_{o1}cos\theta \\ sin\theta & cos\theta & x_{o1}cos\theta - y_{o1}sin\theta \end{bmatrix} \\
H2 &= \begin{bmatrix} cos\theta & -sin\theta & -x_{o2}sin\theta - y_{o2}cos\theta \\ sin\theta & cos\theta & x_{o2}cos\theta - y_{o2}sin\theta \end{bmatrix}
\end{aligned} \tag{17}
$$

Extended Kalman Filter

The Kalman filter has two stages: prediction and update. In the prediction stage, a prediction $\widehat{x}(k|k-1)$ of the state at time k and state covariance $P(k|k-1)$ are computed according to Equation (18) using the previous estimations and the current control input.

$$
\begin{aligned}
\widehat{x}(k|k-1) &= f(\widehat{x}(k-1|k-1), u(k)) \\
P(k|k-1) &= A_k P(k-1|k-1) A_k^T + Q_{k-1}
\end{aligned} \tag{18}
$$

After the prediction stage, a Kalman gain matrix K is computed as in Equation (19).

$$
K_k = P(k|k-1) H_k^T [H_k P(k|k-1) H_k^T + R_k]^{-1} \tag{19}
$$

In the update stage, the observation matrix $z(k)$ is formed using the measurements to estimate the current state and state covariances $\widehat{x}(k|k)$ and $P(k|k)$ according to Equation (20).

$$
\begin{aligned}
\widehat{x}(k|k) &= \widehat{x}(k|k-1) + K_k[z(k) - H\widehat{x}(k|k-1)] \\
P(k|k) &= (I - K_k H_k) P(k|k-1)
\end{aligned} \tag{20}
$$

Typical Extended Kalman filter equations are designed for a single ob-

servation model. For multi-sensor systems, sensor fusion techniques becomes necessary. There are three methods for sensor-fusion employing Kalman filter [60]: the group-sensor method, the sequential-sensor method, and the inverse covariance form.

2.2.2 Sensor Fusion

Typical Kalman filter equations are derived for a single observation model. Under the effect of multiple sensors; there exists multiple methods to implement a Kalman filter. The first method is to apply multiple sensor measurements directly to the system. However, this approach is practically limited to relatively small number of sensors, due to the computational burden involved, since it requires the inverse of matrices with the size of number of included sensors. A second approach is to consider each sensor individually in separate Kalman filter estimate calculations. Due to the number of calculations for a single time step; it is can also be computationally expensive for large number of sensors. The last approach is to adjust the Kalman filter equations such that the invertible matrices should be diagonal to reduce the computational burden.

The Group-Sensor Method

The group-sensor method is the easiest way to apply a multi-sensor Kalman filter. The basic idea is to combine all sensor measurements and observation models into a single "observation matrix" and run a single Kalman filter for each time step. The combination of sensor measurements are represented in Equation (21).

$$
\begin{aligned}
z(k) &= [z1^T; z2^T] \\
H_k &= [H12^T; H34^T] \\
R(k) &= blockdiag[R1(k), R2(k)]
\end{aligned}
\tag{21}
$$

After modifying the measurement and observation matrices, single-sensor Kalman filter formulas can be applied easily.

The group sensor method is the simplest sensor fusion method. However, the dimension of the observation and the covariance matrix increases with the number of sensors. The complexity of the matrices increase the computational burden. Therefore, it is suitable only for small number of sensors.

The Sequential-Sensor Method

The second approach of multi-sensor Kalman filter is to deal with each sensor measurements sequentially. In other words; the update stage of the Kalman filter is computed for each sensor measurements independently. Therefore, update stage is repeated as the number of existing sensors. The prediction stage of the Kalman filter has been calculated using Equation (22).

$$
\begin{aligned}
\widehat{x}(k|k,0) &= \widehat{x}(k|k-1) \\
P(k|k,0) &= P(k|k-1)
\end{aligned}
\tag{22}
$$

The following step is to update the estimated states with the first sensor as Equation (23).

$$
\begin{aligned}
S_{k1} &= H_{k1} P(k|k,0) H_{k1}^T + R_{k1} \\
K_{k1} &= P(k|k,0) H_{k1}^T [S_{k1}]^{-1} \\
\widehat{x}(k|k,1) &= \widehat{x}(k|k,0) + K_{k1}[z_{k1} - H_{k1}\widehat{x}(k|k,0)] \\
P(k|k,1) &= P(k|k,0) - K_{k1} S_{k1} K_{k1}^T
\end{aligned}
\tag{23}
$$

The first update results are then used in the second update and the process continues until the last sensor update, p^{th} term as in Equation (24).

$$
\begin{aligned}
S_{kp} &= H_{kp} P(k|k,p-1) H_{kp}^T + R_{kp} \\
K_{kp} &= P(k|k,p-1) H_{kp}^T [S_{kp}]^{-1} \\
\widehat{x}(k|k,p) &= \widehat{x}(k|k,p-1) + K_{kp}[z_{kp} - H_{kp}\widehat{x}(k|k,p-1)] \\
P(k|k,p) &= P(k|k,p-1) - K_{kp} S_{kp} K_{kp}^T
\end{aligned}
\tag{24}
$$

The last term gives the final update state and updated covariance that can be used for the prediction stage of the next time step (k+1).

With the sequential-sensor method, the covariance matrix has a scalar value, which solves the first method's problem. However, the update stage is repeated for each observation model. Therefore, as the number of sensors increase, the repetition of the update stage also increases, adversely affecting the computational burden.

The Inverse-Covariance Form

The previous methods fail when the number of sensors becomes large. In particular, the group-sensor method fails since the invertible matrix is not diagonal and the computational burden gets more complicated as the increasing matrix dimension. If matrices involved can be made diagonal, the

computational burden does not increase much with the number of sensors. The Inverse-Covariance method reorganizes the Kalman Filter equations to make the covariance matrix diagonal.

The weights associated with the prediction and observation are rewritten as in Equations (25) and (26).

$$(I - K_k H_k) = P(k|k)P(k|k-1)^{-1} \tag{25}$$

$$K_k = P(k|k)H_k^T R_k^{-1} \tag{26}$$

After these simplifications, the revised prediction formulas can be transformed into Equation (27).

$$\begin{aligned} W_x &= \sum (H_k i^T R_k i^{-1} z_i(k)) \\ \widehat{x}(k|k) &= P(k|k)[P(k|k-1)^{-1}\widehat{x}(k|k) + W_x] \\ W_P &= \sum (H_k i^T R_k i^{-1} H_k i) \\ P(k|k) &= [P(k|k-1)^{-1} + W_P]^{-1} \end{aligned} \tag{27}$$

In these equations; since R is a diagonal matrix; $P(k|k)$ and $\widehat{x}(k|k)$ are diagonal either. Unlike the group-sensor method, the addition of new sensors will require new W_x and W_P values so the complexity of the process grows only linearly. And unlike the sequential-sensor method, the update stage takes place only once at each time step.

2.2.3 Results

Sensor fusion techniques explained in Subsection 2.2.1 have been tested through experiments on AssistOn-Mobile combining data from motor encoders and

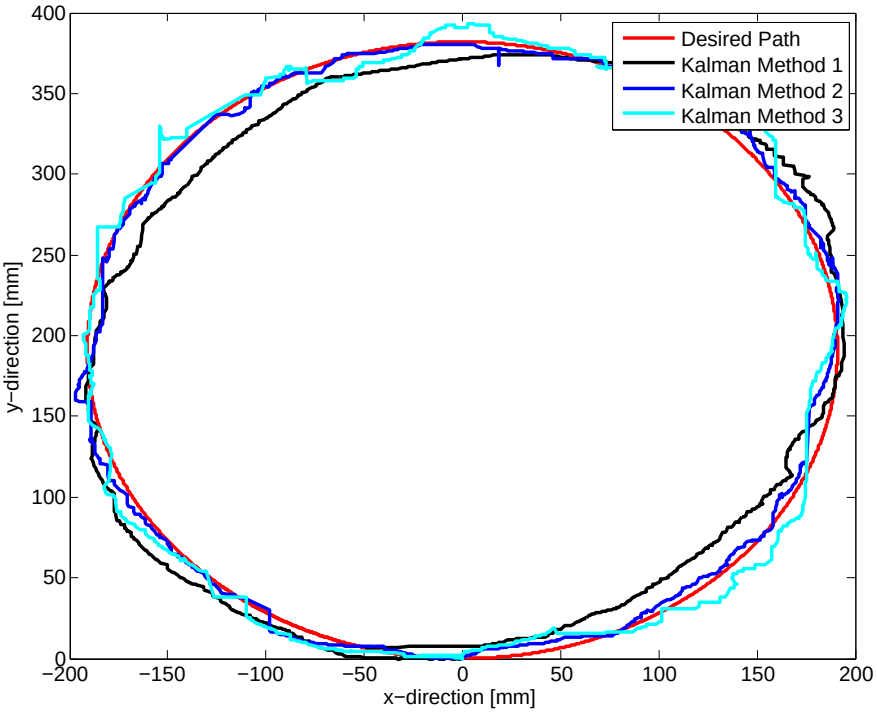

Figure 2.6: Comparison of Kalman filter based sensor fusion methods

Table 2.1: RMS error values for Kalman filter based sensor fusion methods during a circle tracking task

	x	**y**	**radial**
Method 1	2.10 %	2.70 %	3.45 %
Method 2	1.67 %	2.50 %	3.05 %
Method 3	1.80 %	2.90 %	3.47 %

optical flow sensors. A comparison of the performance of these methods are shown in Figure 2.6. The RMS error values of each method along x and y directions during a circle tracking task are given in Table 2.1. The resulting RMS values are well enough for a circle tracking task for 400 mm diameter during the rehabilitation exercises. Moreover, since only 2 optical flow sensor measurement are integrated to the odometry of AssistOn-Mobile the RMS values are close enough to each other.

2.3 Series Elastic Actuation

Rehabilitation therapies are more effective if they control the interaction forces between the patient and the device. Those devices should have low output impedance to be easily manipulated. Moreover, the backdriveability allows patients to move the device freely under the effect of applied forces. Even though the actuators of the proposed holonomic mobile platform are passively backdriveable, the use of Mecanum wheels prevents passive backdriveability of the mobile platform. To achieve backdriveability under control, the holonomic mobile platform is transformed into a Series Elastic Actuator (SEA) by introducing a compliant element between the patients and the mobile platform.

Rehabilitation devices under force control mostly use stiff force sensors to

measure the interaction forces between the device itself and the patient. However, the use of sensors with high stiffness has several drawbacks. First of all, placing a force sensor at the end effector of the device creates non-collocation in the system as shown in Figure 2.7. This non-collocation introduces poles and zeros to the overall system as depicted in Figure 2.8 and causes the system to be stable for bounded closed loop gains. In other words; using a force sensor places an upper limit on the loop gain of the closed-loop system [56]. The presence of force sensor with high stiffness causes the controller gains to be chosen lower, limiting the performance and robustness of the controller to ensure stability. Another disadvantage is the inherent noise involved force sensors. Moreover, the commercial force sensors increase the overall cost of the system due to their very high-cost.

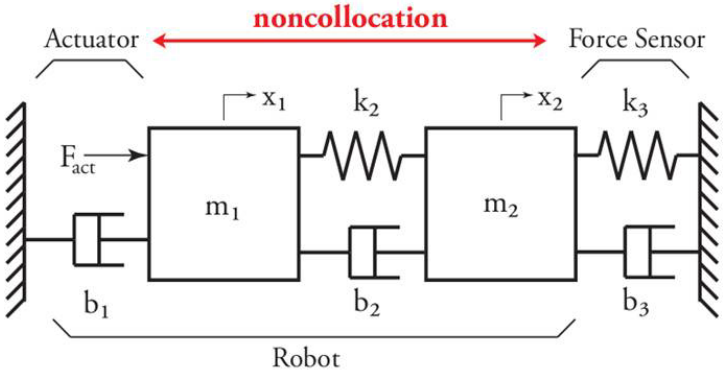

Figure 2.7: The non-collocation in the system

The main idea of SEA is to intentionally introduce a compliant coupling element between the actuator and the environment, measuring and controlling the deflections on it. In particular, the applied forces are estimated by measuring the deflections. Although force sensors work with the same principle as well, SEA has orders of magnitudes lower stiffness than a typi-

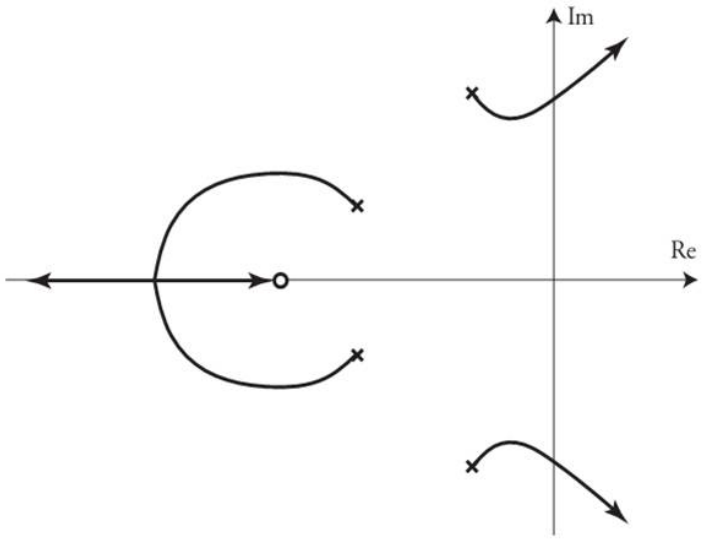

Figure 2.8: Root locus of a system with non-collocation

cal commercial force sensor [61]. For instance, the commercial ATI Nano17 transducer has a stiffness on the order of 10^7 N/m where the proposed compliant term in this thesis has a stiffness on the order of 10^3 N/m.

SEA has many advantages for force control. First of all; the force control problem is simplified into a position control problem. Due to the compliant element, the output impedance is decreased resulting in improved safety, especially under impacts. Moreover, the controller gains can be selected orders of magnitudes higher, since the stiffness of the force sensor is decreased. Increasing the controller gains improve the robustness and the performance of the closed-loop system. Therefore; the actuation and the transmission units can be selected simpler and lower cost.

One disadvantage of SEA is that the soft coupling of the compliant element limits the bandwidth of the system; however, in rehabilitation the desired tasks are slow so that they can be executed by the patients and high

bandwidth is often not necessary.

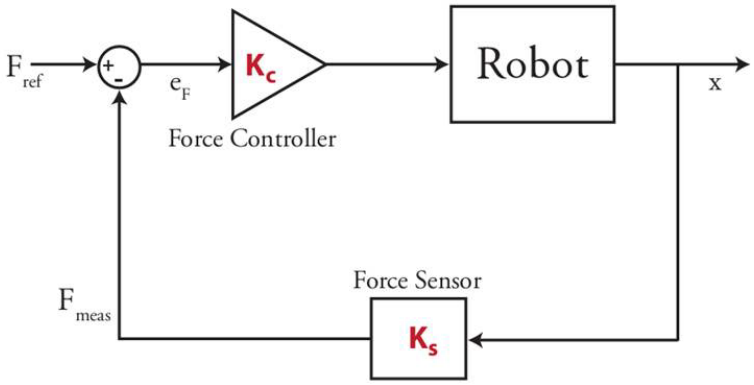

Figure 2.9: Force control with SEA

2.3.1 Design of the Compliant Element

The most important part of SEA is the design of the compliant term. A 3-DoF compliant element is required to turn 3-DoF holonomic mobile platform into AssistOn-Mobile, a 3-DoF mobile series elastic actuator. With this motivation, a compliant, 3-PaRR planar parallel mechanism is chosen as the underlying kinematics of the compliant element. This mechanism is chosen since it allows for the measurement of the in-plane forces and torques acting on the robot by simply measuring the deflections of grounded prismatic joints on this element using linear encoders.

A compliant mechanism is chosen for the design due to its advantages such as:

- the flexible property,
- the ease of manufacturing with low-cost thanks to its monolithic structure and

- friction/lubrication free nature,

Despite of the advantages, compliant mechanisms also have some disadvantages such as:

- the difficulty of design and analysis,
- the weak tolerance to large loads due to possible buckling, and
- the possibility of fatigue and plastic deformation.

3-DoF movement is achieved using a parallel planar mechanism for the design of the compliant element. A parallel planar mechanism is a closed kinematic chain in which the moving platform is connected to the ground by at least two kinematic chains. Parallel mechanisms have many advantages [62] such as:

- better robustness to manufacturing errors,
- more precise motion at the task space,
- compact design with higher stiffness, and
- grounded sensors/actuators.

In particular, a compliant parallel 3-PaRR mechanism is chosen as the underlying kinematic structure of the compliant element. In this mechanism, the compliant revolute joints are implemented using V-shaped flexure hinges while prismatic joints are implemented using 4 hinges in a shape of a parallelogram. The position of the output links of the compliant parallelogram mechanism are measured with respect to the base link. The choice of 3-PaRR allows linear deflection measurements at prismatic (Pa) joints.

V-shaped Filleted Flexure Hinges

Compliant mechanisms can be designed using flexure hinges that deform through a short segment and behave like a revolute joint. Flexure hinges are advantageous since they can achieve small motions with good repeatability and can overcome shortcomings such as friction and backlash. They are made of rectangular blank, removing two symmetric cut-outs with different shapes to have low rotational stiffness about one axis and higher stiffness in other axes.

V-shaped flexure hinges depicted in Figure 2.10 provide better rotational precision than other hinges [63]. The largest elastic deformation of the V-shaped flexure hinge occurs at the point of minimum thickness. To lower stress concentration on this point, corners of the cut-outs are filleted by a fixed angle.

In Figure 2.10; b, h, t, and l denote the width, height, minimum thickness and half length of the flexure hinges, respectively. The symbol c is the height of the profile that is equal to $(h-t)/2$, while R shows the radius of circular section, and θ denotes the separation angle of the profile from horizontal axis [64]. Analytical solution for the deflection of V-shaped hinges is given in Equation (28).

$$\frac{\alpha_z}{M_z} = \frac{3}{2EbR^2}\left\{\frac{1}{2\beta+\beta^2}\left\{\frac{(1+\beta)\sin\theta}{(1+\beta-\cos\theta)^2}+\frac{(3+2\beta+\beta^2)\sin\theta}{(2\beta+\beta^2)(1+\beta-\cos\theta)}\right.\right.$$
$$\left.\left.+\frac{6(1+\beta)}{(2\beta+\beta^2)^{3/2}}\arctan\left(\sqrt{\frac{2+\beta}{\beta}}\tan\frac{\theta}{2}-\frac{\gamma^2\cot\theta}{\beta^2(1+\gamma)^2}\right)\right\}\right.$$
$$\left.+\frac{\cot\theta}{(1+\beta-\cos\theta)^2}\right\} \tag{28}$$

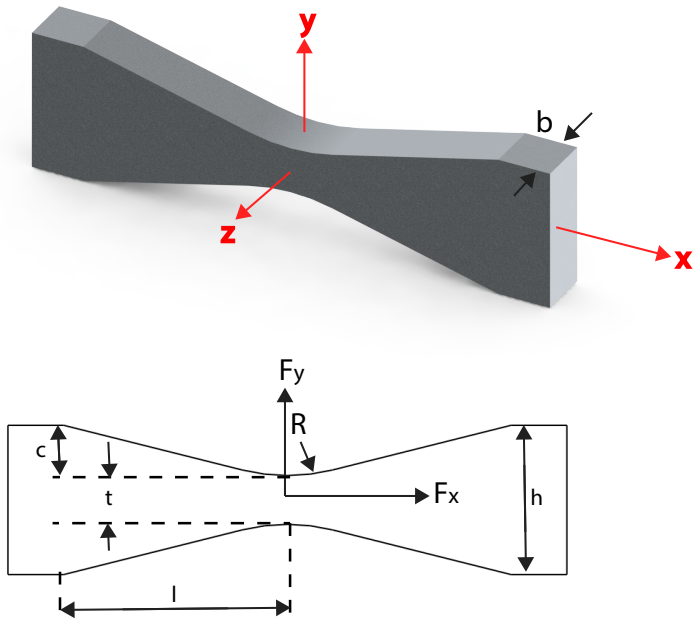

Figure 2.10: Geometric parameters of and forces acting on a filleted V-shaped flexure hinge

where $\beta = t/2R$ and $\gamma = t/2c$. Here, α_z represents the angular displacement and M_z denotes the bending moment about z axis. The maximum deflection is calculated by matching the maximum bending moment with the yield stress of the selected material [63] using Equation (29).

$$K_{joint} = \left(\frac{M_z}{\alpha_z}\right) \tag{29}$$

where E is the Young's modulus of the selected material. In the design of the compliant element which is used for AssistOn-Mobile, each filleted V-shaped flexure hinge is designed to have 1.3° maximum angular deflection and 6.3 Nm/rad joint stiffness.

2.3.2 Kinematics

Using V-shaped flexure hinges, a 3-PaRR mechanism is designed which connects the moving platform to ground with 3 legs as in Figure 2.11. Applied forces and torques acting on the end-effector of the moving platform are estimated by measuring the deflections on the grounded joints of 3-PaRR. Independent joint displacements of the compliant mechanism can be measured using linear encoders and given the joint stiffness, end-effector forces/torques can be estimated.

Although the kinematic analysis of the compliant mechanisms is challenging, the use of flexure hinges allows for the approximation using Pseudo Rigid Body Method (PRBM) [65]. PRBM approximates the motion of a compliant mechanism by replacing the flexible links with rigid links and introducing torsional springs at both ends of rigid ones. The PRBM for the designed 3-PaRR is drawn in Figure 2.11.

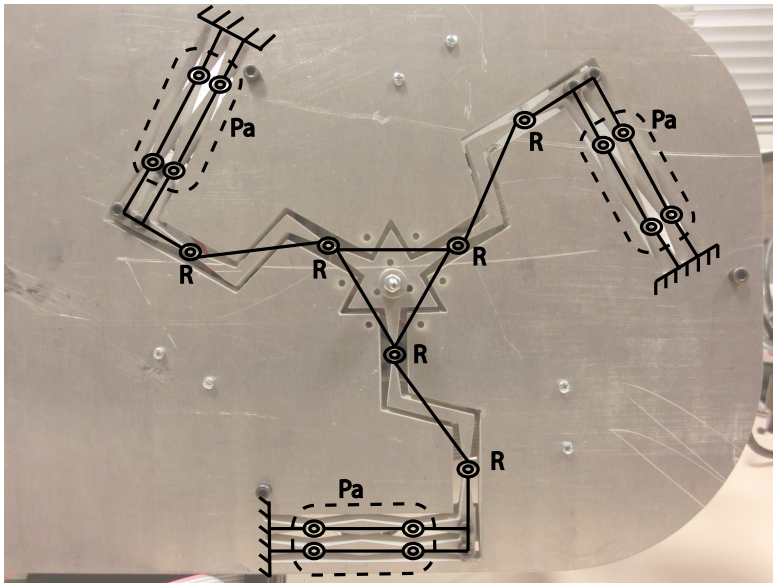

Figure 2.11: Pseudo-rigid body model of 3-PaRR mechanism

A schematic representation of the pseudo-rigid body model of a single leg of 3-PaRR is depicted in Figure 2.12. N and E represent the base reference frame and end-effector frame, respectively. Points H and O mark the end-effector where the handle is placed and the center of the workspace. Bodies A_i, B_i and C_i, (for $i = 1, 2, 3$), denote the three bodies on each leg that connects the end-effector E to the ground N, while K_i, L_i and P_i mark the centers of revolute joints. To study the kinematics of 3-PaRR, three vector loop equations can be written in plane as in Equation (30).

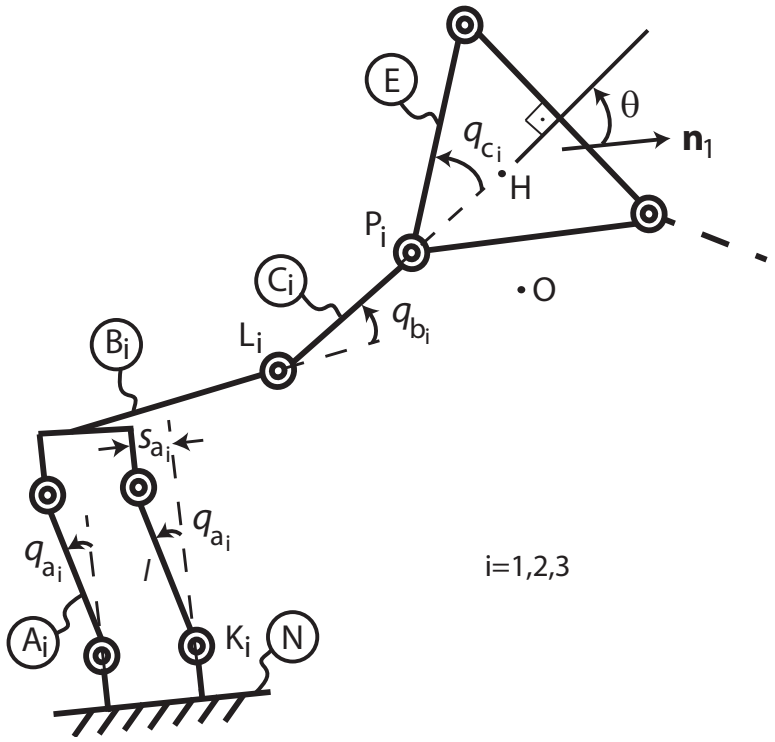

Figure 2.12: Kinematic model on a single leg of 3-PaRR mechanism

$$\vec{r}^{OK_i} + \vec{r}^{K_iL_i} + \vec{r}^{L_iP_i} + \vec{r}^{P_iH} - \vec{r}^{OH} = \vec{0} \tag{30}$$

where $\vec{r}$ represents the position vector from the left superscript to the right

superscript and $i = 1, 2, 3$ is the loop index. It is possible to derive six independent scalar equations from these three planar vector loop equations, while three more independent scalar equations can be derived from the relationship between joint rotations and the end-effector rotations. These equations can be solved analytically to determine all nine joint angles q_{a_i}, q_{b_i} and q_{c_i}, which are required to calculate the task space deflection and stiffness of the device. However, since the defections of the compliant mechanism is relatively small, differential kinematics of the device dominate its movements. In particular, determining the initial configuration of the device together with its Jacobian matrix is sufficient to resolve its kinematics. The Jacobian of the model can be calculated by differentiating the vector loop equations in Equation (30) in N and solving together with the angular velocity equation as Equation (31).

$$\triangle \theta = \triangle q_{b_i} + \triangle q_{c_i} \tag{31}$$

where $\triangle$ signifies small quantities. The resulting Jacobian can be partitioned into kinematic Jacobian J_T , which gives the relation between the joint space and task space velocities, and the constraint Jacobian J_C, which imposes the motion constraints to the system. The kinematic and constraint Jacobian matrices can further be grouped by the type of the joint: measured or passive. This form of the Jacobian matrix provides more insight about the system, since the sub-blocks of the matrix clearly reflects the contributions of the measured and passive joints. Equation (32) is the Jacobian matrix.

$$\begin{bmatrix} \triangle x_T \\ 0 \end{bmatrix} = \begin{bmatrix} J_{T_m} & J_{T_p} \\ J_{C_m} & J_{C_p} \end{bmatrix} \begin{bmatrix} \triangle q_m \\ \triangle q_p \end{bmatrix} \tag{32}$$

where J_{T_m} is the Jacobian matrix for unconstrained measured joints, J_{T_p} is the Jacobian matrix of unconstrained passive joints, J_{C_m} is the Jacobian matrix for constrained measured joints and J_{C_p} is the Jacobian matrix for constrained passive joints, while $\triangle q_{mc}$ and $\triangle q_{pa}$ represent small displacement of measured and passive joints, and $\triangle x_T$ denotes the small configuration changes of the end-effector. In 3-PaRR case, the position of the output links of three grounded parallelogram mechanisms (that effectively act as prismatic joints) are measured, while all the remaining revolute joints are passive. The joint angles of compliant parallelogram linkages are calculated from Equation (33).

$$q_{m_i} = \sin^{-1}(s_{m_i}/l) \tag{33}$$

where s_{m_i} is the measured linear displacement, and l is the length of body A_i.

Using the Jacobian matrices, the relationship between measured joint displacement and the task space displacement of the end-effector can be derived as Equation (34) [66].

$$\begin{aligned} \triangle x_T &= (J_{T_m} - J_{T_p} J_{C_p}^{-1} J_{C_m}) \triangle q_m \\ &= J_{T_{comp}} \triangle q_m \end{aligned} \tag{34}$$

where $J_{T_{comp}}$ denotes the Jacobian matrix of the overall compliant mechanism. Once the Jacobian matrix of the compliant 3-PaRR mechanism is obtained, the task space stiffness matrix K_T of the mechanism can be derived as Equation (35).

$$K_T = J_{T_{comp}}^{-T} (K_{q_m} + J_{C_m}^T J_{C_p}^{-T} K_{q_p} J_{C_p}^{-1} J_{C_m}) J_{T_{comp}}^{-1} \tag{35}$$

where K_{q_m} and K_{q_p} are the individual stiffness values of measured and passive joints.

2.3.3 Implementation of the Compliant Element

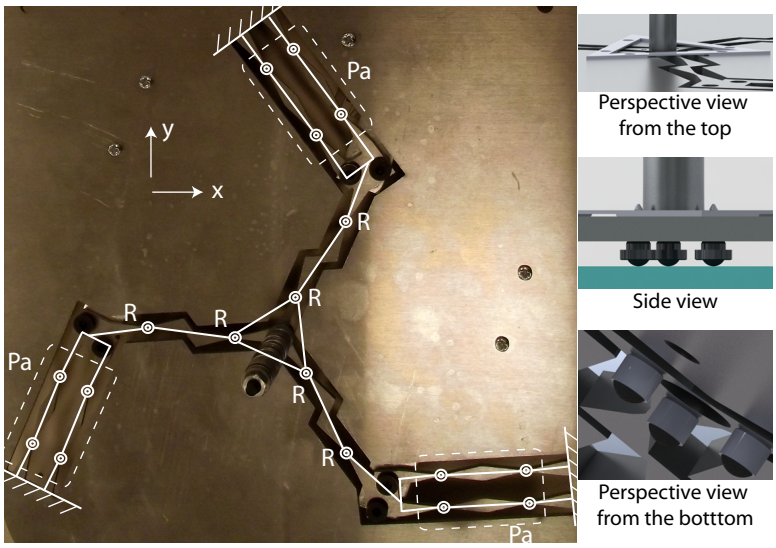

Figure 2.13: Left: Monolithic implementation of compliant 3-PaRR mechanism; Right: Constraints against out-of-plane movements

The monolithic physical implementation of 3-PaRR mechanism based compliant element is shown on the left side of Figure 2.13. The prismatic joints of the compliant mechanism are instrumented with linear incremental optical encoders with 2000 counts per inches resolution under quadrature decoding. For this 3-PaRR compliant mechanism with V-shaped flexure hinges, $K_{q_m} = K_{q_p} = K_{joint}$ are calculated as 0.014 Nm/rad following Equation (29). These values are obtained choosing the parameters in Table 2.2 in order to obtain the highest deflections in the end-effector of the compliant mechanism with approximately 3 Factor of Safety fitting the shape of AssistOn-Mobile.

Table 2.2: Parameters used for implementation of the compliant element

Flexure Hinge Parameters	**Value**
h	5.34 mm
θ	8^o
t	0.99 mm
R	15 mm
b	6 mm
l	16.5 mm

The diagonal terms of task space stiffness reads as $K_{T_x} = K_{T_y} = 14$ N/mm along x and y directions and $K_{T_\theta} = 4.4$ Nm/rad about the rotation axis, while the off diagonal terms are negligibly small.

The out-of-plane movements of the compliant mechanism are restricted as depicted on the right side of Figure 2.13.

Under the assumption of the compliant element will be applied maximum 50 N force, the structural analysis has been made as shown in Figure 2.14. The maximum stress of the mechanism under 50 N load at the end-effector results in a safety factor of 2.99, ensuring its safety. The deflections at the end-effector are physically limited to 10 mm to prevent the plastic deformations of the compliant mechanism.

2.3.4 Verification of Force Sensing using the Compliant Element

To verify the force estimation with the 3-PaRR compliant element, a ATI Nano17 force sensor is attached to the end-effector of the compliant mechanism as in Figure 2.15. Figure 2.16 shows that the compliant mechanism is able to follow the force measurements of the commercial force sensor.

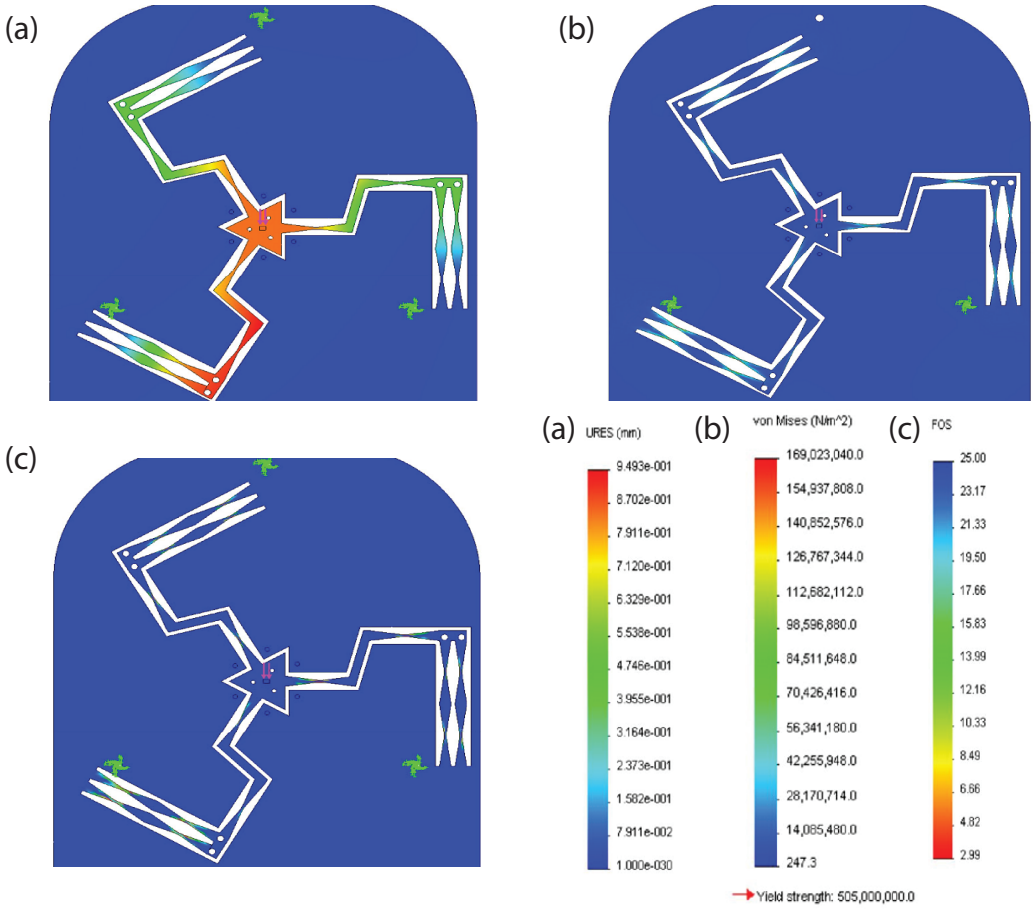

Figure 2.14: Static analysis of the compliant element

% RMS error values along x, y and θ directions are calculated as 5.7%, 7.3% and 8.5%. In particular, the estimated forces using compliant mechanism are efficient enough to be used for rehabilitation therapies.

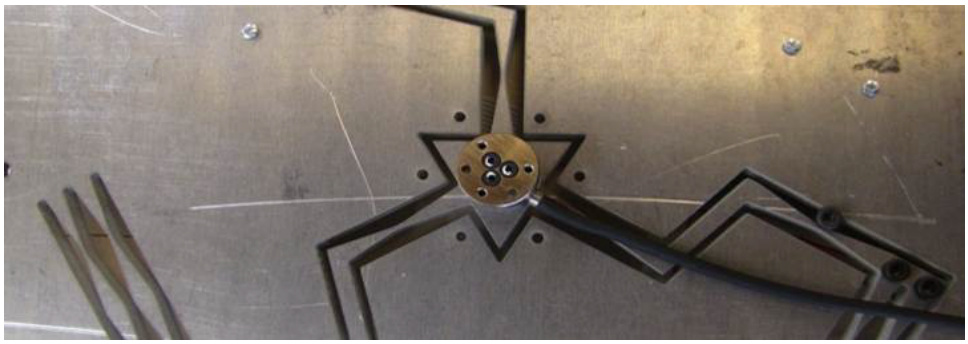

Figure 2.15: ATI Nano17 force sensor attached to 3-PaRR compliant mechanism

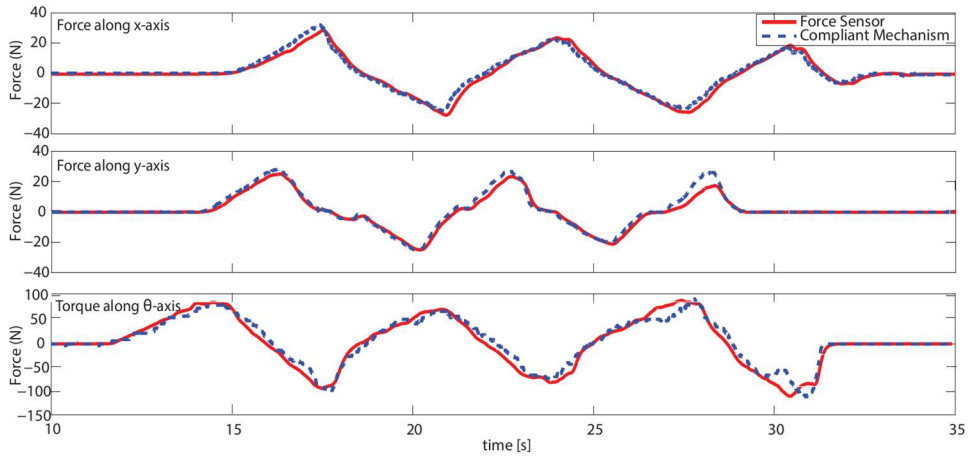

Figure 2.16: 3-PaRR verification in x, y, θ directions

2.4 Integration of Kinect Sensor for Limiting Compensatory Movements of Patients

During therapies; patients with arm disabilities may tend to complete the desired exercise by moving their torso instead of their arms, and such compensatory movements decreases the efficiency of training. To control such movements during therapies, as an online feedback to the patient, the task speed of AssistOn-Mobile is adjusted with respect to compensatory shoul-

der movements of the patients. In particular, shoulder movements are measured with a Kinect (RGBD) sensor and the patients are warned though both haptic and audio channels to correct their sittings during the task.

Microsoft Kinect is low-cost camera which uses infra-red (IR) illumination to obtain depth data, color images and sound as presented in Figure 2.17. IR is used as a distance ranging device and enables the sensor to measure distances at 2 m with a 10 mm accuracy and has a resolution of 3 mm at 2 m.

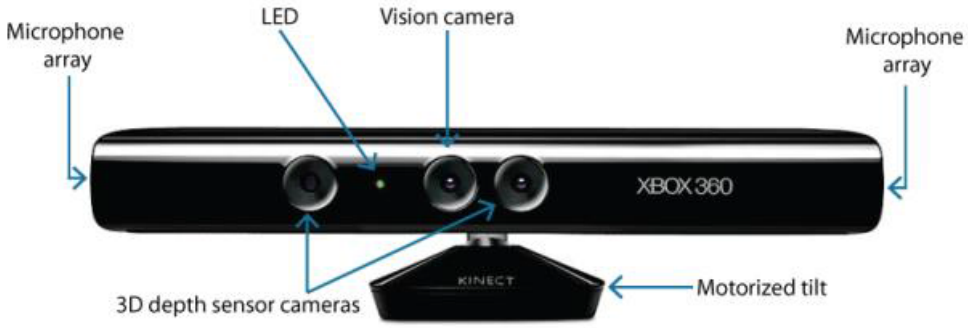

Figure 2.17: Kinect hardware

From the depth data, software provided with Kinect detects human joints which have been represented on the famous drawing by Leonardo da Vinci, the Vitruvian man as in Figure 2.18 and tracks the skeleton instantaneously. Although the skeleton tracking performance of Kinect has been observed lower than an alternative full-body motion capture system in [67], it is suitable to control for instance game protocols for rehabilitation. Kinect has been used for the home-based rehabilitation therapies in [68–70].

Skeleton tracking with Kinect can be achieved using various open source tools. MATLAB provides skeleton tracking using Microsoft SDK for Win-

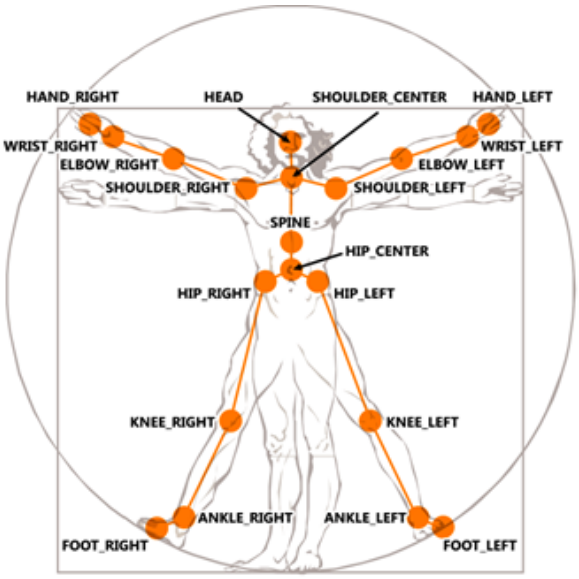

Figure 2.18: Skeleton joints detected by Kinect

dows and does not require a calibration phase before each trial [71]. Figure 2.19 shows an image of a skeleton taken from Kinect, where head, torso, right and left arms and legs are represented with the same color.

The basic idea behind skeleton tracking is to detect human joints in x, y and z coordinates and to measure the movement as in Figure 2.20.

Figure 2.21 represents the set-up for the Kinect integration to the AssistOn-Mobile system to limit compensatory movements of the patients. For a feasibility experiment, Kinect has been placed in front of the subject and the right shoulder displacement of a healthy subject has been measured. These measurements are used to adjust the task-speed of AssistOn-Mobile as shown Table 2.3, while simultaneously providing a warning tone for auditory feedback. In particular; AssistOn-Mobile moves with a maximum speed until the shoulder deflections exceed 50 mm threshold. Between 50 mm and 90 mm thresholds; the task speed of AssistOn-Mobile starts to get de-

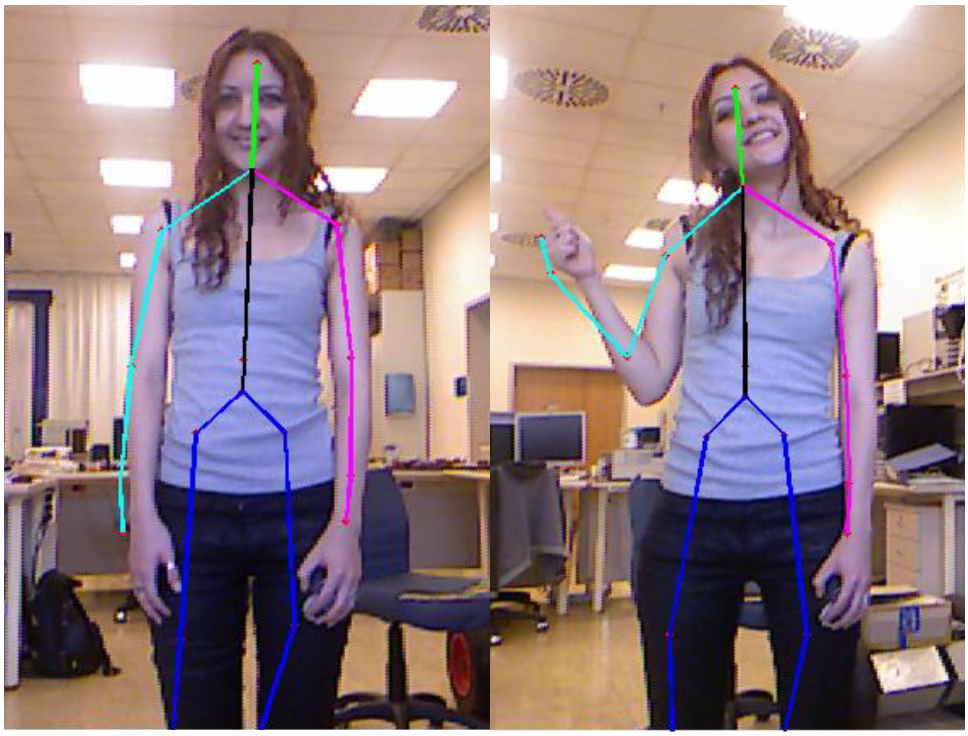

(a) (b)

Figure 2.19: Skeleton tracking by Kinect

creased with a linear function until it stops. The task speed returns back to its original value whenever the subject returns to the defined shoulder deflection range. At each speed change; subjects are also informed by proving them a different tone.

Figure 2.22 shows the results of a sample experimental where the shoulder movement of the subject modifies the task speed of AssistOn-Mobile to limit the compensatory movements. In particular, the task speed of AssistOn-Mobile changes whenever the defined shoulder limits in Table 2.3 are exceeded by the users during the exercise. Moreover, informing subjects with haptic and audio cue, the subjects are forced to correct their

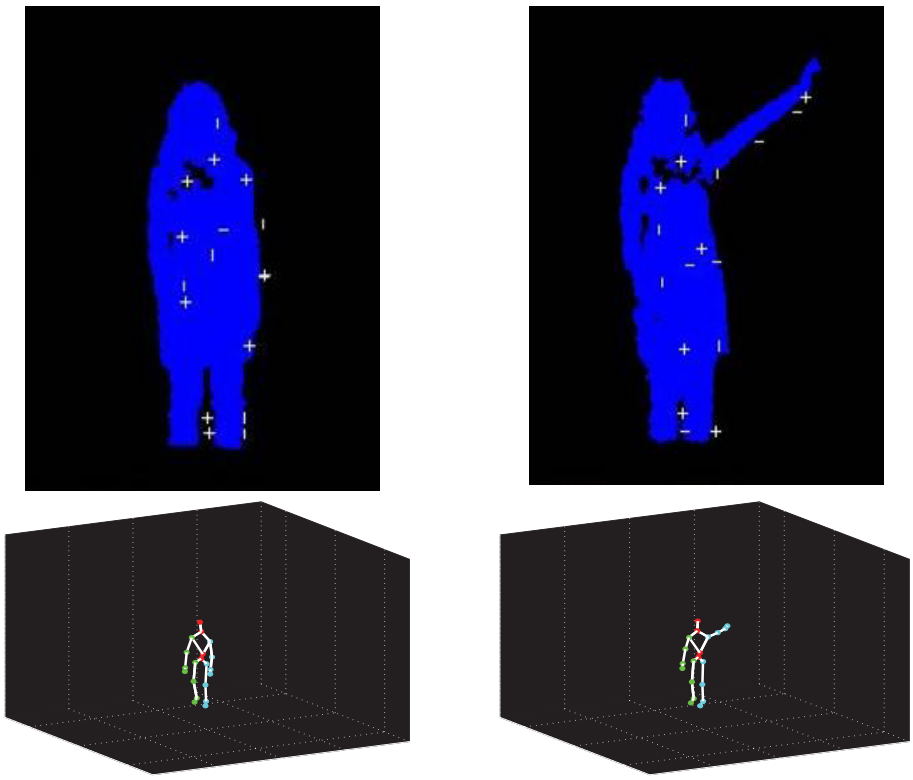

Figure 2.20: Skeleton tracking by Kinect

pose during the movement in an online manner. To reduce the noisy estimations of Kinect during the experiments; the measurements have been passed through a low pass filter.

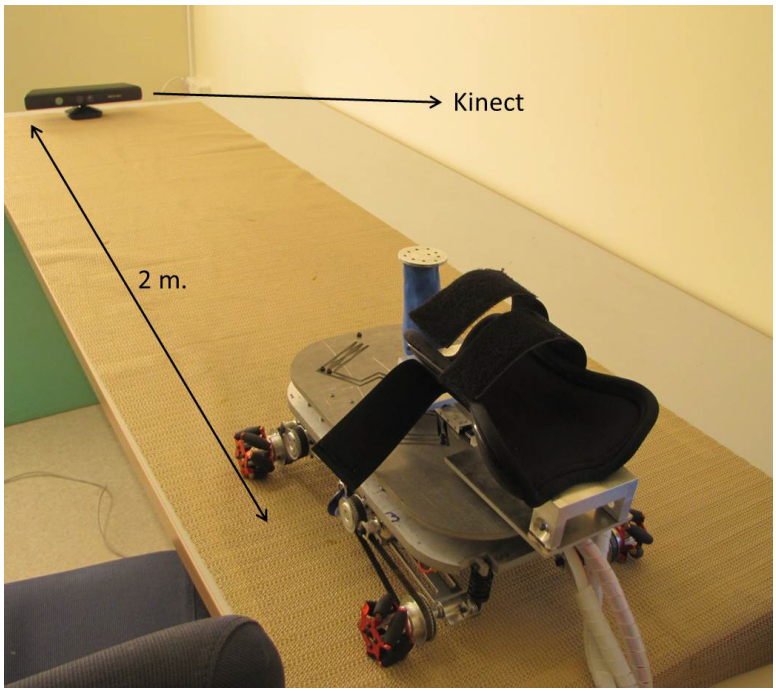

Figure 2.21: Set-up with Kinect

Table 2.3: Experiment Conditions

Shoulder Movements	**Task Speed Scaling**
0 - 50 mm	1
50 - 90 mm	linear function between 0 - 1
$>$ 90 mm	0

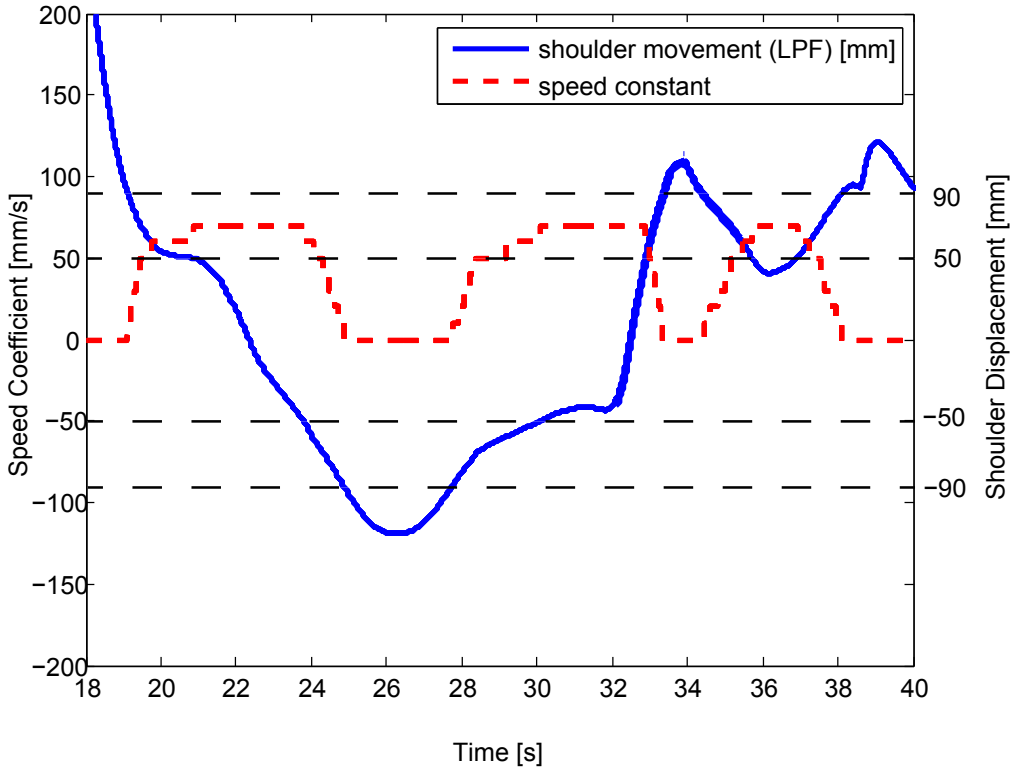

Figure 2.22: Shoulder movements and the adjusted task speed of AssistOn-Mobile

Chapter III

3 Control of AssistOn-Mobile

For effective rehabilitation therapies, patients are required to be actively involved in the exercise. This chapter presents different "assist-as-needed" controllers implemented on AssistOn-Mobile. In particular, admittance control is implemented such that the device becomes actively backdriveable. The integration of the virtual fixtures introduces virtual constraints to limit errors and improve safety during competition of a task. However, mere backdriveability provides no assistance to patients when they are within the virtual fixtures.

In rehabilitation; the timing along the path is not important. Allowing patients to complete the task with their own effort at their own pace with minimum path error is more critical. Therefore, Passive Velocity Field Control (PVFC) is implemented on AssistOn-Mobile for contour tracking tasks. This method not only provides natural assistance to the patients but also ensures safety by guaranteeing passivity of the coupled system with respect to external applied forces.

3.1 Admittance Control

Active backdriveability of AssistOn-Mobile is ensured using admittance control under the action of forces applied by the patient at the end-effector

of the compliant mechanism. Figure 3.1 presents the block diagram of the admittance controller of AssistOn-Mobile. In this cascaded structure, the external forces acting at the handle are estimated through the deflections of the compliant element and its kinematic model. The outer admittance controller transforms the applied forces to the desired task space velocities of the mobile platform. Finally, the inner velocity controller ensures that AssistOn-Mobile tracks the desired velocities by minimizing the velocity errors.

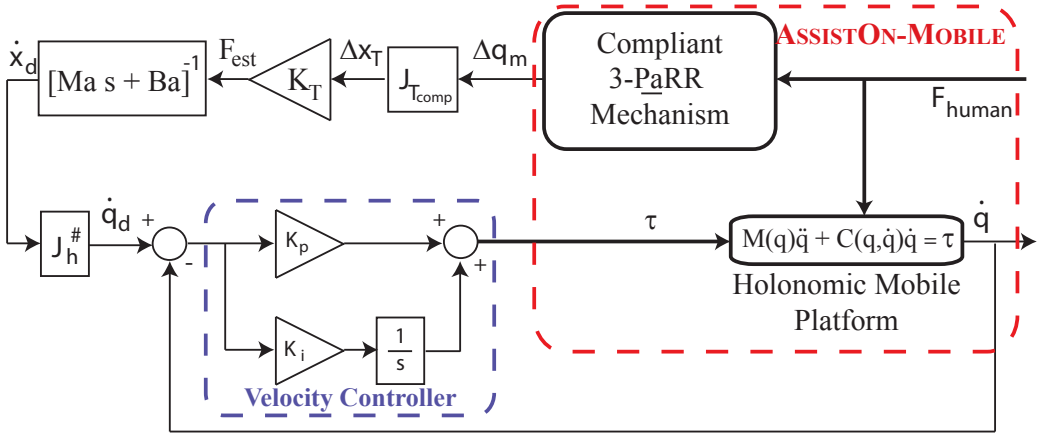

Figure 3.1: Cascaded admittance controller of AssistOn-Mobile

In particular, M denotes robot inertia matrix, while C is the Coriolis matrix of the holonomic mobile platform. $J_h^\sharp$ represents the pseudo-inverse Jacobian of the holonomic mobile platform and F_{human} is the physical interaction forces acting on the robot by the patients. $q, \dot{q}, \ddot{q}$ represent the actual position, velocity and acceleration of the DC motors, $\dot{q}_d$ is the desired velocity of motors and $\dot{x}_d$ denotes the desired task space velocity of the mobile platform. Δq_m is the joint deflections and Δx_T is the deflection on the end-effector of the compliant element. J_{Tcomp} is the Jacobian matrix and K_T is

the stiffness of the compliant term. Symbols K_p and K_i denote the PI gains of the inner-loop velocity controller of the closed-loop system, whereas M_a and B_a represent the parameters of the desired admittance.

Active backdriveability allows patients to move the robotic device freely by applying physical forces. To limit the possible errors over the desired task to ensure safety, a virtual tunnel is implemented along the desired path. The active backdriveability of AssistOn-Mobile has been demonstrated with an experiment where a healthy subject is asked to move the robotic device forward as in Figure 3.2. As addition, virtual walls have been implemented between $\mp$50mm along y direction to limit the robot movements in the task space. In particular, even tough the robot can move freely inside the tunnel, the virtual walls prevent the further movement. It can be observed on Figure 3.2 that AssistOn-Mobile can move along the direction of applied forces by the user inside the implemented virtual tunnel. However, whenever AssistOn-Mobile reaches the boundaries of the virtual walls the controller imposes virtual constrains to the mechanical system such that it cannot exceed the boundaries except penetrations on the wall, which is acceptable in terms of rehabilitation.

3.2 Passive Velocity Field Control

Trajectory-based controllers that provide assistance to patients as they need require patients to complete a task in a pre-determined amount of time. Due to this coupling between the task itself and the timing of the task, trajectory tracking error does not always reflect how well the contour has been followed [72]. Such controllers try to catch up the time, as well as the path itself and may sacrifice the path tracking to improve errors in timing.

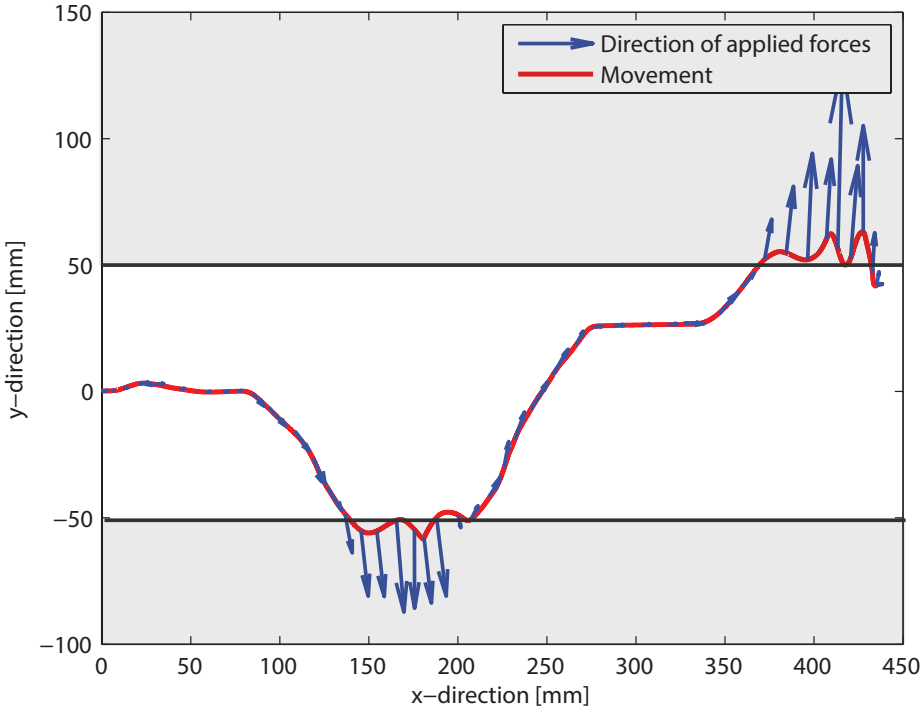

Figure 3.2: Admittance control with virtual wall

This may be detrimental for therapies as large deviation from the path can potentially harm the patients. For applications such as rehabilitation where the timing along the path is not crucial, minimizing the contour error is more critical.

Passive Velocity Field Control (PVFC) is a contour (path) following control technique, where the coordination and synchronization between various degrees of freedom is ensured, while exact timing along the path is left to the patient/therapist. PVFC concept has first been proposed in [73] as an exercise protocol and detailed in [72, 74]. Moreover, it has been implemented for various applications in [75–78].

PVFC has many advantages in rehabilitation, since the decoupling be-

tween the time and the task allows patients to complete the desired tasks at their preferred pace, while the assistance is provided to complete the task with minimum contour error. In particular, PVFC defines a time invariant velocity field V for a given path, and the speed of the task depends on the instantaneous energy of the closed-loop system. PVFC mimics the dynamics of a flywheel; it cannot generate energy, but store and release the energy supplied to it. As a result, PVFC renders the closed-loop system passive with respect to external forces.

PVFC uses velocity fields to define a desired velocity at each configuration of the mechanical system, so that the system will be guided towards the desired contour. The velocity field is the combination of the tangent vector ($V^{||}$) and the normal vector ($V^{\perp}$) to the desired path as in Equation (36).

$$\begin{aligned} V^{||} &= v f_s(s^*) \\ V^{\perp} &= x(r^{EE} - f(s^*)) \end{aligned} \tag{36}$$

where v and x are coefficients of vector fields, r^{EE} is the position of the AssistOn-Mobile. $f(s^*)$ represents the closest point on the path, while $f_s(s^*)$ is the unit tangent vector at this point. The velocity field is formed by the combination of these two vectors as in Equation **??**eq:velocityfield)

$$V = -\frac{2}{1+e^{-vE}} V^{\perp} + \left(\frac{2}{1+e^{-vE}} - 1 \right) V^{||} \tag{37}$$

where E is the instantaneous contour error, the difference between the mechanical position of the robotic device, r^{EE} and the closest point on the curve, $f_s(s^*)$.

The dynamics of a mechanical manipulator in joint space is given respectively as in Equation (38)

$$M(q)\ddot{q} + C(q,\dot{q})\dot{q} = \tau + \tau_e \tag{38}$$

where $M(q)$, $C(q,\dot{q})$, τ and τ_e are inertia matrix, Coriolis matrix, control torques, and external torques, respectively and the local coordinates are represented by $q = [q_1, .., q_n]^T$. PVFC ensures the passivity of the system with respect to external forces, as shown in Equation (39)

$$\int_0^t \tau_e^T \dot{q} d\tau \geq -c^2 \tag{39}$$

where c is a real number. PVFC decouples the desired task from the the speed of the task. For a desired velocity field V, velocity field error can be defined as Equation (40)

$$e_\rho = \dot{q}(t) - \rho V(q(t)) \tag{40}$$

where $\dot{q}(t)$ is the actual velocity of the system, and $\rho > 0$ is a constant. The objective of the velocity field controller is to make e_ρ go to 0 by modulating ρ which is proportional to the traversal speed of the system. Since the mechanical system is not required to be located in a specific position at a particular time, an appropriately desired velocity field directs the system from its current configuration, to approach the contour.

3.2.1 Augmented Mechanical System

In order to satisfy Equations (39) (40), flywheel dynamics are augmented with the mechanical system. The augmented system consists of the robotic system and a fictitious flywheel with dynamical model in Equation (41)

$$M_F \ddot{q}_(n+1) = \tau^{n+1} \tag{41}$$

M_F is the mass of the flywheel and τ^{n+1} represents the coupling control input to the flywheel. The local coordinates of the augmented system with the fictitious flywheel become $q = [q_1, .., q_n, q_{n+1}]^T$. Moreover, the dynamics of the augmented system can be defined as

$$\bar{M}(\bar{q})\ddot{\bar{q}} + \bar{C}(\bar{q}, \dot{\bar{q}})\dot{\bar{q}} = \bar{\tau} + \bar{\tau}_e \tag{42}$$

where $\bar{M}$ denotes the inertia matrix of the augmented system. The total kinetic energy function of the augmented system is given in Equation (43)

$$\bar{k}(\bar{q}, \dot{\bar{q}}) = \frac{1}{2}\dot{\bar{q}}^T \bar{M}(\bar{q})\dot{\bar{q}} \tag{43}$$

Kinetic energy of the augmented system $\bar{k}(\bar{q}, \bar{V}(\bar{q}))$ is equal to a positive number $\bar{E}$ as in Equation (44)

$$\bar{k}(\bar{q}, \bar{V}(\bar{q})) = \frac{1}{2}\bar{V}(\bar{q})^T \bar{M}(\bar{q})\bar{V}(\bar{q}) = \bar{E} > 0 \tag{44}$$

assuming that the velocity of the flywheel $V_{n+1}(q)$ is calculated according to Equation (45)

$$V_{n+1}(q) = \sqrt{\frac{2}{M_F}\left(\bar{E} - \frac{1}{2}V(q)^T M(q) V(q)\right)} \tag{45}$$

3.2.2 Coupling Control

The skew-symmetric control law contains feed-forward compensation and a feedback term for a given velocity field. In particular; the feed-forward term

in Equation (46) implements dynamic compensation while the feedback term in Equation (47) reduces the contour error.

$$\bar{\tau}_c = \frac{1}{2\bar{E}}(\bar{w}\bar{P}^T - \bar{P}\bar{w}^T)\dot{\bar{q}} \tag{46}$$

$$\bar{\tau}_f = \gamma(\bar{P}\bar{p}^T - \bar{p}\bar{P}^T)\dot{\bar{q}} \tag{47}$$

where γ is a control gain which determines the rate of convergence, the speed of the system to follow the desired velocity field. The momentum of the augmented system $\bar{p}(\bar{q}, \dot{\bar{q}})$, the desired momentum of the augmented system $\bar{P}(\bar{q})$ and the inverse dynamics $\bar{w}(\bar{q}, \dot{\bar{q}})$ are defined as

$$\begin{aligned} \bar{p}(\bar{q}, \dot{\bar{q}}) &= \bar{M}(\bar{q})\dot{\bar{q}} \\ \bar{P}(\bar{q}) &= \bar{M}(\bar{q})\bar{V}(\bar{q}) \\ \bar{w}(\bar{q}, \dot{\bar{q}}) &= \bar{M}(\bar{q})\dot{\bar{V}}(\bar{q}) + \bar{C}(\bar{q}, \dot{\bar{q}})\bar{V}(\bar{q}) \end{aligned} \tag{48}$$

The error dynamics under the skew-symmetric control is finally obtained as

$$\bar{\tau}(\bar{q}, \dot{\bar{q}}) = \bar{\tau}_c(\bar{q}, \dot{\bar{q}}) + \bar{\tau}_f(\bar{q}, \dot{\bar{q}}) \tag{49}$$

3.2.3 Speed Regulation

PVFC ensures the total energy of the augmented system to be constant and the task speed of the mechanical system is determined due to the initial energy level of the system and the work done by the external forces. In particular; the timing along the path is due to the initial energy level of the augmented system and the external energies supplied or subtracted by

the patients during the task. Figure 3.3 represents the the change of the task speed during a contour following task with respect to applied forces to the system. In particular, this figure shows that the speed of AssistOn-Mobile increases for additional forces along the direction of the movement. Moreover, AssistOn-Mobile decreases its speed for applied forces along the reverse direction. The green area shows where the task speed obtains negative values due to applied forces and starts to move backwards.

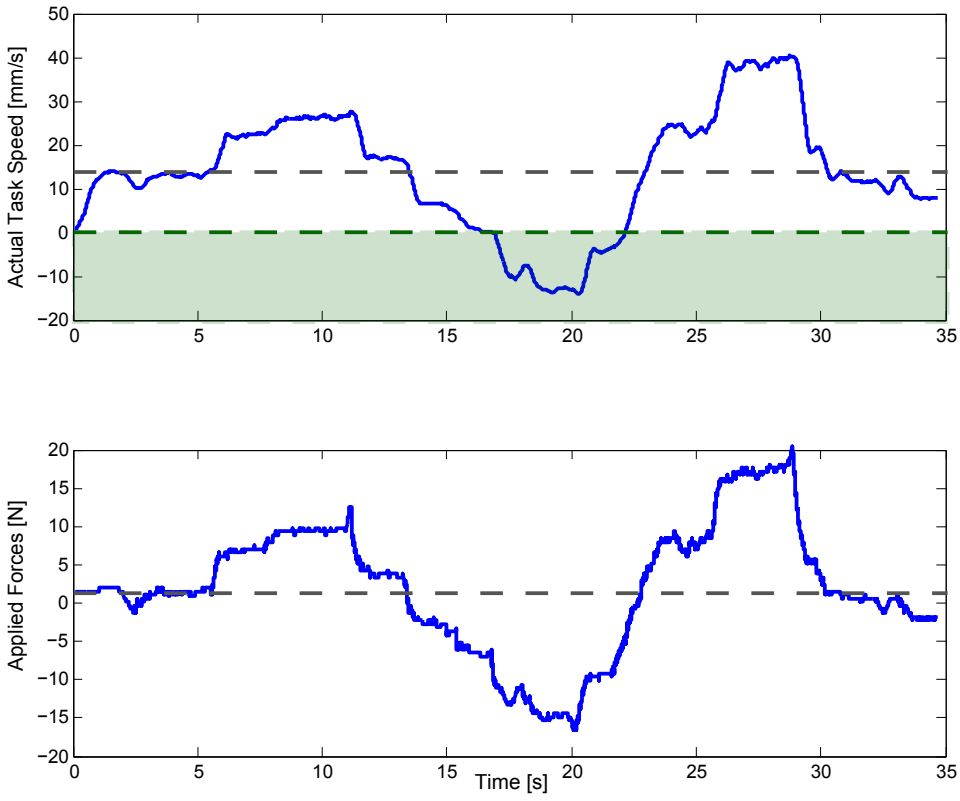

Figure 3.3: Task speed adjustment with respect to applied forces

Besides, the speed of the contour tracking tasks can be controlled by regulating the total energy of the system by the actuators through an extra

control term as in Equation (50).

$$\tau_{forced} = \zeta \bar{P}(r - \frac{\bar{P}^T \dot{\bar{q}}}{2\bar{E}}) \tag{50}$$

where $\zeta > 0$ is the damping coefficient and r is the speed coefficient. Equation (50) clearly states that τ_{forced} minimizes the error between $\dot{\bar{q}}$ and $r\bar{V}$. Figure 3.4 shows the relationship between the applied forces and the speed coefficient r implemented using AssistOn-Mobile.

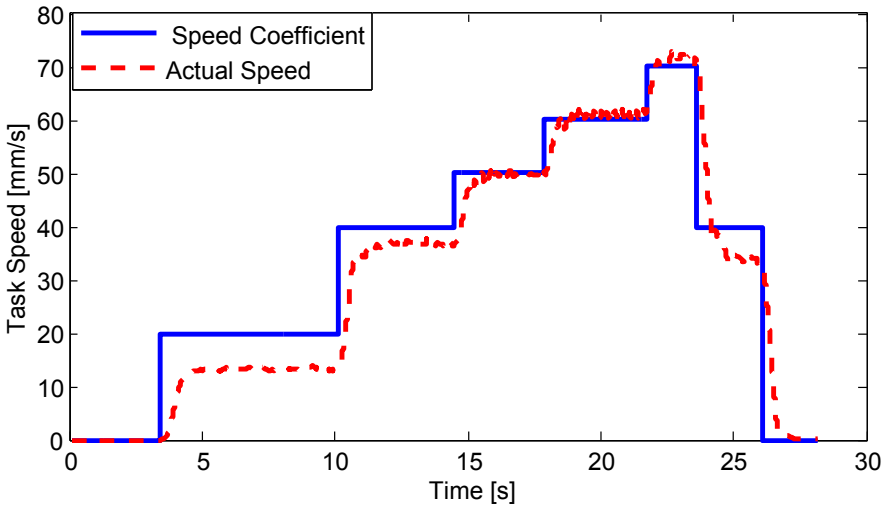

Figure 3.4: Task speed adjustment with respect to speed coefficient

3.2.4 Implementation on AssistOn-Mobile

Since PVFC requires the actual dynamics of the mechanical system, the dynamic analysis is significant. To avoid the difference between the dynamic model and the mechanical system itself, admittance control is used to impose desired dynamics to AssistOn-Mobile.

The basic idea of admittance control is to describe a relationship between

the torque output of the PVFC and the wheel velocities such as

$$q_d(s) = \frac{1}{M_a s + B_a} \tau_d(s) \tag{51}$$

where M_a and B_a are inertia and viscosity parameters for each wheel, respectively. Velocity output of admittance control is used as the reference value for the inner loop velocity control. As a result, the complex dynamics of AssistOn-Mobileis simplified to desired dynamics. The overall control scheme is shown as in Figure 3.5.

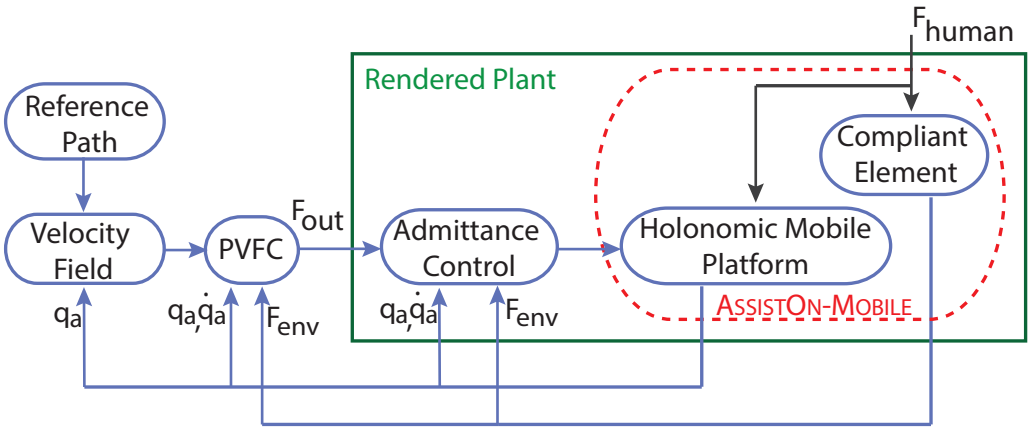

Figure 3.5: Control scheme of PVFC with rendered dynamics

3.2.5 Experimental Results

To see the path tracking performance of AssistOn-Mobile, an experiment has been implemented as in Figure 3.6. In particular, the reference path and the actual robot path has been represented on the x-y plane in Figure 3.6. From the figure, it is clear that AssistOn-Mobile can perform the path tracking tasks with any initial conditions. Table 3.1 shows the RMS error value percentages for x,y and radial movement.

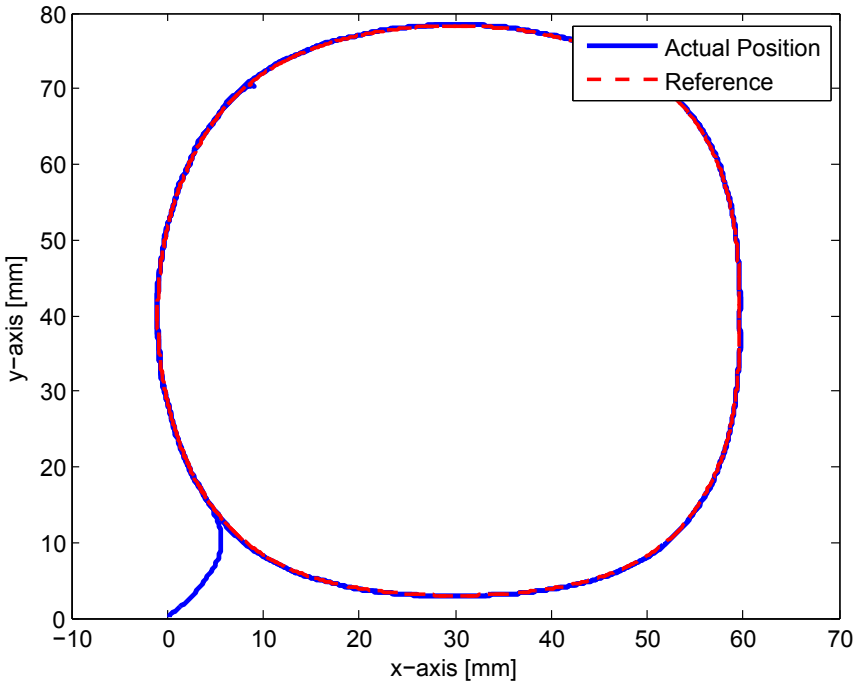

Figure 3.6: Experiment Result of PVFC with AssistOn-Mobile

Table 3.1: RMS error values for PVFC implementation on AssistOn-Mobile

	RMS Error %
x	3.38 %
y	3.53 %
radial	4.8 %

Since PVFC decouples the path and the timing along the path, AssistOn-Mobile converges to the reference path slowly and naturally, unlike a trajectory tracking controller. Therefore, PVFC ensures that the controller does not impose any undesirable trajectory which may harm the patients during therapies. Figure 3.7 shows how AssistOn-Mobile converges to the reference path starting from an initial configuration which is not placed on the

reference path in x and y directions. Once the actual position of AssistOn-Mobile reaches to the reference path, AssistOn-Mobile starts to move faster along the path, without any applied forces under constant speed coefficient.

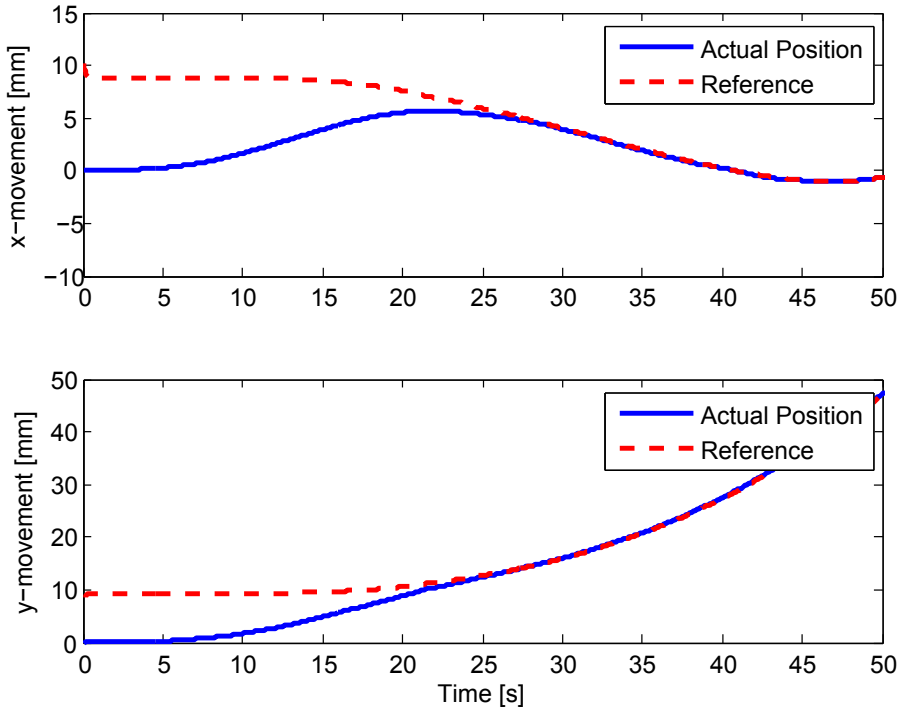

Figure 3.7: Path tracking performance of the AssistOn-Mobile under PVFC from a different initial configuration than reference

Chapter IV

4 BCI Integration with AssistOn-Mobile

"Assist-as-needed" concept discussed in Chapter 3 requires patients to apply physical forces to the active involvement of patients to the therapies are ensured. For patients with severe disabilities who have lost the functionality of their limbs completely, such as spinal cord patients, Brain-Computer Interaction (BCI) provides a communication channel between the rehabilitation tasks and the patients by estimating the instantaneous intention levels of patients. This chapter starts with the introduction of BCI systems and the related literature. Then it discusses the integration of BCI with AssistOn-Mobile. This section introduces the integration of a BCI system with the proposed holonomic mobile platform AssistOn-Mobile as a collaborative work with Sabanci University Computer Vision and Pattern Analysis Laboratory (VPA) **??**.

4.1 Brain-Computer Interaction

A BCI system aims to generate commands about patients' state of mind by measuring the brain activity. The brain activity can be measured using two main methods: the invasive method where the brain signals are measured internally by the electrodes inserted on the brain with an operation and the

non-invasive method where the signals are measured externally by the electrodes placed on a head cap which is worn by the patients. Even though the invasive method enables more accurate signals with minimum noise, the need for the surgery makes it expensive and non-practical. The non-invasive method can be applied by Magnetoencephalography (MEG), X-ray Computed Tomogrophy (CT), Positron Emission Tomography (PET), functional Magnetic Resonance Imaging (fMRI), Electroencephalogram (EEG), etc. For BCI-based rehabilitation, EEG method is commonly favored due to its portability, ease of use, low-cost, lower noise-to-signal ratio and silence.

EEG-based BCI system detects the electrical activity from the scalp and classifies it to estimate the user's intention for the movement. In this thesis, a Biosemi ActiveTwo EEG System is used for EEG recordings. The recording configuration shown in Figure 4.1 uses Ag-Cl electrodes at C3, Cz, C4 at 512 Hz sampling rate. Their upper and lower neighbor channels are used as references. By subtracting the average of the data received from upper and lower neighbor channels of a main channel, 3 referenced main channels are obtained.

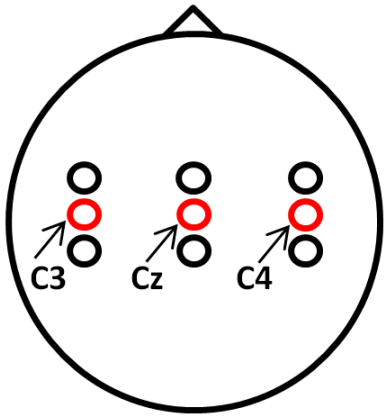

Figure 4.1: Electrode Positions

The motor imagery of movements for users are obtained by extracting various features from the EEG recordings and classifying them with several methods [79]. In particular, event-related synchronization and desynchronization (ERD/ERS) patterns indicate the motor imagery movements where the change of signal amplitude implies the rest or motor imagery. In theory, ERD occurs when the signal values decrease and implies the motor imagery movement and ERS increases the signal after the execution of the movement [80–82]. ERD/ERS patterns are mainly characterized by investigating the spectral powers computed in α (8 Hz-13 Hz) , σ (14 Hz-18 Hz) and β (18 Hz-30 Hz) frequency bands of the EEG data related to the imagery movements [80, 81]. To analyze these frequency bands Short Time Fourier Transform is applied to each trial. These features are classified into two classes: right arm movement and rest using Linear Discriminant Analysis (LDA) which is a non-complex, stationary classification method [83]. In this chapter, unlike the literature, instead of using these binary outputs to provide online adaptation of the BCI system as the rehabilitation protocol, the posterior probabilities of EEG data are used to obtain continuous-valued outputs as shown in Figure 4.2.

A BCI system requires subjects to undergo a cue-based synchronous training sessions where the subjects learn to control the BCI system, while the system generates a pattern from the EEG signals of each subject. During the training sessions, the subjects are asked to sit quietly during the data collection with no actual movement and to relax or imagine moving their right arms with respect to each given cue. Each cue is followed up with a passive period where the EEG signals are not evaluated. In the beginning of the trial, a cross "+" is displayed on the monitor to indicate the passive

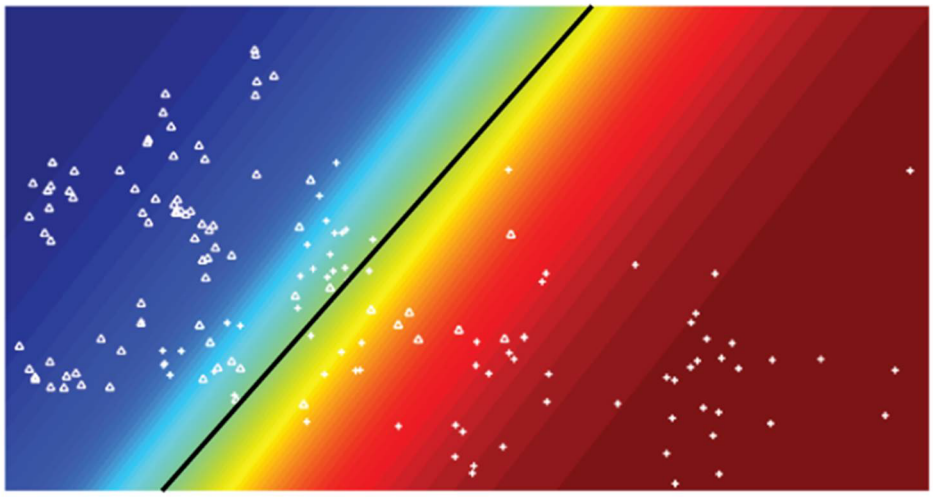

Figure 4.2: Posterior probabilities of EEG data

period. After the passive period, a cue is given which shows either a right arrow or "Relax" with an acoustic stimulus randomly. Each cue is followed by the passive period again. Right arrow asks subjects to concentrate on imagery right arm movements, while "Relax" asks them to relax. The visual cues given to subjects during training are given in Figure 4.3.

Figure 4.3: Graphical interface for the training session

4.2 BCI-based Rehabilitation Protocols

One common way to implement a BCI-based rehabilitation protocol is to integrate the BCI system with virtual reality environments. During such ther-

apies [84–90], the subjects are asked to perform imagery reaching or grasping movements while visual feedback is given on the monitor. In [84], 9 healthy subjects are given visual feedback with "spheroids" game for 7 min. The difficulty parameters are computed in a calibration test where the subjects are asked to move virtual arms to specific locations on a virtual table. BCI system classifies users' intentions into "no movement", "right arm movement" and "left arm movement". In [85], 19 healthy subjects are given visual and auditory feedback during mental imagery tasks. Each subject participated in one session with 4 blocks of 30 reaches per subject. Right arm movements are measured with IR reflective markers. Users are asked to perform straightforward and complicated tasks. The dynamics of the movement is captured with a nonlinear analysis to obtain the information about planning and execution of the movement. The novelty of this technique is to capture the dynamics of the movement. In [86], 5 chronic stroke patients are asked to perform mental imagery tasks with "ball-basket game" besides the physical practice. Patients are asked to attend sessions 2 times a week, for 6 weeks. In [87], 6 healthy subjects are asked to change the position of a cursor with a constant speed for every half second following 3 different tasks. In [88], 15 healthy subjects are asked to control the trajectory of a flying simulated aircraft at a fixed speed and altitude by imagining "right/left" arm movements. In [89], 3 healthy subjects are asked to participate different environmental modes to understand the effect of realistic feedback imagining "right/left" arm movements. In [90], a set of experiments have been performed by 4 healthy subjects where they are asked to perform "left" and "right" imagery movements. The results showed that the participants were able to follow the desired trajectory by controlling a virtual cursor with an EEG-based BCI

system.

In [87, 91], BCI systems are integrated with robotic systems but have no physical interaction with subjects; they are used for visual feedback to correspond with motor imagery of reaching or grasping movements. In [87], 6 healthy subjects are asked to control the movements of FANUS LR Mate 200iB robotic arm. During experiments, subjects try to move the end-effector of robotic arm to right or left imagining "left" and "right" movements. In [91], 1 healthy subject is asked to imagine "left" and "right" arm movements to control the movement of 2-DoF planar robotic arm, PuParm. Two control strategies are applied: controlling the axis and direction of 100 mm linear movement, and controlling the direction of 5° rotation.

The mental imagery tasks supported by a BCI system are only effective if they are combined with physical practice during BCI-based rehabilitation. To make BCI based rehabilitation more intense, mental imagery tasks should be assisted with physical practice tasks using robotic devices that can provide haptic feedback. [92] states the significant difference between MI tasks alone and MI with haptic assistance. Moreover, [93] presents the positive effect of haptic assistance on the accuracy of the classification with respect to virtual feedback only. Therefore, to integrate physical therapy with mental imagery tasks; some studies used robotic rehabilitation devices to provide physical feedback during the mental tasks.

Robotic devices for upper arm rehabilitation have been integrated with BCI systems in [39, 94–102, 102–104] asking subjects or patients to perform imagery reaching and grasping movements. Most of these systems are triggered with respect to intention levels of the users. In [94], 8 stroke patients are asked to trigger 2-DoF MIT-Manus to perform reaching tasks to 8 differ-

ent targets located around a virtual circle. In [95,96], 3 healthy subjects and 4 chronic stroke patients are asked to initialize the movement of Light-Exos arm toward the selected objects by the users. An eye-tracking system allows patients to select the object to reach and a Kinect sensor identifies the 3-D object located in that direction. Each task execution lasts for 5 seconds and the movement itself for 3 to 5 seconds. In [97], 18 stroke patients are divided into two group; one group is asked to trigger MIT-Manus using their intentions to move while other group underwent to conventional physical therapy using MIT-Manus. Moreover, [98, 99] carries out larger clinical studies with the same experimental setup. The same group investigated the efficiency of calibration for long-term BCI users in [101]. [102] shows that it is possible to decode both elbow and hand trajectory from EEG data to exploit natural motor imagery.

In all of these robot-assisted BCI integrated rehabilitation systems, patients' intentions are only used to initiate and stop the movement during therapy. With this approach, once the movement is triggered, the rest of the movement is independent from the intention of subjects. Therefore, the patients may stop focusing on the movement while the robotic devices impose the desired movements to their disabled limbs. Besides, the resulting movement is always the same, invariant of the amount of effort that the patients perform to imagine the movement. Therefore, the consistency of active participation of patients may not be guaranteed with these systems during BCI-based movement therapy.

Recently, [39] advocated the importance of real-time adaptation of the subjects' intention to move to the assisted movement by the rehabilitation device. A 7-DoF robot arm with two part attachment for patient arm with

a magnetic quick release mechanism in case of emergency provides actual movements to subjects. The robot can perform standard rehabilitation therapy modes, as well as an interfering mode where the robot perturbs movements which the interference can be modulated by EEG data measurements. ERD/ERS patterns on μ and β frequency bands are observed for motor imagery estimation. Although the importance of a real-time adaptation of the robotic system to the patient's mental imagery performance is emphasized in this work, real-time adaptation of therapies based on BCI classification has been left as a part of their future work.

In [100], 6 healthy subjects and 3 stroke patients are asked to perform real or imagery movements of flexion/extension right arms or affected arms. The training section of the experiment includes both active robot movement where the robot guides subjects' arm and passive robot movement where the subjects are asked to perform a real or imagery movement. Training section provides neural feedback for either movement type. For each session, a test section follows the training section where the subjects' intention detected by the BCI system switches the WAM robot arm between two modes: active and passive. If the patients' intention is classified as move; the robot becomes active and guides the subjects' arm; however, if the classification determines rest; the robot becomes passive. The mode of the WAM robot is refreshed with every detected intention as "more" or "rest" instead of moving it at the end of the classification. The EEG data is classified in each 250 ms and the output is averaged within a window of increasing size (that start from the first classification instance and covers all classification results to that instant) and given to the rehabilitation device. Similarly, in [103] 6 subjects are asked to control a hand device with EEG-based BCI system. The EEG data is

analyzed at each 150 ms intervals. Each iteration moves the robotic hand to open or closed depending on the present position and previous iteration in an online manner. This device uses signals from the ipsilateral motor planning areas of the brain to detect the intended movements of the hand.

Although the online adaptation between the patients' intention and the robotic device has been implemented by [100], it is implemented by triggering the movement within a small time period and their averaging window washes out the instantaneousness of the interface. In other words, the instantaneous estimates of intention levels for how much the patients are trying cannot be obtained with this approach. Moreover, it cannot guarantee the coupled stability of the human-robot system under the effect of unexpected movements and external forces.

4.3 BCI-Integrated AssistOn-Mobile

Our proposed BCI-based rehabilitation robotic system consists of [105]

- *Real-time BCI system*: For real-time, continual processing of patient intention, EEG system is used to measure the electrical activity of the brain. The LDA algorithm is used to classify ERD/ERS patterns in EEG signals as "move" or "rest". To control the speed of therapeutic movements performed by the robotic system the binary outputs are averaged in a moving window.

- *Rehabilitation robot*: To administer robot assisted therapies, AssistOn-Mobile described in Chapter 2 is used.

- *Contour following tasks and Passive Velocity Field Controller*: For BCI integration, a contour following controller PVFC in Subsection 3.2 has

been used. PVFC enables the intention level of patients to be synchronized with instantaneous task speed to provide online feedback to the patients.

- *Visual feedback module*: Visual feedback is provided to patients during training to give the subjects desired cues.

A representative figure of the BCI-integrated AssistOn-Mobile is given in Figure 4.4. EEG-based BCI system measures the brain signals to control the haptic device, AssistOn-Mobile. Meanwhile, visual and audio feedback are provided to patients. The novelty of this integration is the use of PVFC that ensures online modification by adjusting the speed of the robot with respect to concentration level of patients estimated by the BCI system.

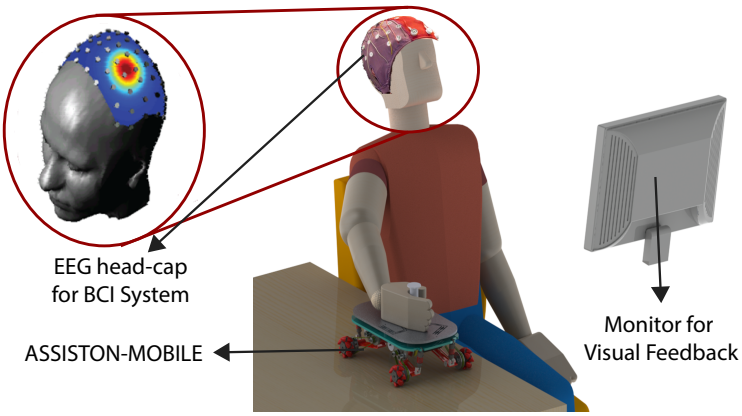

Figure 4.4: BCI-integrated AssistOn-Mobile

4.4 Control of BCI-based AssistOn-Mobile

During BCI experiments, the posterior probabilities of LDA classifier are used to provide continuous estimates of intention levels for online adaptation of the speed of robot assisted contour tracking exercises. These outputs are

used to guide the speed of the contour following task by directly adjusting the speed coefficient r in Equation (50) of PVFC. Hence, the intention levels of users are mapped into the task speed of AssistOn-Mobile to form the online modification between the user and the rehabilitation protocol. In particular, with increased level of "intention", a higher speed to complete the task is supplied to the user to encourage active participation.

We have performed a feasibility experiment with a healthy subject for a single session in order to validate the applicability of the proposed BCI-based rehabilitation protocol. The experimental setup is shown in Figure 4.5. PVFC is implemented in real-time with a sampling frequency of 500 Hz through a desktop computer equipped with a PC I/O card.

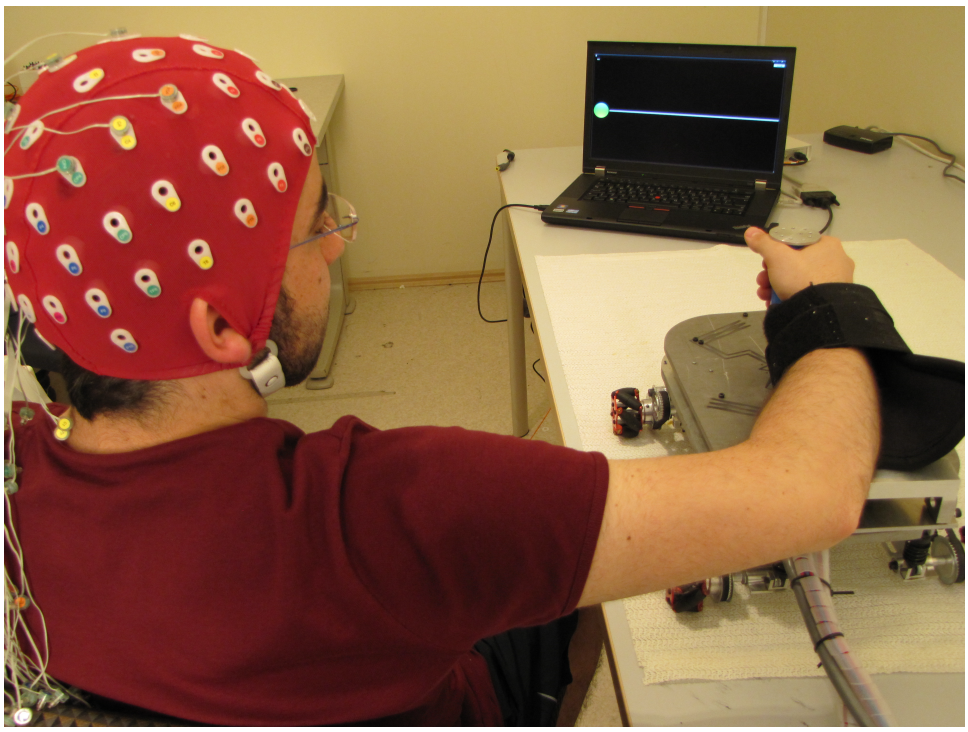

Figure 4.5: Experimental setup of BCI-based AssistOn-Mobile

In the beginning of the experiment, the subject had a training session with 72% averaged classification accuracy. In the first phase of the experiment, the subject is instructed to control AssistOn-Mobile via right arm motor imagery movements tracing the contour. The subject is attached to AssistOn-Mobile and asked not to make any voluntary arm movements during the experiment. Even though AssistOn-Mobile can cover all planar movements; the movement of this experiment is simplified into a straight line task where the subject performs reaching movements forward/backward. In order to avoid sudden variations in the contour tracking speed, instantaneous signals provided by the BCI classifier at each second are averaged over 3 seconds using a moving window for a smoother therapy experience. Figure 4.6 (a) shows the windowed posterior probabilities while AssistOn-Mobile moves forward and backward. Moreover, Figure 4.6 (b) depicts the resultant speed constant of AssistOn-Mobile while performing contour following tasks which is dictated by the BCI signals. The correlation coefficient between the posterior probabilities and the speed coefficients have been calculates as 0.9969.

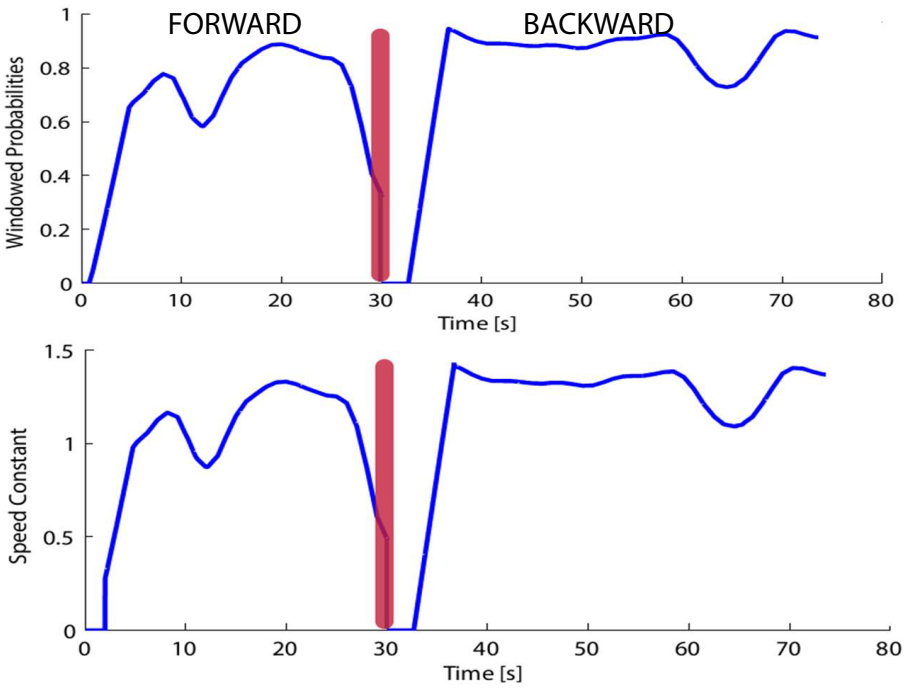

Figure 4.6: (a) Moving window averaged probability of patient intention and (b) speed coefficient of the augmented system

Chapter V

5 Human Subject Experiments

This section presents a set of experiments with healthy volunteers to analyze the efficacy of the proposed BCI-based rehabilitation protocol in Chapter 4 with respect to existing BCI-based and commonly used robot-assisted rehabilitation algorithms in the literature. In particular, this experiment aims to observe:

- The effect of haptic feedback on the active involvement of subjects
- The effect of online adaptation between the subjects and the rehabilitation device in terms of consistent active participation of patients with motor imagery activities
- The effect of proposed robot-assisted BCI-based rehabilitation protocol with online adaptation compared to robot-assisted rehabilitation exercises

This section details the experiment design and procedure used to study the efficacy of the proposed BCI-assisted rehabilitation approach with online modification of task speed to alternative approaches that appear in the literature and discusses the findings. This experiment is a joint work with Sabanci University Computer Vision and Pattern Analysis Laboratory (VPA).

5.1 Experimental Procedure

During the BCI-based rehabilitation exercises, the subjects are asked to control a robotic device where their arms are attached to or a visual object which they are asked to observe while performing mental imagery movements of their limbs. To analyze the effect of haptic feedback, online modification of task speed and the use of BCI in terms of ensuring active participation of subjects to the rehabilitation tasks through mental imagery, an experiment has been designed with 7 consecutive conditions including training and testing blocks as shown in Table 5.1. The experiment consists of one session recorded in a single day. The conditions of the experiment are presented to subjects in a randomized order and short breaks for rest are provided between each condition to prevent fatigue and any systematic effect.

Table 5.1: Experiment Conditions

Conditions	**Training**	**Testing**
C1	Robot moves	BCI assisted robot
C2	Robot does not move	BCI assisted robot
C3	Robot moves	BCI triggered robot
C4	Robot does not move	BCI assisted VR
C5	Robot does not move	BCI triggered VR
PP	-	Patient passive
PA	-	Patient active

13 right-handed healthy subjects among Sabancı University graduate students have volunteered for this study. All subjects gave written informed consent to participate the study. Among these 13 volunteers, 6 of them are excluded from the analysis of the experiment, since their classification accuracy was found to be below 50% for at least 3 of the training sessions. Hence,

the data analysis presented consists of experimental data of 7 subjects; two female and five male volunteers with ages between 24 to 29. All subjects participated in a session where they experienced all of the experimental conditions.

The BCI system in this experiment generates binary outputs classifying the EEG signals of subjects into "rest" and "move" at each 250 ms, similar to existing BCI-based rehabilitation protocols. For the online adaptation of the task speed, these outputs are averaged within a moving window of 1 s. Since this window is moving along time, it provides continuous estimates of the instantaneous intention levels of patients. The EEG signals are measured over C_3, C_z, C_4, CP_3, CP_z, CP_4, FC_3, FC_z and FC_4 locations of the international 10-20 electrode placement system at 2048 Hz sampling rate in the α frequency band.

In the 7 conditions in Table 5.1, the subjects are asked to control either a virtual object in Figure 5.1 or a robotic device, AssistOn-Mobile, as shown in Figure 4.5. The first 5 conditions are BCI-controlled, while the last 2 are conditions that use BCI-system only to observe the brain activity of the subjects during the execution of the task where the movement is either leaded by the user or the device. The timing along the conditions are shown in

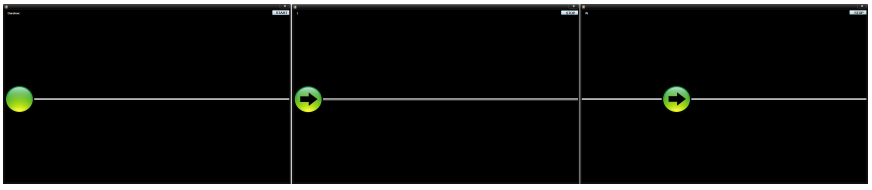

Figure 5.1: Graphical user interface used to provide visual feedback

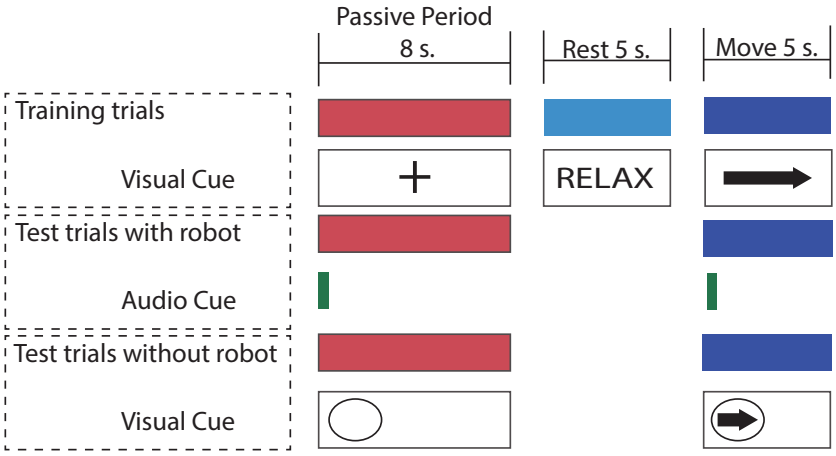

Figure 5.2: Interface used for visual feedback

5.2 Training

Independent training blocks are administered for each of the BCI-controlled conditions. Each training block contains 11 trials in a randomized order (6 Move, 5 Rest) where each trial consists of a 8 s passive period followed by 5 s active period with either a visual or an acoustic cue. Figure 5.3 presents the visual cues for the "move", "rest" and "passive" conditions of the experiment. For training blocks of conditions $C1$ and $C3$, AssistOn-Mobile on which the subjects' right arm is attached moves forward with a constant speed during the right arm imagery movement tasks. The device returns to its initial position during the next passive period. In training blocks of conditions $C2$, $C4$ and $C5$, no haptic feedback is provided to the subjects.

The training session is important for the classification accuracy during the execution of BCI-controlled tasks. In particular, the difference between the mental "move" and "rest" cues results in more accurate BCI classifier.

Figure 5.3: Interface used for the training

Figure 5.4 shows the logarithm of Power Spectrum Density (PSD) values (y-axes) as a function of frequency bands $0-60$ Hz (x-axes) for "move" and "rest" cues with and without haptic feedback for C_3, C_4 and CP_3 electrodes. As expected, the log power values for mental imagery (MI) are smaller than rest cue regarding to ERD/ERS phenomena for each electrode.

A one tailed t-test with $p = 0.05$ was applied to the α band to check whether the PSD values in average are significantly different between MI and rest periods. Figure 5.5 represents the p-values for C_3, C_4 and CP_3 electrodes which obtain statistically significance, indicating discriminative information about the right arm imagery movement and rest periods with and without robotic assistance. This test implies that a classifier model can be built with and without haptic feedback.

The effect of robotic assistance to the motor imagery task is investigated by comparing training sessions of averaged power spectrum densities across the subjects over time for C_3, C_4 and CP_3 electrodes. Figure 5.6 shows the p-values of t-tests for averaged PSDs in the α frequency band over time between with and without robotic assistance training sessions. Under the haptic feedback, the difference between MI and rest periods become significant after 1 s from the given cue throughout the trial. However, without haptic feedback the difference between MI and rest period vanishes and the p values become unsignificant (e.g. for C_3 electrode at 4.75^{th} second). The

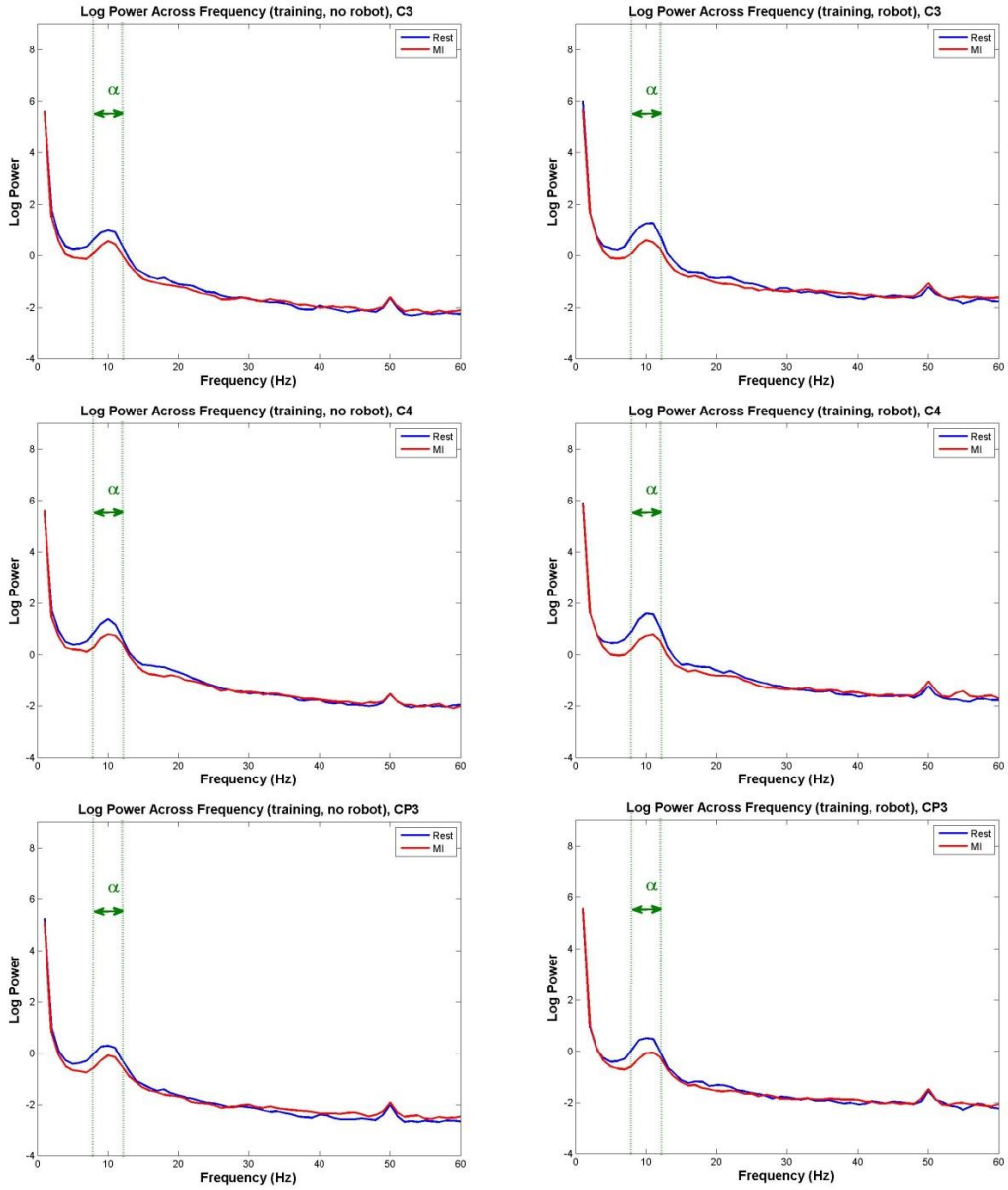

Figure 5.4: Averaged log PSDs for robot and non-robot assisted MI tasks

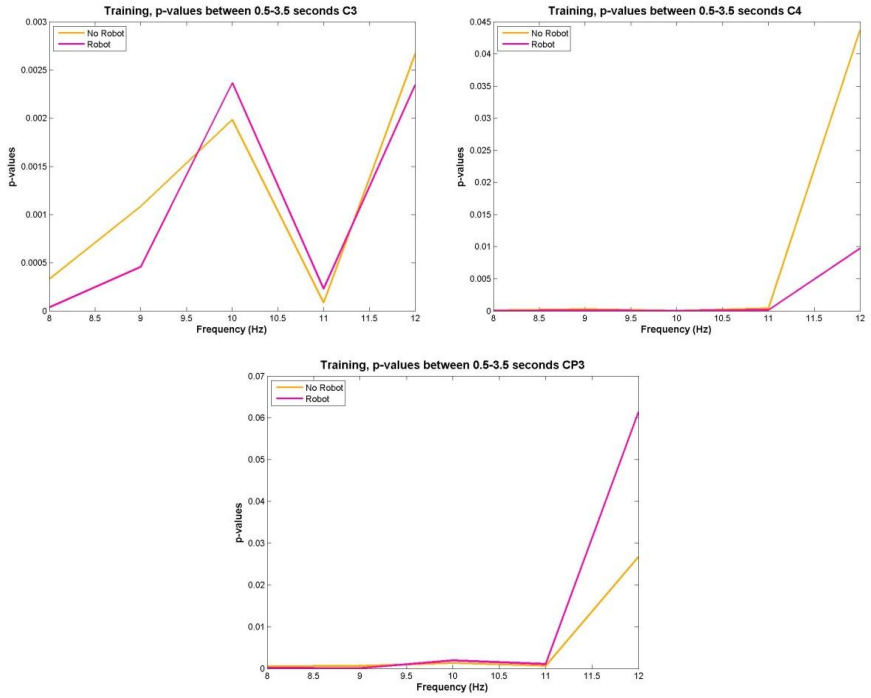

Figure 5.5: p-values of t-test for averaged PSDs in the α band over frequency bands

small p-values indicate that a training model can be built with and without robotic assistance, however the haptic feedback may provide more accurate classifier model since the difference between two classes is more consistent over time under haptic feedback.

5.3 Testing

A test block consists of 16 trials of 5 s mental imagery of right arm movement and a passive period followed by an active period of 8 s. At the beginning

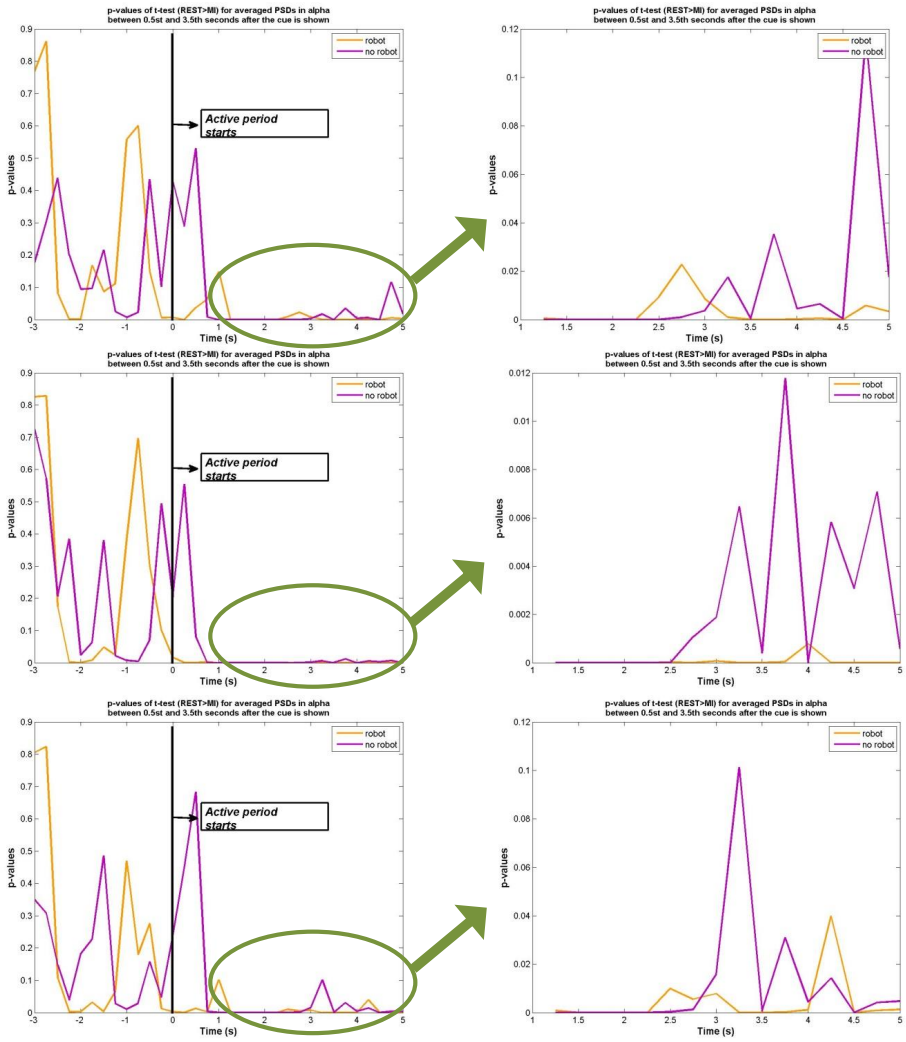

Figure 5.6: p-values of t-test for averaged PSDs in the α band over time

of each period, an acoustic cue indicates the beginning of a trial. During the test, the feedback is provided to the subjects in through either visual channel using a virtual ball or by haptic feedback provided by AssistOn-Mobile. For the conditions under haptic feedback, AssistOn-Mobile returns back

to its initial position for the following passive period with a constant speed and waits for the next active period. The conditions in Table 5.1 are detailed as follows:

- **BCI-assisted** The subjects are asked to perform right arm imagery movements to adjust the task speed with AssistOn-Mobile or of a virtual ball as proposed in Chapter 4. The task speed of the controlled object is updated in each 250 ms according to the outputs obtained from the LDA classifier of BCI, in a correlated fashion with the instantaneous intention level of the subject. In conditions $C1$ and $C2$, AssistOn-Mobile provides haptic feedback, while in condition $C4$ the virtual object provides visual feedback.

- **BCI-triggered** In the triggered conditions, there exists a waiting period between the passive and active periods where the subjects are asked to perform mental imagery right arm movements to trigger a virtual ball or AssistOn-Mobile with a constant speed. The active period starts whenever an intention threshold is exceeded during the waiting period. The minimum and the maximum duration of a waiting period are set as 500 ms and 10 s respectively. The mental imagery of subjects during the active period is not evaluated. In condition $C3$, AssistOn-Mobile provides haptic feedback, while in condition $C5$ the virtual object provides visual feedback.

- **Patient Passive** AssistOn-Mobile guides the right arm of subjects forward with a constant speed while the patient stays passive. Meanwhile, the BCI system is employed to measure the brain activity so that comparison can be made with the BCI-controlled conditions.

- **Patient Active** The subjects are asked to move AssistOn-Mobile by applying external forces to the end-effector. The task speed of AssistOn-Mobile is adjusted with respect to these applied forces. Meanwhile, the BCI system is used to measure the brain activity so that comparison can be made with the BCI-controlled conditions.

5.3.1 Experimental Results

This set of experiment has been designed to compare the proposed robot-assisted BCI based rehabilitation protocol with online modification of task speed with respect to existing protocols in terms of active participation of subjects. The participation level of subjects are estimated with the PSD values of brain activity. According to ERD/ERS patterns, the low PSD values imply higher intention levels of subjects throughout the mental imagery tasks. For the rehabilitation, the objective of this experiment is to find a condition where the PSD values are continuously smaller than other protocols. To be able to check the continuity of the intention levels of subjects; the data is analyzed in 4 small timing windows (0-1, 1.25-2.25, 2.5-3.5, 3.75-4.75 s).

This experiment is designed to test validity of the following three hypothesis.

Hypothesis 1: Beneficial effects of haptic feedback BCI-based rehabilitation systems with mere integration of visual feedback require patients to observe the effect of their motor imagery without providing any haptic feedback. Therefore, the neural activity for such systems exist as long as the patients keep concentrating. On the other hand, under the effect of physical robotic assistance during BCI-based therapies, actual movement further engages the neural pathways in addition to mental imagery of the movement.

As a result, overall brain activity and engagement of the patients are hypothesized to be higher for BCI-based rehabilitation protocols with robotic assistance when compared to protocols with visual feedback only.

Hypothesis 2: Beneficial effects of online modification of the task speed During triggered BCI-based rehabilitation therapies, the subjects are only required to initiate the movement by exceeding a predetermined intention threshold and once initiated, the motion continues without the need for further human involvement. Under this type of therapy, the patients are not encouraged to concentrate throughout the task, since patients mental imagery does not effect the execution of the task that is performed with a constant speed on a determined trajectory once it is initiated. It is hypothesized that involvement of the patients decreases after motion initiation in triggered BCI-based rehabilitation therapies and online adjustment of the speed of the task execution (with or without haptic feedback) can further engage patients throughout the task, recovering active involvement of patients throughout the therapy.

Hypothesis 3: Beneficial effects of BCI-based robot-assisted rehabilitation with online modification of the task speed This hypothesis is a superposition of hypothesis 1 and 2; that is, we hypothesize that beneficial effects of online modification and haptic feedback adds up to result in more effective therapies when both of these aspects are simultaneously employed. In particular, robot-assisted BCI-based rehabilitation protocol with online adaptation is hypothesized to be as effective as patient active control therapies in terms of achieving active involvement of the patients.

These hypothesis are analyzed in details by comparing different conditions to each other. In particular, two tailed t-tests have been performed to

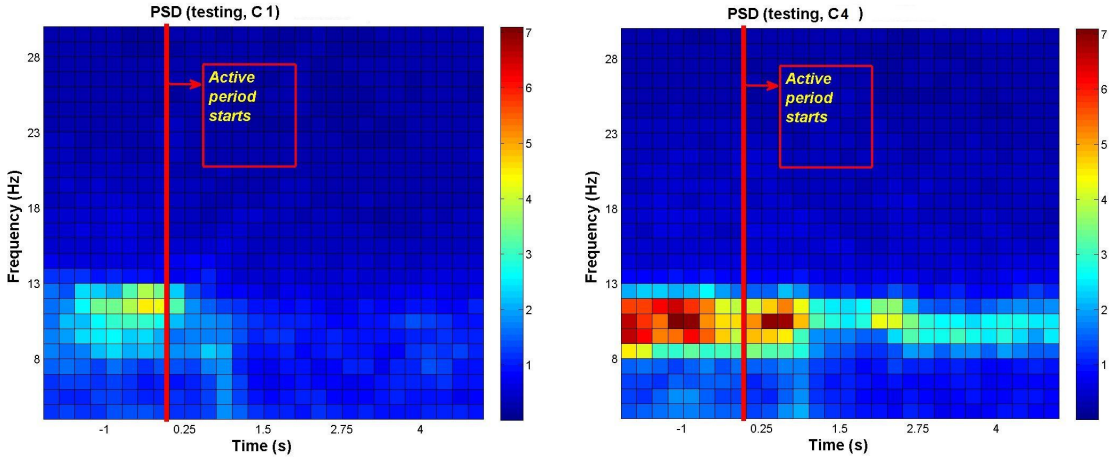

Figure 5.7: PSD across time for conditions C1, C4

observe the possible differences and one tailed t-tests have been performed to observe the significant smaller/higher situations between the PSD values for different conditions where p-value limit has been chosen as 0.05 for statistical significance.

Hypothesis 1: Beneficial effects of haptic feedback

The effect of haptic feedback is first analyzed for BCI-assisted conditions C1 and C4 as in Figure 5.7 where the averaged PSD values have been shown as a function of frequency band $0 - 30\ Hz$ (y-axes) over time (x-axes). In particular, the α frequency band is observed (8-12 Hz) during the analysis.

Since condition C1 provides haptic feedback and C4 provides virtual feedback, the PSD values in C1 are observed to be more intense than PSDs of C4 in Figure 5.7 as expected. This observation implies that condition C1 supports subjects to be more involved with the movement than con-

dition C4. To be able to have a strong statement, one tailed and two tailed t-tests show the difference of the PSD values in 4 timing windows $(0-1, 1.25-2.25, 2.5-3.5, 3.75-4.75$ s). The p-values in Table 5.3.1 show that PSD values of condition $C1$ are significantly smaller than $C4$ for all time windows.

Table 5.2: t-test results for C1, C4

	0-1	**1.25-2.25**	**2.5-3.5**	**3.75-4.75**
$\mathbf{PSD_{C1} < PSD_{C4}}$	2,80E-06	1,69E-03	1,02E-05	0,000178
$\mathbf{PSD_{C1}/PSD_{C4}}$	5,60E-06	0,00338	2,05E-05	0,000356

The effect of haptic feedback can also be analyzed for BCI triggered conditions by comparing the PSD values for conditions C3 and C5. Figure 5.8 shows that the PSD values are lower for condition $C3$ than condition $C5$, since the subjects are provided haptic feedback during condition $C3$.

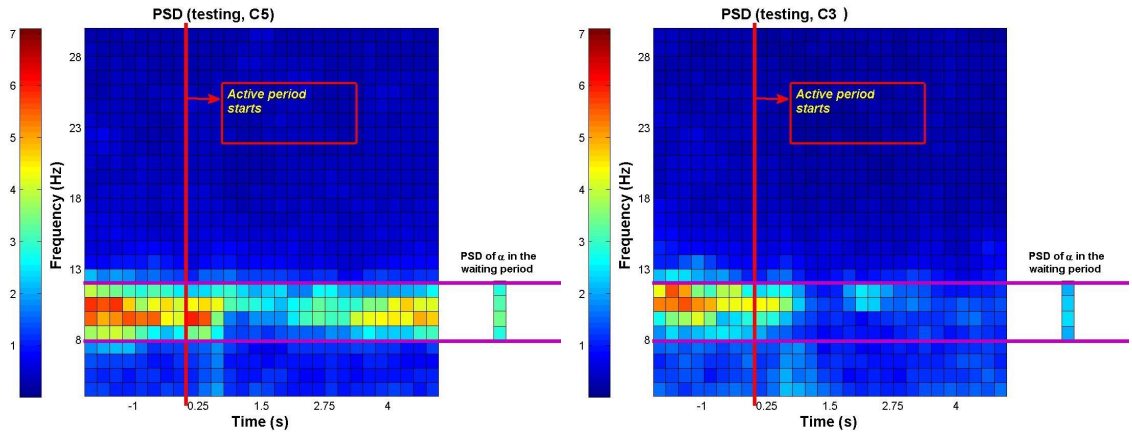

Figure 5.8: PSD across time for conditions C3, C5

Table 5.3 shows the resulting p-values from the t-test and states the statistically significant difference between two conditions.

Table 5.3: t-test results for C3, C5

	0-1	**1.25-2.25**	**2.5-3.5**	**3.75-4.75**
$\mathbf{PSD_{C3} < PSD_{C5}}$	0,026538	0,048532	2,91E-04	3,02E-07
$\mathbf{PSD_{C3}/PSD_{C5}}$	0,053076	0,097065	0,000582	6,05E-07

To sum up; PSD values can be stated for BCI-assisted conditions as $PSD_{C1} < PSD_{C4}$ and for BCI-triggered conditions as $PSD_{C3} < PSD_{C5}$ throughout the movement. These results support the beneficial effect of haptic feedback on the motor imagery activity of subjects.

Hypothesis 2: Beneficial effects of online modification of the task speed

The effect of online modification of the task speed as proposed with respect to initializing the movement only is investigated under haptic and visual feedbacks. Figure 5.9 represents the averaged PSD values across the subjects for BCI-assisted and BCI-triggered conditions with robotic assistance, C1 and C3. From this figure, the condition C1 is observed to be more continuous and intense than condition C3 since the PSD values tend to increase in Condition C3. One and two tailed t-test results in Table 5.3.1 also show that the PSD values of condition C1 are significantly smaller than C3 only in one timing window.

Table 5.4: t-test results for C1, C3

	0-1	**1.25-2.25**	**2.5-3.5**	**3.75-4.75**
$\mathbf{PSD_{C1} < PSD_{C3}}$	0,11222	0,098301	0,006446	0,109945
$\mathbf{PSD_{C1}/PSD_{C3}}$	0,22444	0,196602	0,012893	0,219889

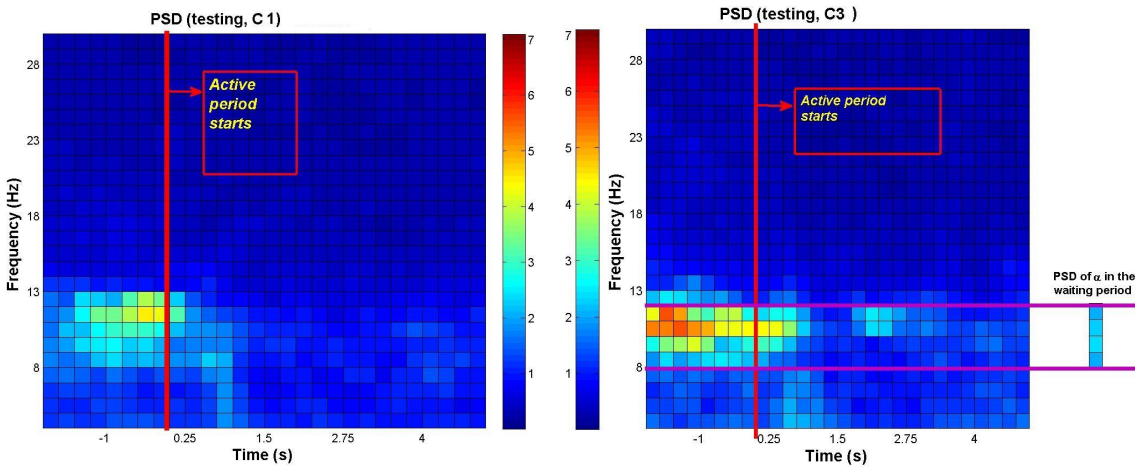

Figure 5.9: PSD across time for conditions C1, C3

Similarly, the effect of online adaptation of task speed under visual feedback is observed as in Figure 5.10. The statistically significant difference between these two conditions are investigated by the t-test and the resultant p values are represented in Table 5.5. The p-values also show that the PSD values of condition C4 is statistically significantly smaller than C5 in only one timing window.

Table 5.5: t-test results for C4, C5

	0-1	**1.25-2.25**	**2.5-3.5**	**3.75-4.75**
$\mathbf{PSD_{C4} < PSD_{C5}}$	0,927666	0,685656	0,064351	0,001429
$\mathbf{PSD_{C4}/PSD_{C5}}$	0,144667	0,628689	0,128702	0,002859

To sum up; using a BCI system with the online adaptation of the task speed may help the subjects to be continuously involved to their tasks. In particular, during BCI-triggered conditions, the subjects may tend to decrease their intentions on the movement which causes the discontinuity in the PSD

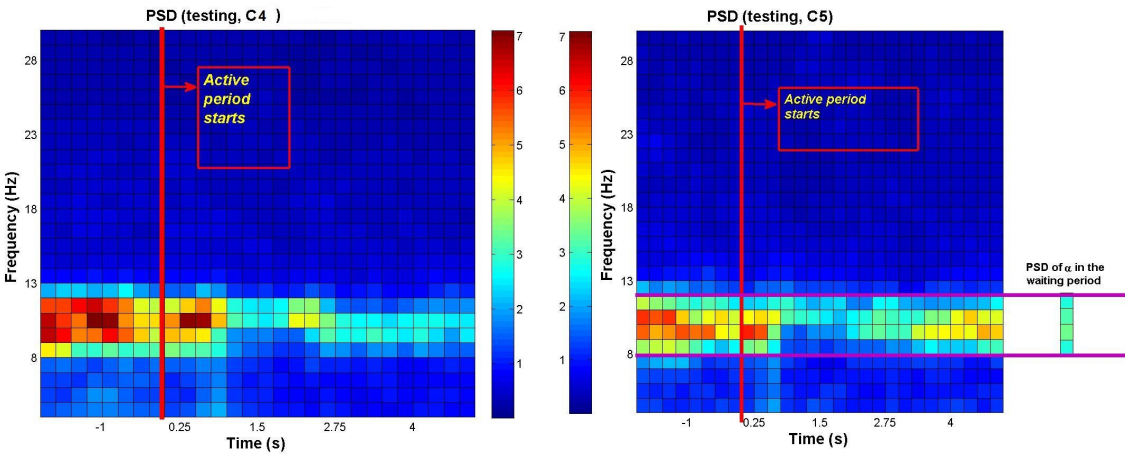

Figure 5.10: PSD across time for conditions C4, C5

plots while the BCI-assisted conditions may promise better consistency in the intention levels of subjects. Although the t-tests in this experiment do not provide enough evidence to make a statistically significant claim about the effect of online adaptation of the task speed compared to triggering the movement, a trend of online modification seems promising in terms of keeping the subjects actively involved with the task throughout the movement. For a stronger claim, further experiments are required comparing these two conditions.

5.3.2 Hypothesis 3: Beneficial effects of BCI-based robot-assisted rehabilitation with online modification of the task speed

The previous analyses showed that the haptic feedback has a significant effect on the involvement of subjects and online adaptation of the task speed may help subjects to be involved more consistently. To provide a comparison of BCI-assisted robotic rehabilitation protocol with online modification of task

speed with respect to commonly employed robotic rehabilitation protocols, subjects are asked to perform PA and PP conditions, where they are asked to apply forces to the end-effector of the device or let the robot to guide their arms to complete the desired tasks, respectively. During conditions PA and PP, the BCI system is used only to measure the brain activity.

Figure 5.11 shows the averaged PSD values across the subjects for C1, PA and PP conditions. The averaged PSDs in PP are greater than conditions C1 and PA throughout the movement. However, looking at the Figure, the PSDs in PA and C1 are similar in α frequency band after the active period. For further analysis, one and two tailed t-tests have been performed and the resultant p-values are shown in Table 5.6.

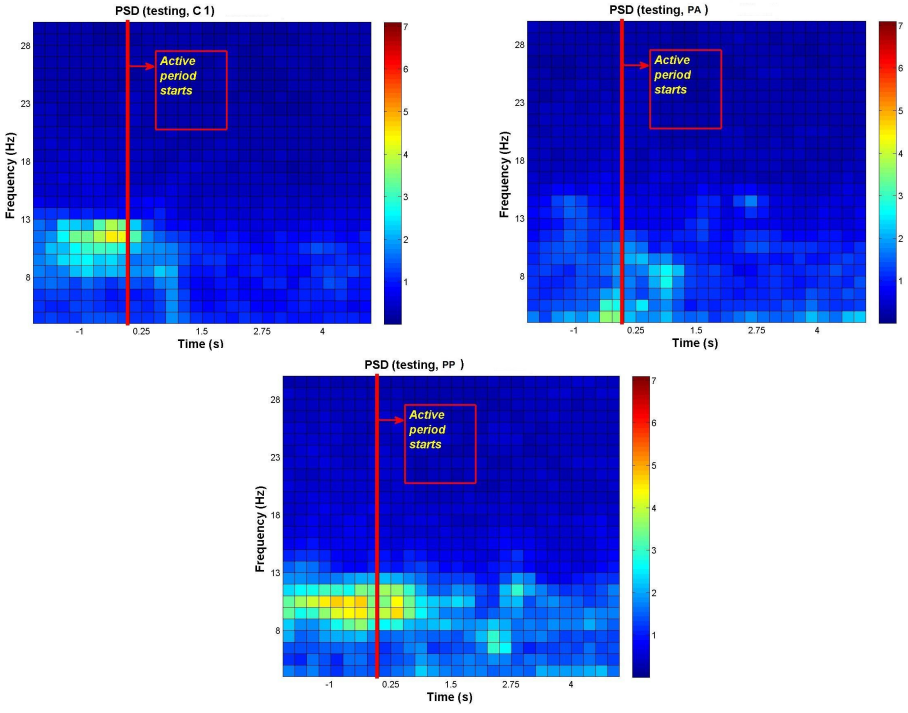

Figure 5.11: PSD values of conditions C1, PA, PP

Table 5.6: t-test results for C1, PA, PP

	0-1	**1.25-2.25**	**2.5-3.5**	**3.75-4.75**
$\mathbf{PSD_{C1} < PSD_{PA}}$	0,596088	0,119425	0,077717	0,54833
$\mathbf{PSD_{C1} < PSD_{PP}}$	5,68E-03	3,20E-05	0,022491	0,00065
$\mathbf{PSD_{PA} < PSD_{PP}}$	0,013885	0,01782	0,106211	0,014598
$\mathbf{PSD_{C1}/PSD_{PA}}$	0,807825	0,238849	0,155435	0,903339
$\mathbf{PSD_{C1}/PSD_{PP}}$	0,011365	6,39E-05	0,044982	0,0013
$\mathbf{PSD_{PA}/PSD_{PP}}$	0,02777	0,03564	0,212421	0,029196

As expected, no statistically significant difference is observed between conditions C1 and PA while PSDs of PP are statistically significantly higher than C1 and PA. These results on average can be summarized as $PSD_{C1} = PSD_{PA} < PSD_{PP}$, implying the active involvement of subjects. For the BCI-based rehabilitation, this finding is promising since it shows that a BCI-based rehabilitation protocol under robot assistance with online modification of the task speed can help subjects to be actively involved throughout the rehabilitation exercises, as much as them applying external forces to the rehabilitation device. As a result, this protocol possesses high promise to provide a positive effect on treatments.

5.3.3 Overall Results

Considering Table 5.7 and Table 5.8 presenting the overall t-test results for each condition, the following conclusions can be extracted:

- **The effect of haptic feedback with robotic assistance:** During both BCI-assisted and BCI-triggered conditions, the PSD values of the brain activity under the effect of robotic assistance are statistically significantly smaller than under visual feedback. These results have been

summarized as $PSD_{C1} < PSD_{C4}$ and $PSD_{C3} < PSD_{C5}$ throughout the movement. Therefore, the beneficial effect of the robotic assistance on the motor imagery activity of subjects have been observed.

- **The effect of online modification of the task speed:** The t-test results between the BCI-assisted and BCI-triggered conditions under both haptic and visual feedbacks has shown statistically significant difference in only one timing window each. However, there is a trend where the PSD values under BCI-assisted conditions are more consistent and continuous than BCI-triggered conditions. This trend may imply that BCI-assisted conditions impose active participation of subjects throughout the movement where under BCI-triggered conditions, the subjects may tend to lose their involvement. Yet, further experiments are necessary to make a strong statement about the effect of online modification of the task speed.

- **The effect of using a BCI system in rehabilitation:** The proposed BCI-based rehabilitation protocol under robotic assistance with online modification of the task speed has no statistically significant difference compared to PA condition where the subjects are asked to perform the real movement with their own efforts. This PA condition is the gold standard in rehabilitation, therefore the proposed system may be promising for the rehabilitation of patients with severe disabilities. Moreover, the statistically significant difference between the proposed BCI-assisted condition and PP condition where the robotic device leads the subjects' arm to complete the task claims that the use of proposed protocol helps subjects to be more involved with the

tasks throughout the movement. These findings can be summarized as $PSD_{C1} = PSD_{PA} < PSD_{PP}$

The findings of this set of experiment is promising in terms of discussing the beneficial effects of the proposed BCI-based protocol under robotic assistance with online modification of the task speed. However, the effect of online modification with respect to triggered control requires more investigation. Moreover, such experiments have been tested on patients instead of healthy subjects.

Table 5.7: t-test results for all conditions - I

	0-1	**1.25-2.25**	**2.5-3.5**	**3.75-4.75**
$\mathbf{PSD_{C1} < PSD_{C2}}$	0,001874	0,100908	0,045632	0,080617
$\mathbf{PSD_{C1} < PSD_{C3}}$	0,11222	0,098301	0,006446	0,109945
$\mathbf{PSD_{C1} < PSD_{C4}}$	2,80E-06	1,69E-03	1,02E-05	0,000178
$\mathbf{PSD_{C1} < PSD_{C5}}$	0,000753	4,84E-04	6,64E-07	1,51E-06
$\mathbf{PSD_{C1} < PSD_{PA}}$	0,596088	0,119425	0,077717	0,54833
$\mathbf{PSD_{C1} < PSD_{PP}}$	5,68E-03	3,20E-05	0,022491	0,00065
$\mathbf{PSD_{C2} < PSD_{C3}}$	0,631996	0,943474	0,39661	0,516314
$\mathbf{PSD_{C2} < PSD_{C4}}$	0,01322	0,013722	0,018646	0,110799
$\mathbf{PSD_{C2} < PSD_{C5}}$	0,130193	0,003783	0,00015	0,000159
$\mathbf{PSD_{C2} < PSD_{PA}}$	0,188848	0,227043	0,346034	0,445784
$\mathbf{PSD_{C2} < PSD_{PP}}$	0,115803	0,005504	0,070347	0,131887
$\mathbf{PSD_{C3} < PSD_{C4}}$	0,001237	0,04188	0,003073	0,000206
$\mathbf{PSD_{C3} < PSD_{C5}}$	0,026538	0,048532	2,91E-04	3,02E-07
$\mathbf{PSD_{C3} > PSD_{PA}}$	0,185512	0,162465	0,185022	0,805987
$\mathbf{PSD_{C3} < PSD_{PP}}$	0,046812	0,114913	0,165211	0,004412
$\mathbf{PSD_{C4} < PSD_{C5}}$	0,927666	0,685656	0,064351	0,001429
$\mathbf{PSD_{C4} > PSD_{PA}}$	0,003292	0,016636	0,005742	0,002358
$\mathbf{PSD_{C4} > PSD_{PP}}$	0,048138	0,11567	0,291817	0,022569
$\mathbf{PSD_{C5} > PSD_{PA}}$	0,024382	0,045381	0,010116	0,000176
$\mathbf{PSD_{C5} > PSD_{PP}}$	0,419453	0,190689	0,092892	7,81E-06
$\mathbf{PSD_{PA} < PSD_{PP}}$	0,013885	0,01782	0,106211	0,014598

Table 5.8: t-test results for all conditions - II

	0-1	**1.25-2.25**	**2.5-3.5**	**3.75-4.75**
$\mathbf{PSD_{C1}/PSD_{C2}}$	0,003749	0,201815	0,091264	0,161234
$\mathbf{PSD_{C1}/PSD_{C3}}$	0,22444	0,196602	0,012893	0,219889
$\mathbf{PSD_{C1}/PSD_{C4}}$	5,60E-06	0,00338	2,05E-05	0,000356
$\mathbf{PSD_{C1}/PSD_{C5}}$	0,001507	0,000969	1,33E-06	3,01E-06
$\mathbf{PSD_{C1}/PSD_{PA}}$	0,807825	0,238849	0,155435	0,903339
$\mathbf{PSD_{C1}/PSD_{PP}}$	0,011365	6,39E-05	0,044982	0,0013
$\mathbf{PSD_{C2}/PSD_{C3}}$	0,736007	0,113052	0,793219	0,967373
$\mathbf{PSD_{C2}/PSD_{C4}}$	0,026441	0,027445	0,037293	0,221598
$\mathbf{PSD_{C2}/PSD_{C5}}$	0,260385	0,007565	0,0003	0,000319
$\mathbf{PSD_{C2}/PSD_{PA}}$	0,377695	0,454086	0,692068	0,891569
$\mathbf{PSD_{C2}/PSD_{PP}}$	0,231607	0,011008	0,140693	0,263774
$\mathbf{PSD_{C3}/PSD_{C4}}$	0,002475	0,083761	0,006146	0,000412
$\mathbf{PSD_{C3}/PSD_{C5}}$	0,053076	0,097065	0,000582	6,05E-07
$\mathbf{PSD_{C3}/PSD_{PA}}$	0,371025	0,324931	0,370045	0,388026
$\mathbf{PSD_{C3}/PSD_{PP}}$	0,093625	0,229827	0,330422	0,008824
$\mathbf{PSD_{C4}/PSD_{C5}}$	0,144667	0,628689	0,128702	0,002859
$\mathbf{PSD_{C4}/PSD_{PA}}$	0,006583	0,033273	0,011484	0,004716
$\mathbf{PSD_{C4}/PSD_{PP}}$	0,096276	0,23134	0,583634	0,045137
$\mathbf{PSD_{C5}/PSD_{PA}}$	0,048765	0,090763	0,020232	0,000352
$\mathbf{PSD_{C5}/PSD_{PP}}$	0,838905	0,381378	0,185783	1,56E-05
$\mathbf{PSD_{PA}/PSD_{PP}}$	0,02777	0,03564	0,212421	0,029196

Chapter VI

6 Conclusions and Future Works

We have developed AssistOn-Mobile a multi-DoF series-elastic actuator based on a holonomic mobile platform to administer active therapeutic table-top exercises with unlimited workspace. This device can provide assistice/resistive forces to patients. The localization of AssistOn-Mobile implemented through an Extended Kalman Filter that fuses measurements of optical flow sensors with motor encoders. To prevent compensatory movements of the patients while performing therapies with AssistOn-Mobile, shoulder and trunk movements of the patient is continuously monitored with a Kinect (RGBD) sensor and online feedback is provided to the patient to correct their posture by regulating the task speed. We have also implemented passive velocity field controller (PVFC) to ensure inherently safe, coordinated and synchronized path tracking and reaching exercises performed with a speed determined by the patient.

We also integrated a BCI with AssistOn-Mobile to control the speed of contour following tasks based on the intention levels of patients estimated by the EEG-based BCI system. In particular, continuous intention estimates are extracted from LDA classified by utilizing moving windows and/or posterior probabilities and the speed of the task is modulated through PFVC of AssistOn-Mobile. As a result, the more patients concentrate on the

movement, the faster the robot moves, providing online haptic feedback and helping increase the motivation of the patients. To compare the efficacy of the proposed BCI-assisted rehabilitation with AssistOn-Mobile, an experiment has been designed and conducted with healthy volunteers. The results of human subject experiments suggest that robotic BCI framework with online modification of task speed can ensure a higher level of engagement for patients and promises to be as effective as human active rehabilitation protocols.

The future works include conducting human subject experiments with a larger group of volunteers and testing the feasibility and efficacy of the proposed protocol on spline-cord injury patients. Increasing the robustness of AssistOn-Mobile by properly constraining out-of-plane movements of the series elastic element, addition of an inertial measurement unit to achieve better short-term localization accuracy and integration of Kinect as a global position/orientation sensor to help with global localization of the device are also among our future works.

References

[1] Neurological injury. http://www.oshmanlaw.com/personal_injury/neurological-injury-lawyer.html.

[2] Global burden of disease. http://www.who.int/healthinfo/global_burden_disease/GBD_report_2004update_full.pdf.

[3] C. C. Edward, C. Jeffrey, S. Sergio, and R. Robert. *Stroke - the American Psychiatric Press Textbook of Geriatric Neuropsychiatry (Second ed.)*. Washington DC: American Psychiatric Press, 2000.

[4] C. Bütefisch, H. Hummelsheim, P. Denzler, and K.-H. Mauritz. Repetitive training of isolated movements improves the outcome of motor rehabilitation of the centrally paretic hand. *Journal of the Neurological Sciences*, 130(1):59 – 68, 1995.

[5] G. Kwakkel, R. C. Wagenaar, J. W. R. Twisk, G. J. Lankhorst, and J. C. Koetsier. Intensity of leg and arm training after primary middle-cerebral-artery stroke: A randomised trial. *The Lancet*, 354(9174):191 – 196, 1999.

[6] A. Sunderland, D. J. Tinson, E. L. Bradley, D. Fletcher, R. Langton Hewer, and D. T. Wade. Enhanced physical therapy improves recovery of arm function after stroke. A randomised controlled trial. *Journal of Neurology, Neurosurgery and Psychiatry*, 55(7):530–535, 1992.

[7] N. A. Bayona, J. Bitensky, K. Salter, and R. Teasell. The role of task-specific training in rehabilitation therapies. *Topics in Stroke Rehabilitation*, 12(3):58–65, 2005.

[8] G. Kwakkel, B. J. Kollen, and H. I. Krebs. Effects of robot-assisted therapy on upper limb recovery after stroke: A systematic review. *Neurorehab. and Neural Repair*, 22(2):111–121, 2008.

[9] J. Mehrholz, T. Platz, J. Kugler, and M. Pohl. Electromechanical and robot-assisted arm training for improving arm function and activities of daily living after stroke. *Stroke*, 40, 2009.

[10] G. B. Prange, M. J. Jannink, C. G. Groothuis-Oudshoorn, H. J. Hermens, and M. J. Ijzerman. Systematic review of the effect of robot-aided therapy on recovery of the hemiparetic arm after stroke. *Journal of rehabilitation research and development*, 43(2):171–184, 2006.

[11] K. Nykanen. The effectiveness of robot-aided upper limb therapy in stroke rehabilitation: A systematic review of randomized controlled studies. Master's thesis, University of Jyväskylä, Institute of Health Sciences, Physiotherapy, 2010.

[12] T. Nef, M. Guidali, and R. Riener. ARMin III arm therapy exoskeleton with an ergonomic shoulder actuation. *Applied Bionics and Biomechanics*, 2(6):127–142, 2009.

[13] A. Frisoli, M. Bergamasco, M. C. Carboncini, and B. Rossi. Robotic assisted rehabilitation in virtual reality with the L-EXOS. *Stud Health Technol Inform*, 145:40–54, 2009.

[14] M. A. Ergin and V. Patoglu. AssistOn-SE: A self-adjusting shoulder-elbow exoskeleton. In *IEEE International Conference on Robotics and Automation*, 2012.

[15] C. Carignan, M. Liszka, and S. Roderick. Design of an arm exoskeleton with scapula motion for shoulder rehabilitation. In *International Conference on Advanced Robotics*, pages 524 –531, 2005.

[16] R. J. Sanchez, J. Liu, S. Rao, P. Shah, R. Smith, T. Rahman, S. C. Cramer, J. E. Bobrow, and D. J. Reinkensmeyer. Automating arm movement training following severe stroke: Functional exercises with quantitative feedback in a gravity-reduced environment. volume 14, pages 378 –389, 2006.

[17] M. Yalcin and V. Patoglu. Kinematics and design of AssistOn-SE: A self-adjusting shoulder-elbow exoskeleton. In *IEEE International Conference on Biomedical Robotics and Biomechatronics*, 2012.

[18] A. H. A. Stienen, E. E. G. Hekman, F. C. T. Van der Helm, G. B. Prange, M. J. A. Jannink, A. M. M. Aalsma, and H. Van der Kooij. Dampace: dynamic force-coordination trainer for the upper extremities. In *IEEE International Conference on Rehabilitation Robotics*, pages 820 –826, 2007.

[19] W. Ye, C. Yang, and Q. Xie. The development of an Exoskeleton Robot for Co-Manipulation of Human Upper Limb Movement. *World Congress on Intelligent Control and Automation.*

[20] R.-J. Wang and H.P. Huang. AVSER - Active Variable Stiffness Exoskeleton Robot System: Design and Application for Safe Active-Passive Elbow Rehabilitation. *IEEE International Conference on Advanced Intelligent Mechatronics.*

[21] Y. Mao and S. K. Agrawal. Transation from Mechanical Arm to Human Arm with CAREX: a Cable Driven Arm Exoskeleton (CAREX) for Neural Rehabilitation. *IEEE International Conference on Robotics and Automation.*

[22] Y. Ren, S. Hoon Kang, H.-S. Park, Y.-N. Wu, and L.Q. Zhang. Developing a Multi-Joint Upper Limb Exoskeleton Robot for Diagnosis, Therapy, and Outcome Evaluation in Neurorehabilitation. *IEEE Transactions on Neural Systems and Rehabilitation Engineering.*

[23] A. U. Pehlivan, S. Lee, and M. K. O'Malley. Mechanical Design of RiceWrist-S: a Forearm-Wrist Exoskeleton for Stroke and Spinal Cord Injury Rehabilitation. *IEEE International Conference on Biomedical Robotics and Biomechatronics.*

[24] J. Bae and I. Moon. Design and Control of an Exoskeleton Device for Active Wrist Rehabilitation. *IEEE International Conference on Control, Automation and Systems.*

[25] D. Broetz, C. Braun, C. Weber, S.R. Soekadar, A. Caria, and N. Birbaumer. Combination of Brain-Computer Interface Training and Goal-Directed Physical Therapy in Chronic Stroke: A Case Report. *Neurorehabilitation and Neural Repair.*

[26] A. R. Murguialday, V. Aggarwal, A. Chatterjee, C. Yoonju, R. Rasmussen, B. O'Rourke, S. Acharya, and N. V. Thakor. Brain-computer interface for a prosthetic hand using local machine control and haptic feedback. In *IEEE 10th International Conference on Rehabilitation Robotics (ICORR)*, pages 609 –613, june 2007.

[27] J. d. R. Millan, F. Galan, D. Vanhooydonck, E. Lew, J. Philips, and M. Nuttin. Asynchronous non-invasive brain-actuated control of an intelligent wheelchair. In *Annual International Conference of the IEEE Engineering in Medicine and Biology Society(EMBC)*, pages 3361 – 3364, 2009.

[28] D. Huang, K. Qian, D. Fei, W. Jia, X. Chen, and O. Bai. Electroencephalography (eeg)-based brain computer interface (bci): A 2-d virtual wheelchair control based on event-related desynchronization/synchronization and state control. *IEEE Transactions on Neural Systems and Rehabilitation Engineering*, 20(3):379 –388, 2012.

[29] D. Huang, P. Lin, D. Fei, X. Chen, and O. Bai. Eeg-based online two-dimensional cursor control. In *Annual International Conference of the IEEE Engineering in Medicine and Biology Society (EMBC)*, pages 4547 –4550, 2009.

[30] S. P. Kim, J. D. Simeral, L. R. Hochberg, J. P. Donoghue, G. M. Friehs, and M. J. Black. Point-and-click cursor control with an intracortical neural interface system by humans with tetraplegia. *IEEE Transactions on Neural Systems and Rehabilitation Engineering*, 19(2):193 – 203, 2011.

[31] K. K. Ang, C. Guan, K. S. G. Chua, B. T. Ang, C. Kuah, C. Wang, K. S. Phua, Z. Y. Chin, and H. Zhang. Clinical study of neurorehabilitation in stroke using eeg-based motor imagery brain-computer interface with robotic feedback. In *Annual International Conference of the IEEE Engineering in Medicine and Biology Society (EMBC)*, pages 5549 –5552, 31 2010-sept. 4 2010.

[32] H. K. Kim, J. Biggs, W. Schloerb, M. Carmena, M. A. Lebedev, M. A. L. Nicolelis, and M. A. Srinivasan. Continuous shared control for stabilizing reaching and grasping with brain-machine interfaces. *IEEE Transactions on Biomedical Engineering*, 53(6):1164 –1173, 2006.

[33] A. S. Royer, A. J. Doud, M. L. Rose, and B. He. Eeg control of a virtual helicopter in 3-dimensional space using intelligent control strategies. *IEEE Transactions on Neural Systems and Rehabilitation Engineering*, 18(6):581 –589, 2010.

[34] R. Carabalona, P. Castiglioni, and F. Gramatica. Brain-computer interfaces and neurorehabilitation. *Studies in Health Technology and Informatics*.

[35] E. Buch, C. Weber, L. G. Cohen, C. Braun, M. A. Dimyan, T. Ard, J. Mellinger, A. Caria, S. Soekadar, A. Fourkas, and N. Birbaumer. Think to move: a neuromagnetic brain-computer interface (bci) system for chronic stroke. *Stroke*, 39(3):910–917, 2008.

[36] G. Pfurtscheller, G. R. Muller-Putz, R. Scherer, and C. Neuper. Rehabilitation with brain-computer interface systems. *IEEE Computer Society*, 41(10):58 –65, 2008.

[37] K. K. Ang, C. Guan, K. S. G. Chua, B. T. Ang, C. W. K. Kuah, C. Wang, K. S. Phua, Z. Y. Chin, and H. Zhang. A clinical evaluation of non-invasive motor imagery-based brain-computer interface in stroke. In *IEEE International Conference on Engineering in Medicine and Biology Society (EMBS)*, pages 4178 –4181, 2008.

[38] A. Ramos-Murguialday, D. Broetz, M. Rea, L. Läer, O. Yilmaz, F.L. Brasil, G. Liberati, M.R. Curado, E. Garcia-Cossio, A. Vyziotis, M. Agostini W. Cho, E. Soares, S. Soekadar, A. Caria, L.G. Cohen, and N. Birbaumer. Brain–machine interface in chronic stroke rehabilitation: A controlled study. *Annals of Neurology*.

[39] T. Meyer, J. Peters, D. Brtz, T. O. Zander, B. Scholkopf, S. R. Soekadar, and M. Grosse-Wentrup. A brain-robot interface for studying motor learning after stroke. In *IEEE/RSJ International Conference on Intelligent Robots and Systems (IROS)*, pages 4078 –4083, 2012.

[40] M. Sarac, M. A. Ergin, and V. Patoglu. ASSISTon-Mobile A Series Elastic Holonomic Mobile Platform for Upper Extremity Rehabilitation. *IEEE World Haptics Conference*, 2013.

[41] H. Krebs, M. Ferraro, S. Buerger, M. Newbery, A. Makiyama, M. Sandmann, D. Lynch, B. Volpe, and N. Hogan. Rehabilitation robotics: pilot trial of a spatial extension for MIT-Manus. *Journal of Neuro-Engineering and Rehabilitation*, 1(5), 2004.

[42] R. C. V. Loureiro and W. S. Harwin. Robot aided therapy: Challenges ahead for upper limb stroke rehabilitation. In *International Conference on Disability, Virtual Reality and Associated Technologies*, 2004.

[43] P. Lammertse, E. Frederiksen, and B. Ruiter. The hapticmaster, a new high-performance haptic interface. In *Eurohaptics*, 2002.

[44] R. Chemuturi and and K. Dautenhahn F. Amirabdollahian. Impact of lead-lag contributions of subject on adaptability of the GENTLE/A

system: an exploratory study . *IEEE International Conference on Biomedical Robotics and Biomechatronics.*

[45] S. Hesse, H. Schmidt, C. Werner, C. Rybski, U. Puzich, and A. Bardeleben. A new mechanical arm trainer to intensify the upper limb rehabilitation of severely affected patients after stroke: Design, concept and first case series. *Eura Medicophys*, 43(4):463–8, 2007.

[46] F. Meng, Y. Dai, Y. Jin, and Y. Wang. The Design of a New Upper Limb Rehabilitation Robot System Based on Multi-Source Data Fusion. *World Congress on Intelligent Control and Automation.*

[47] Y. L. Chen, T. S. Kuo, and W. H. Chang. Aid training system for upper extremity rehabilitation. In *Int. Conference of the IEEE Engineering in Medicine and Biology Society*, volume 2, pages 1360 – 1363, 2001.

[48] A. Peattie, A. Korevaar, J. Wilson, B. Sandilands, X.Q. Chen, and M. King. Automated variable resistance system for upper limb rehabilitation. In *Australasian Conf. on Robotics and Automation*, 2009.

[49] G. C. Burdea, D. Cioi, J. Martin, D. Fensterheim, and M. Holenski. The Rutgers Arm II Rehabilitation System–A feasibility study. *IEEE Transactions on Neural Systems and Rehabilitation Engineering*, 18(5):505 –514, 2010.

[50] J. C. Perry, H. Zabaleta, A. Belloso, C. Rodriguez de Pablo, F. I. Cavallaro, and T. Keller. ARMassist: Development of a functional prototype for at-home telerehabilitation of post-stroke arm impairment. In *IEEE International Conference on Biomedical Robotics and Biomechatronics*, pages 1561 –1566, 2012.

[51] J. H. Jung, D. B. Valencia, C. Rodríguez de Pablo, T. Keller, and J. C. Perry. Development of a powered mobile module for the ArmAssist home-based telerehabilitation platform. *IEEE International Conference on Rehabilitation Robotics*.

[52] C. A. Avizzano, M. Satler, G.i Cappiello, A. Scoglio, E. Ruffaldi, and M. Bergamasco. MOTORE: A Mobile Haptic Interface for Neuro-Rehabilitation. In *IEEE International Symposium on Robot and Human Interactive Communication*, pages 383–388, 2011.

[53] D. Luo, M. Roth, C. Wiesener, T. Schauer, H. Schmidt, and J. Raisch. Reha-Manus: A novel robot for upper limb rehabilitation. In *Workshop Automatisierungstechnische Verfahren fur die Medizin (AUTOMED)*, pages 33–34, 2010.

[54] D. Luo, T. Schauer, M. Roth, and J. Raisch. Position and Orientation Control of an Omni-Directional Mobile Rehabilitation Robot. *IEEE International Conference on Control Applications*.

[55] C. H. An and J. M. Hollerbach. Dynamic stability issues in force control of manipulators. In *American Control Conference*, pages 821 –827, 1987.

[56] S. Eppinger and W. Seering. Understanding bandwidth limitations in robot force control. In *IEEE International Conference on Robotics and Automation*, pages 904 – 909, 1987.

[57] K. L. Han, O. K. Choi, I. Lee, I. Hwang, J. S. Lee, and S. Choi. Design and control of omni-directional mobile robot for mobile haptic

interface. In *International Conference on Control, Automation and Systems*, pages 1290 –1295, 2008.

[58] S. K. Agrawal. Multibody dynamics: A formulation using kane's method and dual vectors. In *Journal of Mechanical Design*, volume 115, pages 833–838, 1988.

[59] G. Welch and G. Bishop. *An Introduction to the Kalman Filter*. Chapel Hill, NC, 2001.

[60] H. Durrant-Whyte. *Introduction to Decentralised Data Fusion*. BAE SYSTEMS, 2001.

[61] D. W. Robinson. Design and analysis of series elasticity in closed-loop actuator force control. *Doctor of Philosophy in Mechanical Engineering, Massachusetts Institute Of Technology*, 2000.

[62] J. P. Merlet. *Parallel Mechanisms*. Springer-Verlag, 2006.

[63] Y. Tian, B. Shirinzadeh, D. Zhang, and Y. Zhong. 3 flexure hinges for compliant mechanism designs based on dimensionless graph analysis. *Precision Engineering*, 34(1):92–100, 2010.

[64] Y. Tian, B. Shirinzadeh, and D. Zhang. Closed-form Compliance Equations of Filleted V-Shaped Flexure Hinges for Compliant Mechanism Design. *Precision Engineering*, 34:408–418, 2010.

[65] A. J. Nielson and L. L. Howell. An Inverstigation of Compliant Micro Half Pantographs Using the Pseudorigid Body Model. *Mechanics Based Design of Structures and Machines*, 29:317–330, 2001.

[66] B. H. Kang, J. T. Wen, N. G. Dagalakis, and J. J. Gorman. Analysis and Design of Parallel Mechanisms with Flexure Joints. *IEEE Transactions on Robotics*, 21:1179–1185, 2005.

[67] C. Schonauer, T. Pintaric, H. Kaufmann, S. Jansen – Kosterink, and M. Vollenbroek-Hutten. Chronic Pain Rehabilitation with a Serious Game using Multimodal Input. *International Conference on Virtual Rehabilitation*, 2011.

[68] W. Ilg. Video Game-based Coordinative Training Improves Ataxia in Children with Degenerative Ataxia. *Neurology*, 79(20):2056–60, 2012.

[69] Y.-J. Chang, S.-F. Chen, and J.-D. Huang. A Kinect-based System for Physical Rehabilitation: A Pilot Study for Young Adults with Motor Disabilities. *Research in Developmental Disabilities*, 32(6):2566–70, 2011.

[70] E. B. Brokaw, P. S. Lum, R. A. Cooper, and B. R. Brewer. Using the Kinect to Limit Abnormal Kinematics and Compensation Strategies During Therapy with End Effector Robots. *IEEE International Conference on Rehabilitation Robotics*, 2013.

[71] Kinect skeleton detection. `http://www.mathworks.com/`.

[72] P. Y. Li and R. Horowitz. Passive velocity field control of mechanical manipulators. *IEEE Transactions on Robotic and Automation*, 15:751–763, 1999.

[73] P.Li and R. Horowitz. Control of Smart Exercise Machines, I. Problem Formulation and Nonadaptive Control. *IEEE/ASME Transactions on Mechatronics*, 2:237–247, 1997.

[74] P. Y. Li and R. Horowitz. Passive velocity field control (pvfc): Part i - geometry and robustness. *IEEE Transactions on Automatic Control*, 46:2001, 2001.

[75] D. Lee and P.Li. Passive Bilateral Feedforward Control of Linear Dynamically Similar Teleoperated Manipulators. *IEEE Transactions on Robotics and Automation*, 19:443–456, 2003.

[76] D. Lee and P.Li. Passive Bilateral Control and Tool Dynamics Rendering for Nonlinear Mechanical Teleoperators. *IEEE Transactions on Robotics*, 21:936–951, 2005.

[77] J. Moreno-Valenzuela. On Passive Velocity Field Control of Robot Arms. *IEEE Conference on Decision and Control*, pages 2955–2960, 2006.

[78] J. Moreno-Valenzuela. Velocity Field Comtrol of Robot Manipulators by Using Only Position Measurements. *Journal of the Franklin Institute*, 344:1021–1038, 2007.

[79] F. Lotte, M. Congedo, A. Lecuyer, F. Lamarche, and B. Arnaldi. A review of classification algorithms for EEG-based brain-computer interfaces. *Journal of neural engineering*, 4(2), 2007.

[80] S. Sanei and J. A. Chambers. *EEG Signal Processing chapter 1*. Chichester: Wiley, 2007.

[81] Event-related EEG/MEG synchronization and desynchronization: basic principles. *Clinical neurophysiology*, 110(11):1842–1857, 1999.

[82] G. Pfurtscheller. Brain-Computer Interface—a new communication device for handicapped persons. *Journal of Microcomputer Applications*, 16(3):293–299, 1993.

[83] K. Fukunaga. *Introduction to Statistical Pattern Recognition*. Academic Press, 2 edition, 1990.

[84] S. Bermudez i Badia, H. Samaha, A. G. Morgade, and P. F. M. J. Verschure. Exploring the synergies of a hybrid bci - vr neurorehabilitation system. In *International Conference on Virtual Rehabilitation (ICVR)*, pages 1 –8, 2011.

[85] A. Faith, Y. Chen, T. Rikakis, and L. Iasemidis. Interactive rehabilitation and dynamical analysis of scalp eeg. In *Annual International Conference of the IEEE, Engineering in Medicine and Biology Society (EMBC)*, pages 1387 –1390, 2011.

[86] G. Prasad, P. Herman, D. Coyle, S. McDonough, and J. Crosbie. Applying a brain-computer interface to support motor imagery practice in people with stroke for upper limb recovery: a feasibility study. *Neuroengineering and rehabilitation*, 7(60):1–17, 2010.

[87] E. Ianez, J. M. Azorin, A. Ubeda, and E. Fernandez J. M. Ferrandez, and. Mental tasks-based brain robot interface. *Robotics and Autonomous Systems*, 58(12):1238 – 1245, 2010.

[88] A. Akce, Miles Johnson, O. Dantsker, and T. Bretl. A Brain–Machine Interface to Navigate a Mobile Robot in a Planar Workspace: Enabling Humans to Fly Simulated Aircraft With EEG. *IEEE Transactions On Neural Systems and Rehabilitation Engineering*.

[89] R. Ortner, D.C. Irimia, J. Scharinger, and C. Guger. Brain-Computer Interfaces for stroke rehabilitation: evaluation of feedback and classification strategies in healthy users. *IEEE International Conference on Biomedical Robotics and Biomechatronics.*

[90] A. Ubeda, E. Ianez, J.M. Azorin, and C. Perez-Vidal. Endogenous Brain-Machine Interface based on the Correlation of EEG Maps. *Computer Methods and Pragrams in Biomedicine.*

[91] A. Ubeda, E. Ianez, J. Badesa, R. Morales, J. M. Azorin, and N. Garcia. Control strategies of an assistive robot using a Brain-Machine Interface. In *IEEE/RSJ International Conference on Intelligent Robots and Systems (IROS)*, pages 3553 –3558, 2012.

[92] S.J. Page, P. Levine, and A. Leonard. Mental Practice in Chronic Stroke: Results of a Randomized, Placebo-Controlled Trial. *Stroke.*

[93] D. Leonardis, A. Frisoli, M. Barsotti, N. Vanello, and M. Bergamasco. Combination of Brain-Computer Interface Training and Goal-Directed Physical Therapy in Chronic Stroke: A Case Report. *IEEE International Conference on Biomedical Robotics and Biomechantronics.*

[94] C. Wang, K. S. Phua, K. K. Ang, C. Guan, H. Zhang, R. Lin, K.S.G. Chua, B. T. Ang, and C.W.K. Kuah. A feasibility study of non-invasive motor-imagery bci-based robotic rehabilitation for stroke patients. In *4th International IEEE/EMBS Conference on Neural Engineering, NER'09*, pages 271 –274, 2009.

[95] A. Frisoli, C. Loconsole, D. Leonardis, F. Banno, M. Barsotti, C. Chisari, and M. Bergamasco. A new gaze-bci-driven control of an upper

limb exoskeleton for rehabilitation in real-world tasks. *IEEE Transactions on Systems, Man, and Cybernetics,Part C: Applications and Reviews*, 42(6):1169 –1179, 2012.

[96] C. Loconsole, F. Banno, A. Frisoli, and M. Bergamasco. A new Kinect-based guidance mode for upper limb robot-aided neurorehabilitation. *IEEE International Conference on Intelligent Robots and Systems*.

[97] K. K. Ang, C. Guan, K. S. G. Chua, B. T. Ang, C. Kuah, C. Wang, K. S. Phua, Z. Y. Chin, and H. Zhang. A clinical study of motor imagery-based brain-computer interface for upper limb robotic rehabilitation. In *IEEE International Conference on Engineering in Medicine and Biology Society(EMBC)*, pages 5981 –5984, 2009.

[98] K. K. Ang, C. Guan, K. S. G. Chua, Ang B, T, C. Kuah, C. Wang, K. S. Phua, Z. Y. Chin, and H. Zhang. Clinical study of neurorehabilitation in stroke using eeg-based motor imagery brain-computer interface with robotic feedback. In *Annual International Conference of the IEEE Engineering in Medicine and Biology Society (EMBC)*, pages 5549 – 5552, 2010.

[99] K. K. Ang, C. Guan, K. Chua, B. T. Ang, C. Kuah, C. Wang, K. S. Phua, Z. Y. Chin, and H. Zhang. A large clinical study on the ability of stroke patients to use an eeg-based motor imagery brain-computer interface. 42(4):253–258, 2011.

[100] M. Gomez-Rodriguez, M. Grosse-Wentrup, J. Hill, A. Gharabaghi, B. Scholkopf, and J. Peters. Towards brain-robot interfaces in stroke rehabilitation. 8(3), 2011.

[101] M. Arvaneh, C. Guan, K. K. Ang, and C. Quek. Omitting the Intra-session Calibration in EEG-based Brain Computer Interface Used for Stroke Rehabilitation. *IEEE International Conference on Engineering in Medicine and Biology Society.*

[102] J.-H. Kim, R. Chavarriaga, J.R. Millan, and S.-W. Lee. Three-Dimensional Upper Limb Movement Decoding from EEG Signals. *International Winter Workshop on Brain-Computer Interface(BCI).*

[103] C.D. Holmes, M. Wronkiewicz, T. Somers, J. Liu, E. Russell, D. Kim, C. Rhoades, J. Dunkley, D. Bundy, E. Galboa, and E. Leuthardt. IPSIHAND BRAVO: An Improved EEG-based Brain-Computer Interface for Hand Motor Control Rehabilitation. *IEEE International Conference on Engineering in Medicine and Biology Society.*

[104] Y. Hayashi, K. Nagai, K. Ito, S. J. Nasuto, R. C. V. Loureiro, and W. S. Harwin. A feasible study of eeg-driven assistive robotic system for stroke rehabilitation. In *4th IEEE RAS EMBS International Conference on Biomedical Robotics and Biomechatronics (BioRob)*, pages 1733 –1739, 2012.

[105] M. Sarac, E. Koyas, A. Erdogan, M. Cetin, and V. Patoglu. Brain Computer Interface based Robotic Rehabilitation with Online Modification of Task Speed. *IEEE International Conference on Rehabilitation Robotics*, 2013.